Mechanical and Control Department.

Design of Efficient Propeller for A Flight in Thin-Density Atmosphere

Space Dynamics and Control Laboratory

Umunna, Reuben Jikeme
January, 2020

This dissertation is submitted to Kyushu Institute of Technology in Partial fulfilment of the requirements for the award of A Doctor of Philosophy

Advisor: Prof. Koju Hiraki

ACKNOWLEDGEMENT

My tenure at Kyushu Institute of Technology was supported by Japan Student Service Organization (JASSO) and the Kyutech 100th anniversary scholarship. I remain deeply grateful for the generosity from these institutions.

I would also like to thank my advisor Professor Koju Hiraki for his invaluable technical insights and the opportunity to learn from his thought process. I would also like to say a very big thank you to Prof. Koichi Yonemoto of the Space Club for the opportunity to participate, contribute, and learn from the WiRes project. Special thank you to my amazing laboratory mates, my tutor and ties of friendship I have with great people in Japan – you made my stay in Japan a pleasant and memorable one. Thank you Japan for the experience and gift of an additional lens from which to further view the world.

Lastly, to my father thank you for nurturing my curiosity and to my mother thank you for the strength of spirit.

Indeed, I remain eternally indebted to your collective humanity.

DECLARATION

“I Umunna Jikeme Reuben, declare that this dissertation is my own work. Any section, part or phrasing of words that are copied from any other work or publication has been clearly referenced at point of use and also fully described in the reference chapter of this work.”

……

Umunna Reuben Jikeme

ABSTRACT

Over the last three decades and a half, there has been huge effort to develop high performance propellers suitable for flight in the rarefied Martian atmosphere. At low Reynolds number below 30000 the aerodynamic flow physics makes accurate measurement of airfoil force data difficult. Propellers are currently the most promising means of propulsion in Mars. However, since propellers rotate and translate in the fluid medium in which they operate, the problem of flying in Mars atmosphere is compounded by low speeds of sound, which limits propeller tip speeds. The first section this thesis describes work undertaken in validating vortex theory in the design of a heavily loaded propeller with high solidity and chord-based Reynolds number of ≈60000 (calculated at 75% radius) at design point. SD7037 2D airfoil experiment data used for the entire blade design was collected at Reynolds number of 60000. At design advance ratio, more than 50% of the entire blade radius operated between 40000 – 60000 Reynolds numbers. A design goal of the propeller was to minimize variation in Reynolds number from hub to tip radius. Wind tunnel tests were carried out at Kyushu Institute of Technology.

The second section of the thesis focussed on designing a blade that would operate in a lower Reynolds number of 20000. At these low Reynolds numbers, which is about the Reynolds number Mars propellers are expected to operate, 2D airfoil force experiment data are not available. A numeric code was used to predict the airfoil performance at these low Reynolds number. A propeller was designed to operate at 20000 Reynolds number using 2D airfoil data obtained from the numeric code – Xflr-5. The propeller design was carried out using a Minimum Induced Loss BEMT code Xrotor. Airfoil lift and drag estimates are approximated in Xrotor using a linear function for lift and a quadratic function for drag coefficient. The use of functions in estimating airfoil lift and drag data makes Xrotor a good design tool to under study relationship between airfoil force coefficients and propeller performance. Parameters in the lift and drag estimation functions in Xrotor can be individually manipulated and the overall effect on propeller performance can be isolated and theoretically studied. Using Xrotor, a propeller designated as SDL20M was designed, fabricated and tested at Kyushu institute of technology wind tunnel facility. The result show discrepancy between predicted propeller performance and wind tunnel test data. Through a careful manipulation of four (4) key parameters in the

functions defining lift and drag in Xrotor, it was possible to match predicted propeller performance to wind tunnel test. Following a successful performance matching, a semi-empirical correction function that corrected the flow velocity relationships in the wake and plane of the propeller in classical BEMT formulation was developed. Lastly, the semi-empirical correction function developed was applied on a propeller design. A BEMT code was written in Matlab in which the semi-empirical correction function was integrated. 2D airfoil force data is supplied to the BEMT code in a look-up chart which was populated with data from the numerical code. The Reynolds number regime of interest in this work are in the orders not available from experiment, airfoil force data was obtained from Xflr-5 by setting Ncrit value of 1. Utilizing the developed BEMT code, two (2) propellers designated as SDL20Y and SDL20Y-2 were designed, fabricated and tested in wind tunnel experiments. SDL20Y-2 is a 2-bladed unmodified propeller design output from classical BEMT code written for the purpose of this work, while the design of SDL20Y was modified by applying the semi-empirical correction developed in the course of this research. Beside the semi-empirical correction applied in the design of SDL20Y, all other design parameters were kept exactly the same with SDL20Y-2. Wind tunnel tests from both propellers showed that when compared with SDL20Y-2, SDL20Y has excellent agreement between predicted performance and wind tunnel test data.

MOTIVATION

Earth is about 148 million Km^2 and Mars is about 97% the size of Earth and at 0.1 km altitude, the ratio of Earth's density to Mars is about 80. Pictures taken by rovers on Mars indicate that the surface of Mars is littered with lumps of debris.

For years Man has struggled to find evidence that answers the question of whether or not Mars once had life; whether there was once water on the surface of Mars or does water or ice caps exist anywhere on Mars surface. So far, satellites in orbits around Mars have been used for the exploration of Mars, landers and rovers have all been equally used. Landers and rovers deployed on Mars were equipped with several sensors to perform in-situ data collection and analysis of soil and rock samples. However, spatial and temporal exploration using rovers have been remarkably slow, largely due to difficulties associated with path planning necessary to avoid obstacles such as debris on Mars surface or canyons. Pathfinder for instance travelled only 52m in a period of 30 days. The slow travel rate of pathfinder was largely because it had to transmit telemetry and receive command from Earth million of miles away. Inherent communication delay results in time lag of up to two digits.

Mars air vehicles have long been considered as either faster alternatives for the exploration of Mars than rovers or could be employed to compliment rovers. A Mars Scout is planned to support path planning for next generation rovers. However, Mars environment is known to be a difficult environment to achieve powered flight. The CO_2 dominated Mars atmosphere lacks oxidant necessary for combustion of fuels, thus, reducing the appeal of air breathing engines for propulsion in Mars. Propellers on the other hand, do not require combustion to generate lift and thrust as they can be powered using batteries and/or solar energy. However, the low density and low speed of sounds impose design limitations on Mars usable propellers for vehicle propulsion.

Table of Contents

1 ABSTRACT

Table of figures

NOTATION

Nomenclature

T : Thrust

Q : Torque

P : Power

B : Number of blades

ρ : Density

r : Station radius

r_{tip} : Tip radius

r_{hub} : Hub radius

V_R : Resultant velocity

ϕ : Local flow angle

C_D : Drag coefficient

$C_{D(0)}$: Minimum C_D

C_L : Lift coefficient

$C_{L(0)}$: C_L at $C_{D(0)}$

Re : Reynolds number

c : Blade chord

ω : Angular velocity

v_t : Induced tangential velocity

V : Free airstream velocity

v_a : Induced axial velocity

J : Advance ratio

C_T : Thrust coefficient

C_D : Drag coefficient

a0 : Lift curve slope

$()_{(E)}$: Experiment

$()_{(J)}$: Advance ratio

$()_{(i)}$: Induced inflow angles

v_i : Airflow velocity @ leading edge

Ω : Angular speed in RPS

F : Prandtl loss factor

ϕ_t : Local flow angle at blade tip

ε : Drag to lift ratio

λ : Speed ratio $V/\Omega R$

ξ : Non-dimensional radius, r/R

ς : Displacement velocity ratio v'/V

W : Local total velocity

w_t : Tangential velocity in wake

v' : Vortex displacement velocity

w_a : Axial velocity in wake

w_r : Resultant velocity in wake

Γ : Circulation

a : Axial induction factor

a' : Rotational induction factor

β : Blade pitch

α : Blade angle of attack

CHAPTER ONE

1 INTRODUCTION

1.1 Literature Review

Recently there has been considerable interest in Low-Reynolds flights driven by efforts to develop micro air bots for various applications: achieving flights within the stratosphere and in the rarefied Mars atmosphere. For a Mars flight, extremely low fluid inertia and speed of sound limits the propeller tip speeds, thus, adding to the design complexity. Other design consideration includes; compactness of the design to ensure fit into aerosols from where it would be deployed for operation on entry into Mars atmosphere. Hence, blades with large radius would need to be folded and reliably deployed before the commencement of flight. The propeller design presented in this work was not designed to meet the propulsion demands of any specific air vehicle but rather the goal was to firstly validate the application of lifting line theory and minimum induced losses in the design of high solidity, low Reynolds number operating propellers. The works of Betz [1], Goldstein [2] all assumes light loading for which their respective formulation holds true. Mark Drela replaced the advance ratio ($v/\Omega R$) with wake advance ratio to account for heavy disk loading [3]. However, the implementation of graded momentum formulation in Xrotor notes that the momentum formulation is unsuitable for advance ratios greater than 0.5 [4].

Muller [5] described chord based Low Reynolds number as flows less than 10^6. However, Reynolds numbers <70k are of particular interest in this work. A major challenge that must be overcome towards the realization of low-Reynolds number-high performance flight is an efficient propulsion system. Studies favor a propeller based propulsion system for high efficiency, long endurance flights at high altitude or rarefied Martian atmosphere where propellers may operate at Reynolds numbers lower than 100k. Youngren [6] used Xrotor to redesign a COT propeller and demonstrated that improving the performance of 2D airfoil and optimally distributing propeller load along its radius could enhance the performance of COT propellers operating at Low Reynolds numbers. Wind tunnel tests of the redesigned propeller conducted by Youngren showed better performance than Xrotor predictions. Smedresman et al [7] used Qprop a code based on lifting line theory to create a propeller that operates at about 21000 chord based Reynolds number. The propeller design utilized 2D aero data of a modified MA409 airfoil that was obtained using Xfoil. Wind tunnel test of the fabricated

propeller showed 20% lower efficiency from Qprop predictions. The uncertainties associated with 2D airfoil force coefficients were reported by Smedresman to be partly responsible for the discrepancy between experiment and predicted results. Dexter et al [8] tested several low Reynolds number COT propellers. Experiment data from their wind tunnel tests showed performance dependency on Reynolds number. However, details of airfoil and related force coefficients used in the respective designs of the COT propellers as expected are not in the public domain. As a result, it was difficult to compare design performance data with experimental data. In the performance tests of Black widow's propeller, Grasmeyer et al [9] achieved excellent performance agreement between experimental data and lifting line theory predictions. However, details of 2D airfoil aerodynamic data and propeller operational Reynolds number were not supplied.

The design of a high performance propeller requires the accurate knowledge of the 2D airfoil data to be used for the design. Poor or inaccurate 2D airfoil data results in poor propeller performance and discrepancy between vortex theory prediction and experiment data. For most flows over an airfoil at Reynolds number below 100k, Laminar Separation Bubble (LSB) is not only present, but it also degrades the airfoil performance. Selig [10] suggests that LSB progresses forward towards the leading edge with increasing angle of attack until total flow separation of the flow from the trailing edge is achieved due to "burst" of the laminar bubble eventually causing airfoil stall. Presence of LSB modifies the airfoil shape and consequently the airfoil aerodynamic force coefficients. Depending on the geometry, position and radial spread along a propeller, LSB can drastically affect the overall performance of a propeller.
With decreasing Reynolds number (<40) it becomes increasingly challenging to obtain reliable 2D airfoil force data. At these Low Reynolds number, Aerodynamic force data from experiment or numeric sources cannot be absolutely depended upon. (1) presented experiment data of A18, BE50, and SD8030 at Reynolds number of 40k. However, while it was possible to measure lift for these airfoils, reliable measurement of drag proved difficult to obtain and are hence unavailable.

For most low inertia flows over an airfoil, that result in Reynolds number <100k, the presence of laminar separation degrades the performance of such airfoils. However, airfoils can also be designed so that the LSB modifies the airfoil shape and consequently improves aerodynamic force coefficients of airfoils. (2) suggest that short LSB can act as a turbulator thereby

improving 2D airfoil performance. Grundy (3) measured lift and drag forces acting on E61 airfoil between Reynolds number range of 25k and 60k and concluded that at high angle of attack long LSB break down into short bubbles resulting in an increase in lift and decrease in drag. Grundy further added that high acoustic activity in the vicinity of the measurement promoted a quick transitioning of flow states.

High frictional forces and low inertia associated with Low Reynolds number flows often results in adverse pressure during flow transition at the upper surface of the airfoil. The sensitivity of low-Reynolds number flows makes it onerous to acquire the aerodynamic forces that govern the flow thus, reducing the quality of 2D airfoil data collected from experiments. On the other hand, 2D airfoil characteristics obtained from numeric codes are also not reliable. The limited understanding of the actual physics of low Reynolds number flows further extends to lower the accuracy of force coefficient predictions by numerical codes. (4) used Xfoil to predict the aerodynamic characteristics of MA409 at Reynolds number between 10k and 22k and used the data in the design of a propeller. In their work, uncertainties associated with 2D airfoil force data was partly blamed for observed discrepancy in the propeller performance between theory and experiment. Ultimately, inherent uncertainties from 2-D airfoil aerodynamic force data prevent accurate propeller performance prediction.

1.2 Chapter Summary

This work describes the methodological efforts applied to achieve propeller designs operating in low Reynolds number flight regimes whose theoretical performance closely matches with wind tunnel experiments.

Chapter 1: Introduces literature review of Low Reynolds number propellers and inherent difficulties associated with the measurement of 2D airfoil force data at Reynolds numbers less than 30k. It also captures summary of unique contribution of this work.

Chapter 2: Discusses behaviour of airfoils at low Reynolds number and introduces SD7037, an airfoil used in the design of all propellers presented in this work. It discusses SD7037 at Reynold number regimes where 2D force data are available and not. Xflr-5, a software that uses vortices panel method in the prediction of airfoil 2D force data is presented. Chapter 2 lays out the underlying principles and equation of Blade Element Momentum Theory (BEMT) and present Xrotor – a freely distributed BEMT code used in the design of propellers.

Equations describing the analysis of an arbitrary propeller is presented . The chapter finally describes propeller wind tunnel test set-up as used in all propeller tests carried out in the course of this work. A 9x10" APC propeller tested using this experiment set-up and compared with similar experiment conducted at University of Illinois Urbana Champaign (UIUC) is presented.

Chapter 3: The chapter describes work undertaken in validating vortex theory in the design of a heavily loaded propeller with high solidity and chord-based Reynolds number of about 60000 (calculated at 75% radius) at design point. A propeller designated as SDL60M was designed, fabricated, and tested. At design advance ratio, more than 50% of the entire blade radius operated between 40,000 – 60,000 Reynolds numbers. This was a deliberate design to minimize variation in Reynolds number from hub to tip radius. Wind tunnel tests of the fabricated propeller was carried out in an Eiffel-type, open-no-return wind tunnel at Kyushu Institute of Technology. Results of tests and analysis are also presented.

Chapter 4: In this chapter, discrepancies between theoretically predicted propeller performance and wind tunnel test data at Re ≈ 20,000 is investigated. A propeller designated as SDL20M was design to operate at 20,000 Reynolds number. However, the absence of 2D airfoil experiment data meant that 2D airfoil force data could only be obtained from numeric sources. Theoretical performance prediction of the propeller was compared with wind tunnel test data.

Chapter 5: This chapter begins with a detailed description of the methodology applied in developing a semi-empirical correction function from the theoretical performance prediction and actual wind tunnel tests of SDL20M. Through a careful manipulation of four (4) key parameters in the functions defining lift and drag in Xrotor, it was possible to match predicted propeller performance to wind tunnel test. The effect of induction factors, a and a', on performance parameters were presented. Following successful performance matching, a semi-empirical correction function that corrected the flow velocity relationships in the wake and plane of the propeller in classical BEMT formulation was developed and presented. The semi-empirical correction function developed was applied in the design of a propeller designate as SDL20Y and wind tunnel test compared with a similar control propeller specimen also fabricated and designated as SDL20Y-2.

Chapter 6: Presents the summary of the entire work and recommends future paths the work could be extended.

1.3 Summary of Contribution

This work explored a range of areas within the scope of propeller design, from the design of propellers using airfoil force data obtained from experiment data at Reynolds number of 60000 to reliable propeller design and performance prediction using airfoil force data predicted using numeric codes at Reynolds number of 20000. Unique contributions of this work to existing knowledge on propeller design at Low Reynolds number includes:

- Explored in detail the contributions of non-linear effects of 2D airfoil force experiment data obtained at Reynolds number of 60000 on the accurate prediction of propeller performance.
- Developed and validated a semi-empirical method that can be applied in accurate prediction of propeller performance operating at low Reynolds number of about 20,000 in which 2D airfoil data from experiment is unavailable.
- Implicitly evaluated the reliability of 2D airfoil force prediction using vortice panel method at Reynolds number of 20000 in the design of propellers.
- Showed that for propellers operating at Reynolds number around 20000, a stability criterion is an induction factor that is lower than 1% of airflow and angular velocities of the propeller.
- Demonstrated the applicability of Blade element theory in the design of a heavily loaded blade at Reynolds number of 60000.

CHAPTER TWO

2 PROPELLER DESIGN

2.1 Airfoil Considerations

High frictional forces and low inertia associated with Low Reynolds number flows often results in adverse pressure during flow transition at the upper surface of the airfoil. The sensitivity of low-Reynolds number flows makes it onerous to acquire the aerodynamic forces that govern the flow, thus, reducing the quality of 2D airfoil data collected by experiments. The limited understanding of the flow physics of low Reynolds number flows further extends to lower the accuracy of force coefficient estimated by numerical codes. Ultimately, uncertainties from 2-D airfoil aerodynamic data are cascaded into overall propeller performance.

A single airfoil SD7037 was used for the design of the entire design of all the propellers fabricated and tested in wind tunnel as discussed in this work . The 2D airfoil aerodynamic data used for the design of SD1007 was taken from experiments conducted by H.A Stokely (5).

To ensure structural integrity of the propeller the thickness of the airfoil at blade root (r/R = 0.175) was increased to 35% while at other blade stations (r/R = 0.287 and 0.75) a 9% thickness/chord SD7037 was maintained. Further, to check inherent trailing edge structural concerns, the airfoil trailing edge was thickened to a constant value of 0.05mm along the entire blade radius, corresponding to <0.5% of chords. A NACA report (6) recommends a 1% trailing-edge radius for an airfoil with 10% thickness to chord.

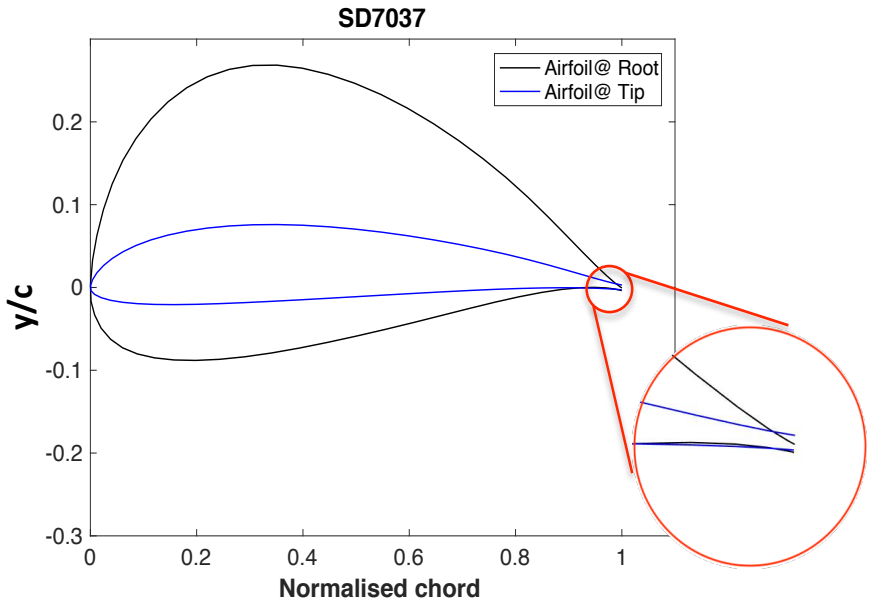

Figure 2-1: Airfoil shape at root and tip showing Trailing edge opening

2.1.1 XFLR-5

Xflr-5 (7) is a numeric code that uses vortices panel method for the analysis of airfoils at low Reynolds numbers. It combines high-order panel methods with coupled interaction between viscous and inviscid layer flows to predict airfoil characteristics. An e^N envelope method allows the inclusion of a representative boundary layer transition effects in solutions within the subsonic flow regime. Airfoils can be directly modified in Xflr-5 by direct specifying new geometric parameters such as maximum thickness and camber, trailing thickness and leading edge radius.

2.2 Blade Element Momentum Theory

Initial blade designs in this work were carried out using Xrotor, which is a freely available and distributable Blade Element Momentum Theory (BEMT) design code written in Fortran language. Xrotor iterates blade chord and twist under the condition of Minimum Induced Losses using either 2D blade momentum theory or Goldstein formulation. In both methods, lifting line is used at various radial stations to represent the blade geometry. Graded blade element momentum theory uses the Betz-Prandtl method for the estimation of induced

velocities at the propeller plane, while the Goldstein method calculates the induced velocities by prescribing a helicoidal wake from the trailing edge vortices of the blade where Helmholtz's condition is imposed. Propeller section thrust and torque are integrated along the entire blade using equations 1 and 2. The blade shape can only be iterated in design mode in Xrotor after which the off-design performance of the iterated blade shape is evaluated in operate mode.

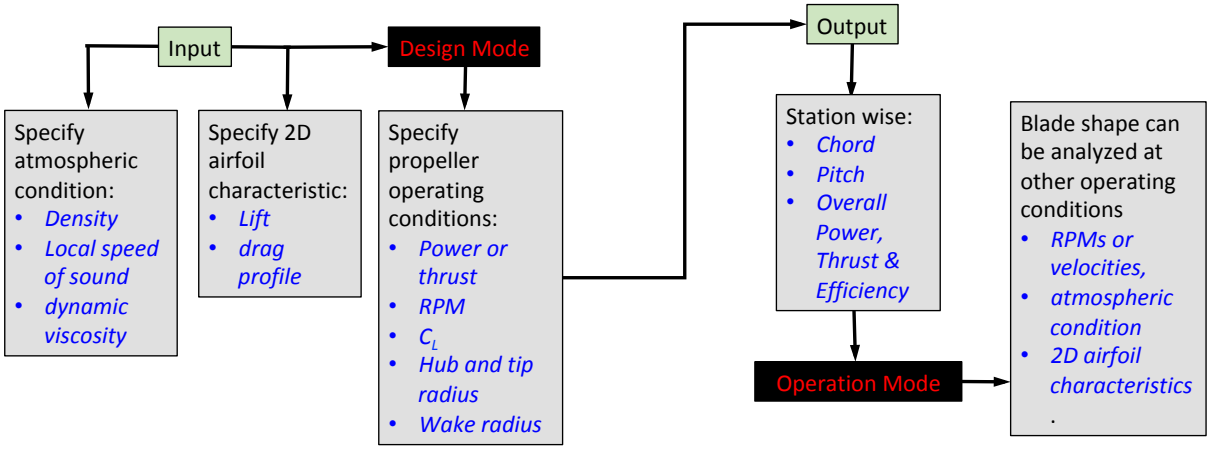

Figure 2-2: Xrotor - Propeller design and off-performance evaluation flow chart

This work uses the Blade element momentum theory reformulated by larrabee. In the BEMT each section is made of a 2D airfoil section at a given angle known as the geometric pitch of a propeller. For fixed pitch propellers, the geometric pitch is fixed. The sections at each propeller radius are discretely analysed on the assumptions that:

(1) The only velocity components acting on each propeller section are the axial and angular components of velocity
(2) Induced velocity from external sources are sufficiently small enough to be neglected
(3) Induced velocity vector is normal to the local velocity relative to the 2D airfoil section.

The local angle of attack is the angle the local velocity vector at each blade section makes with the zero lift line of the 2D airfoil section. Lift and drag of the airfoil section can be obtained from either experiment data or numeric sources. However, note that depending on the BEMT code, the 2D airfoil may have to be provided in a table or linearized form for use in blade design. In Xrotor, a linearized form of the 2D airfoil data is provided as input. There are

advantages of the latter input method: it allows for a perfect agreement of blade performance predictions in both the propeller design and off-performance modes of the design process.

If we consider a free stream fluid element of mass dm upstream of a propeller with velocity V moving towards the propeller, so that at a region near the face of the propeller, V is roughly equal to V_i. Further, at the plane of the propeller, the mass flow rate of fluid element dm in the tube of elemental radius dr passing through the propeller must equal the thrust produced by this blade element for conservation of momentum to hold true. Therefore, the resulting thrust and torque due to momentum between change in the fluid velocity at the region behind the propeller and free stream velocity V_i at the region close to the face of the propeller is given by

$$dT = 2\pi r dr \rho V (V_{As} - V_i) \tag{1}$$

$$dQ = 2\pi r^2 dr \rho \mathrm{V} (V_{Ts} - V_T) \tag{2}$$

Next, if we define the blade's tangential velocity Omega*r, which is slightly reduced because of the propeller swirl at the plane of the propeller. Then taking the velocities together, we arrive at equation 3 and equation 4

$$V_A = V_i \left(1 + \left(\frac{v_a}{V_i}\right)\right) \tag{3}$$

$$V_T = \Omega r \left(1 - \left(\frac{v_t}{\Omega r}\right)\right) \tag{4}$$

The free stream velocity V ahead of the propeller in the stream tube is determined to be the average of velocity of the fluid stream right at the fore and aft of the propeller, V_i and V_s respectively. Combining with equation 1 the slipstream velocity is given by

$$V_{As} = V_i \left(1 + 2\left(\frac{v_a}{V_i}\right)\right) \tag{5}$$

$$V_{Ts} = \Omega r(1 + (\frac{v_t}{\Omega r})) \quad (6)$$

Using equation 1, 3 and 5, along with equation 2, 4 and 6 it can be shown that the final form of the momentum equation including the Prandtl's momentum loss factor *F* is given by

$$dT = 2\pi r dr \rho V(2v_a F) \quad (7)$$

$$dQ = 2\pi r^2 dr \rho \mathrm{V}(2v_t F) \quad (8)$$

Where is defined as

$$F = \left(\frac{2}{\pi}\right) arc\ cos(e^{-f}) \quad (9)$$

$$f = \frac{B}{2}(1 - \frac{r}{R})/\sin\phi_t \quad (10)$$

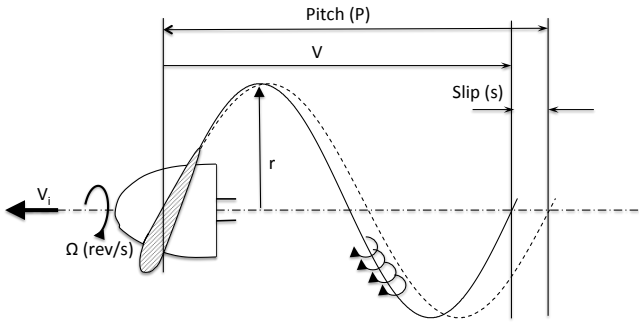

Figure 2-3: 2D propeller section helicoidal wake depicting slip and vortex swirl

From Figure 2-4 the elemental thrust and torque per area of a section of the blade element Figure 2-4(a) can be written as

$$dT = dLcos(\phi) - dDsin(\phi) = dL\ cos(\phi)(1 - \varepsilon\ tan(\phi)) \quad (11)$$

$$\frac{dQ}{r} = dL\ sin(\phi) - dD\ cos(\phi) = dL\ sin(\phi)(1 + \varepsilon/tan(\phi)) \quad (12)$$

$$dL = B\rho W\Gamma dr \tag{13}$$

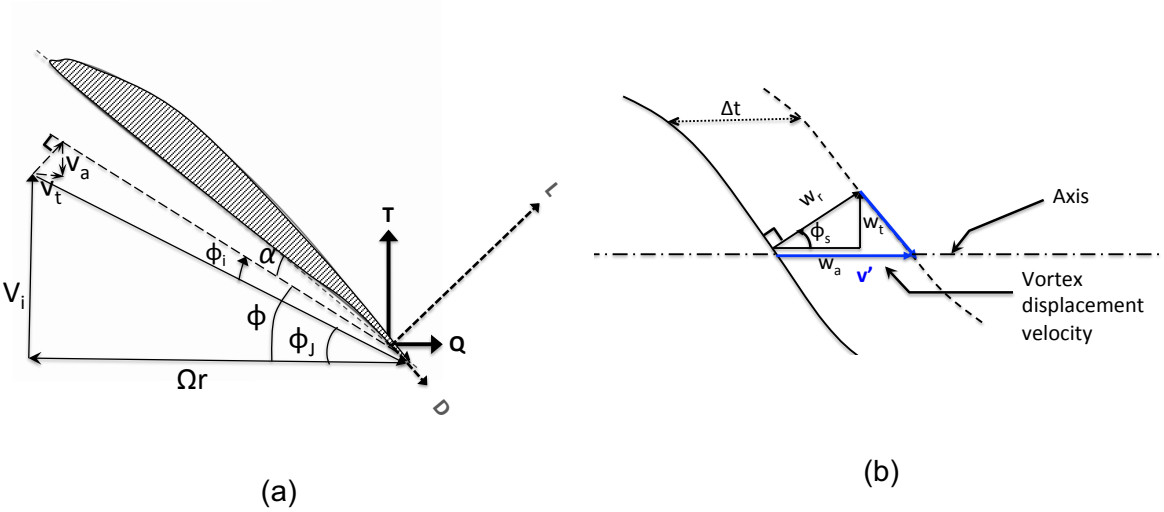

(a) (b)

Figure 2-4: Locally induced axial and tangential velocity at propeller plane (a) and wake (b)

Where ε is the drag/lift ratio of the 2D airfoil. Then, an important assumption on which BEMT prediction is based is that the motion of the vortex sheet must proceed in a perpendicular track relative to the local reference sheet as shown in figure 3-3(b). From figure 3-3(b), the tangential velocity and the axial velocity of fluid as defined at the plane of the propeller is given by equations 14 and 15 respectively.

$$w_t = w_r \sin(\phi) \tag{14}$$

$$v' = w_r / \cos(\phi) \tag{15}$$

Equation 16 defines the average W_t in terms of a displacement velocity ratio $\zeta = v'/V$, using equations 14 and 15, while equation 17 defines the average axial velocity W_a. This is the Betz condition for minimum power induced losses.

$$w_t = V\zeta \sin(\phi)\cos(\phi) \tag{16}$$

$$w_a = \zeta cos^2(\phi) \tag{17}$$

The Betz-Prandtl circulation function is defined as

$$\Gamma = \left(\frac{2\pi V^2 \zeta}{B\Omega}\right) F \sin(\phi)\cos(\phi) \tag{18}$$

Next, by relating the axially induced velocity W_a in the wake and the tangential velocity induced by the rotor on the wake W_t to the corresponding velocities, v_a and v_t, on the plane of the propeller the following relationship satisfies the blade condition at tip where the r/R is unity.

$$\tan(\phi_t) = \left(1 + \frac{\zeta}{2}\right)\left(\frac{r}{R}\right)\frac{V_i}{\Omega R} \tag{19}$$

If c is used to denote chord and C_L is the local coefficient of lift at blade station r, it follows that a strip dr would generate a lift per radius equivalent of

$$\Gamma = \frac{V_R c C_L}{2} \tag{20}$$

By equating equation 18 to equation 20, equation 21 is obtained

$$V_R c = \frac{4\pi\lambda V R \zeta}{B C_L} F cos(\phi) sin(\phi) \tag{21}$$

Multiplying equation 21 with kinematic viscosity yields Reynolds number of the blade strip

$$V_R = (\Omega r - v_t)/\cos(\phi) \tag{22}$$

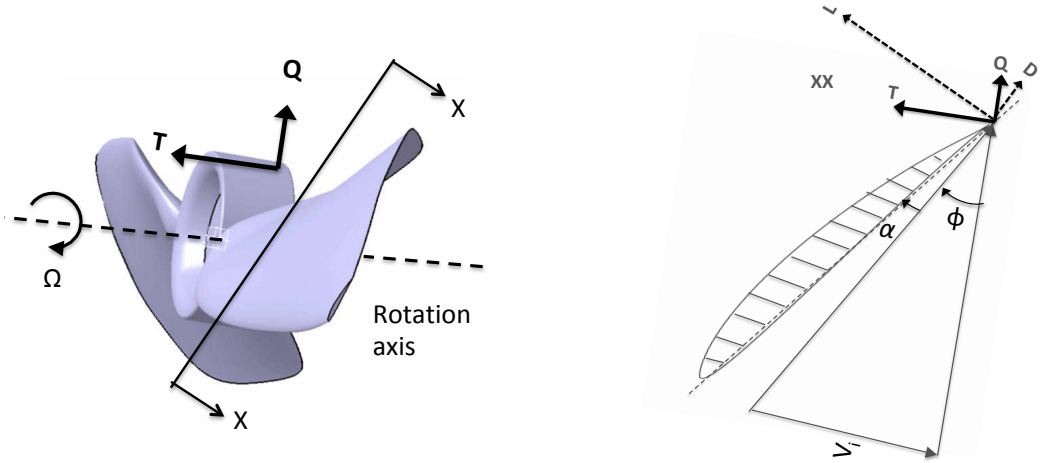

Figure 2-5: blade section showing local velocity profiles

The total thrust delivered by the blade and the total power absorbed by the propeller is given in equation 23 and 24.

$$T = 0.5B\rho \int_{R_{hub}}^{R_{tip}} V_R^2 c_L \left(cos\phi - \frac{c_D}{c_L} sin\phi \right) cdr \tag{23}$$

$$Q = 0.5B\rho \int_{R_{hub}}^{R_{tip}} V_R^2 c_L \left(sin\phi + \frac{c_D}{c_L} cos\phi \right) crdr \tag{24}$$

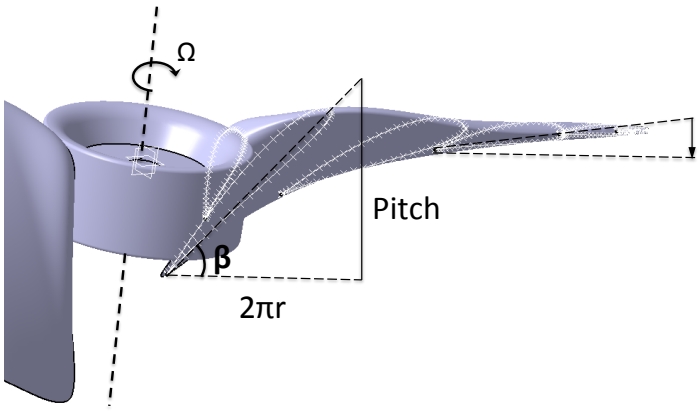

Figure 2-6: Propeller twist distribution root to tip

Figure 2-6shows typical twist distribution achieved from the integration of 2D airfoil of a blade from hub to tip

2.3 Analysis of Arbitrary Blade

The blade element momentum theory was fundamentally developed using the conservation of axial and angular momentum of a propeller in action and the fluid with which it interacts. When power is applied to a propeller so that it possesses angular momentum by which axial flow of the working fluid through the propeller generates desired thrust. BEMT modelling is largely performed in 2-dimensional plane only based on lifting line or strip method. Essentially, a strip or elemental section of the blade is taken and analyzed to obtain the thrust generated due to power delivered to it or vice versa. Each section of the blade is an airfoil with known characteristics as shown in Figure 2-7. The total thrust and power delivered to and by the propeller is predicted by integrating the elemental thrust (dT) and Power (dQ) of the blade along its entire span.

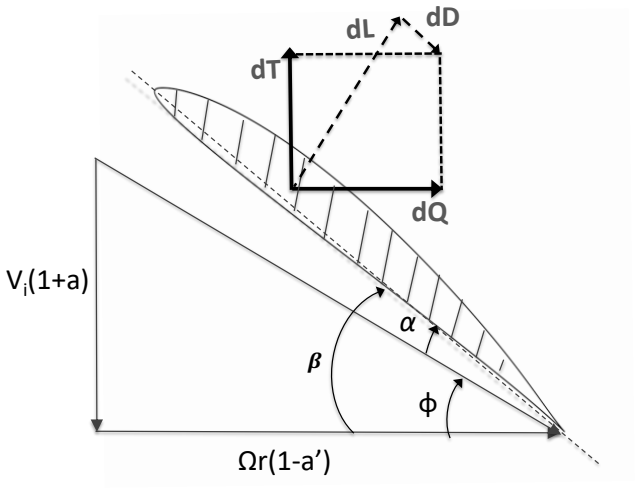

Figure 2-7: Blade section flow geometry at station r/R

Suppose a fluid element of mass *m* far upstream of a propeller approaches the propeller plane at velocity *V,* so that the torque action of the propeller causes a velocity increase to *V*(1+a) where a is the axial induction factor while in the slipstream, aft of the propeller, the velocity is increased to Ωr(1+a'). At the plane of the propeller, the thrust generated per radius due elemental fluid mass travelling in an annular stream tube of magnitude 2πrdr can be estimated using equation 1. Along similar lines, the torque per unit radius can be estimated using equation 2.

$$\frac{dT}{dr} = 4\pi r\rho V^2 F(1+a)a \tag{25}$$

$$\frac{dQ}{dr} = 4\pi r^2\rho V\Omega F(1+a)a' \tag{26}$$

The lift and drag per strip element dr is given in equation 27 and 28.

$$dL = \frac{1}{2} Bc\rho V^2 \frac{(1+a)^2}{sin^2\phi} C_l dr \tag{27}$$

$$dD = \frac{1}{2} Bc\rho V^2 \frac{(1+a)^2}{sin^2\phi} C_d dr \tag{28}$$

Using the relationship between lift and drag, the elemental thrust and torque is given in equations 25 and 26 respectively.

$$\frac{dT}{dr} = \frac{dL}{dr} cos\phi - \frac{dD}{dr} sin\phi \tag{29}$$

$$\frac{dQ}{dr} = \left(\frac{dL}{dr} sin\phi + \frac{dD}{dr} cos\phi\right) r \tag{30}$$

From the momentum theory, it follows that the equation pairs 25, 29 and 26, 30 must be equivalent, so that the induction factors a and a' can be estimated using equations 31 and 31. Thus, the total thrust generated and torque supplied to the blade is the summation of individual contribution dT and dQ from each element strip dr. The thrust and power coefficients C_t and C_p, advance ratio J, and efficiency η are calculate using equations 33 – 36 respectively.

$$a = \frac{1}{\left(\frac{4Fsin^2\phi}{\sigma C_l (cos\phi - \frac{C_d}{C_l} sin\phi)}\right) - 1} \tag{31}$$

$$a' = \frac{1}{\left(\frac{4sin\phi cos\phi}{\sigma C_l(sin\phi + \frac{C_d}{C_l}cos\phi)}\right) + 1} \quad (32)$$

$$C_t = \frac{T}{\varrho\Omega^2 D^3} \quad (33)$$

$$C_p = \frac{P}{\varrho\Omega^3 D^5} \quad (34)$$

$$J = \frac{v}{nD} \quad (35)$$

$$\eta = \frac{C_t J}{C_p} \quad (36)$$

Correction to Hub and Tip losses

As the number blades increase from one to infinity, the Prandtl correction factors ensures the blade behaviours tend to a disk and it also forces the design produces no thrust at the tip radius where R = r. The Prandtl correction factor is given in equation 38.

$$f = \frac{B(R-r)}{2R}\frac{1}{sin\phi} \quad (37)$$

$$F = \frac{2\cos^{-1}(e^{-f})}{\pi} \tag{38}$$

2.4 Experiment Set-Up

Two different experiment set-ups were used for the measurement of thrust and torque. Figure 2-8 and Figure 2-9 depicts the set-up for thrust and torque respectively. A TCLZ-NA load cell was used for the measurement of thrust while torque reading was collected via a UM-II torque meter having an accuracy of 0.0001. In the measurement of thrust and torque, a DC power source supplied power to a Hyperion ZS2213-22 electric motor via an ATLAS 21A ESC. A WF1974 match function generator was used to send PWM command to the electronic speed controller. The angular velocity of propeller was obtained from a HT-5500 contactless tachometer and free airstream velocity was collected using a digital anemometer. Propeller performance measurements were carried out using the Kyushu Institute of Technology wind tunnel. The wind tunnel is an open-ended no-return Eiffel tower type with an open test section. The propeller was mounted about 0.3m away from the exit plane of the convergent section of the open test area that measures 0.5m x 0.5m x 1m.

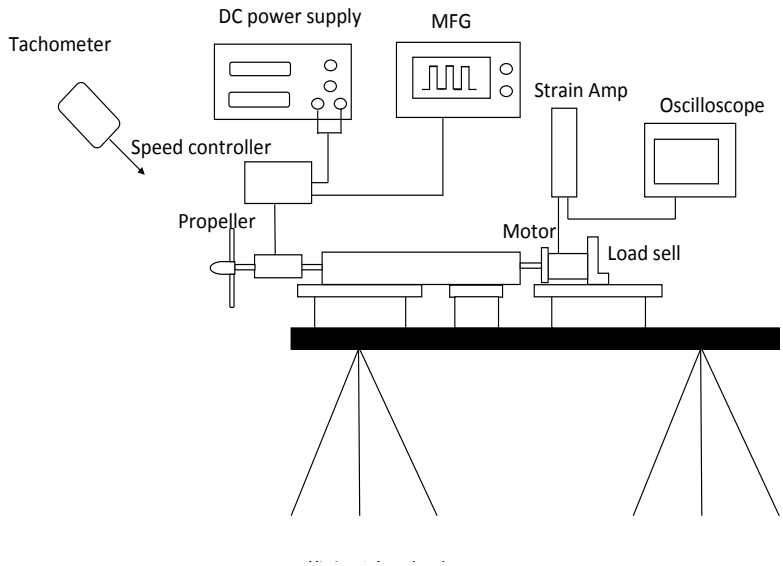

Figure 2-8: Experiment set up for Thrust measurement

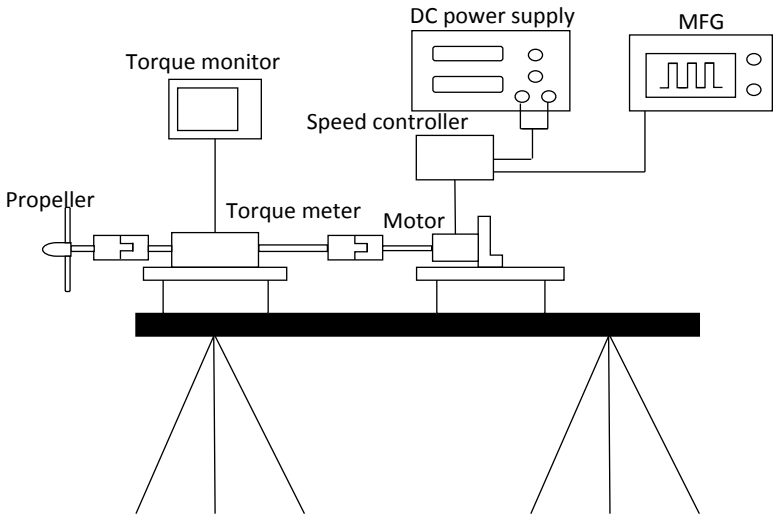

Figure 2-9: Experiment set up for Torque measurement

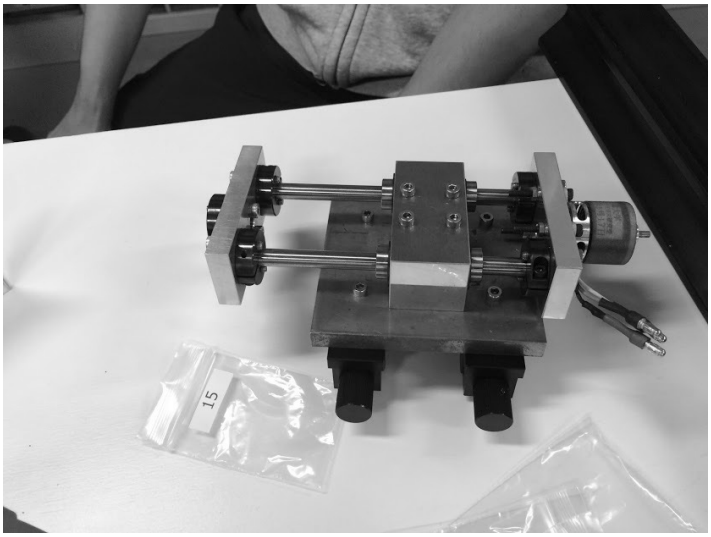

Figure 2-10: Frictionless 1 axis slide bushing for thrust measurement

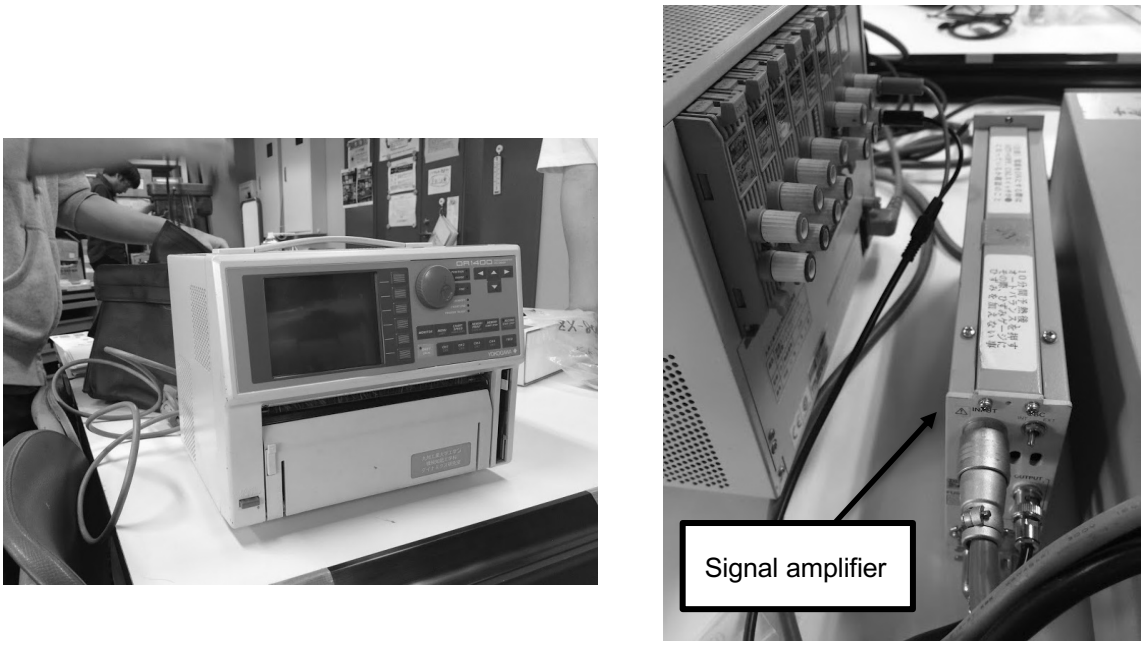

Figure 2-11: Oscilloscope (a) and Signal Amplifier (b) used to collect data from strain guage in the measurement of thrust

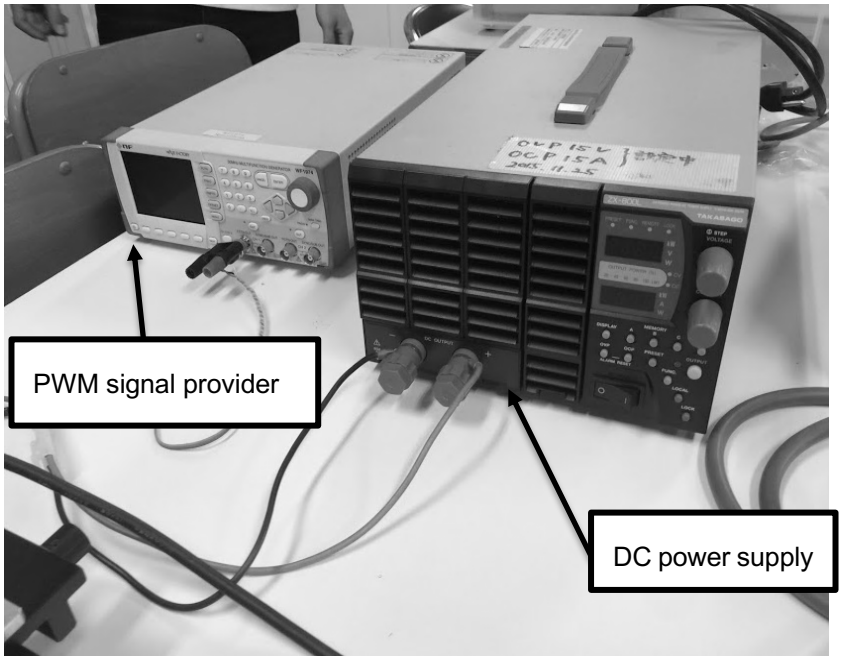

Figure 2-12: PWM signal provider and DC power supply source

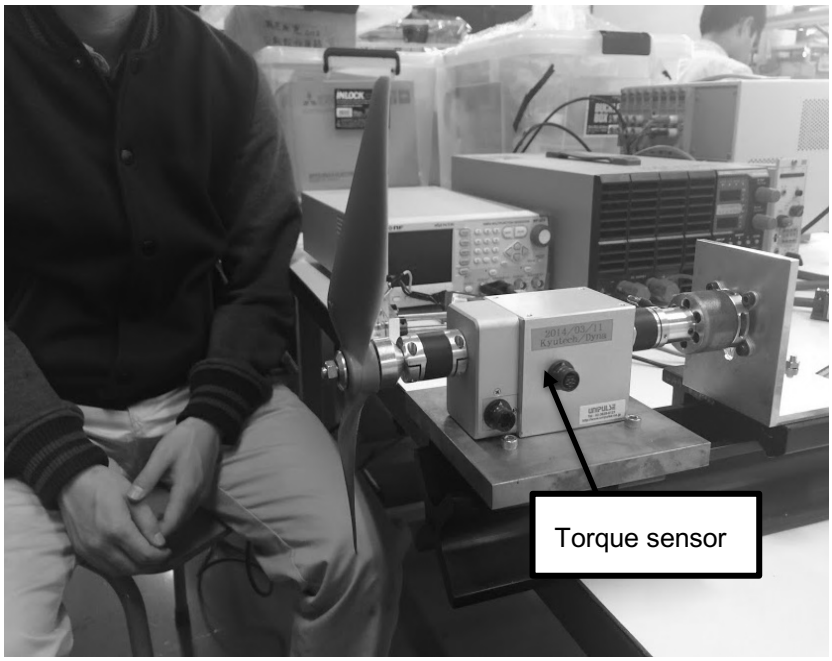

Figure 2-13> A UM Ii torque sensor

Figure 2-14: A UM II torque reading display

2.5 Test of A COT Propeller

An APC 9 x 6” commercial of the shelf propeller was tested as described in experiment test setup section of this paper. The measured thrust was corrected by adjusting drag to account for the propeller mount fixtures. The correction method applied was developed at University of Illinois Urbana Champaign (UIUC) [11] and it resulted in a slightly higher value for the measured Figure 2-16 shows comparison of experiment data obtained from Kyushu Institute of technology with similar data from University of Illinois Urbana Champaign. The results are in good agreement and all point lie within the 95% confidence interval. The acceptable agreements emphasized the and validated the Kyushu Institute of technology wind tunnel experiment set up including the sliding force measurement test stand used in the measurement of thrust.

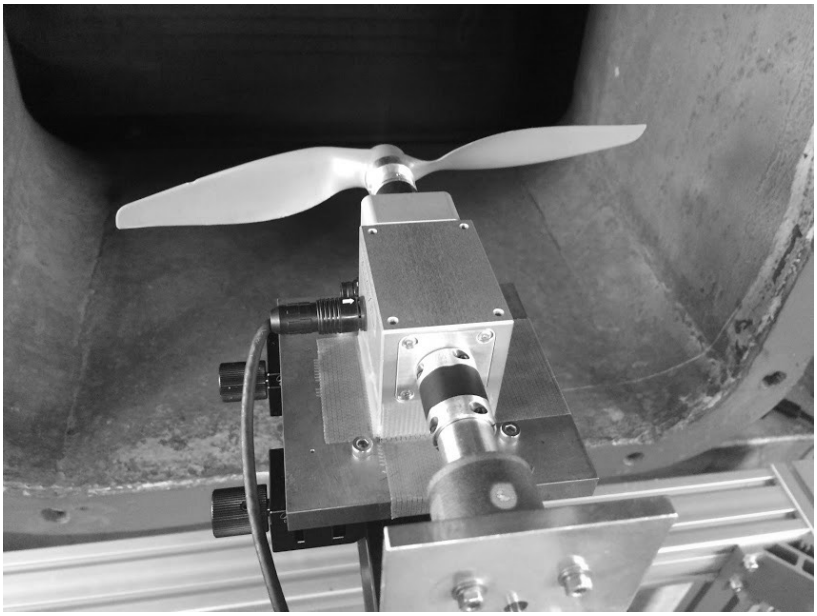

Figure 2-15: APC 9 X 6" Propeller in wind tunnel open test section (torque test configuration)

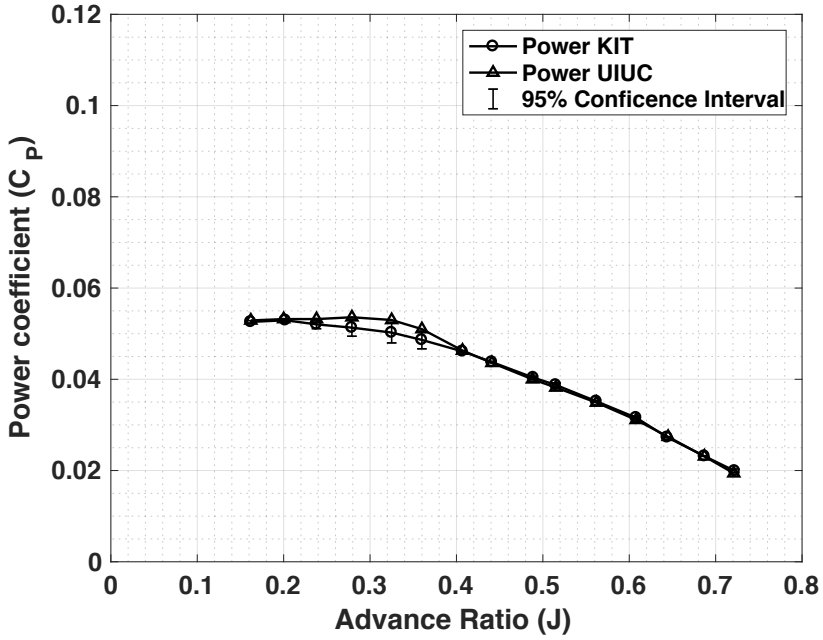

Figure 2-16: Power vs advance ratio experiment data from KIT and UIUC including 95% confidence interval

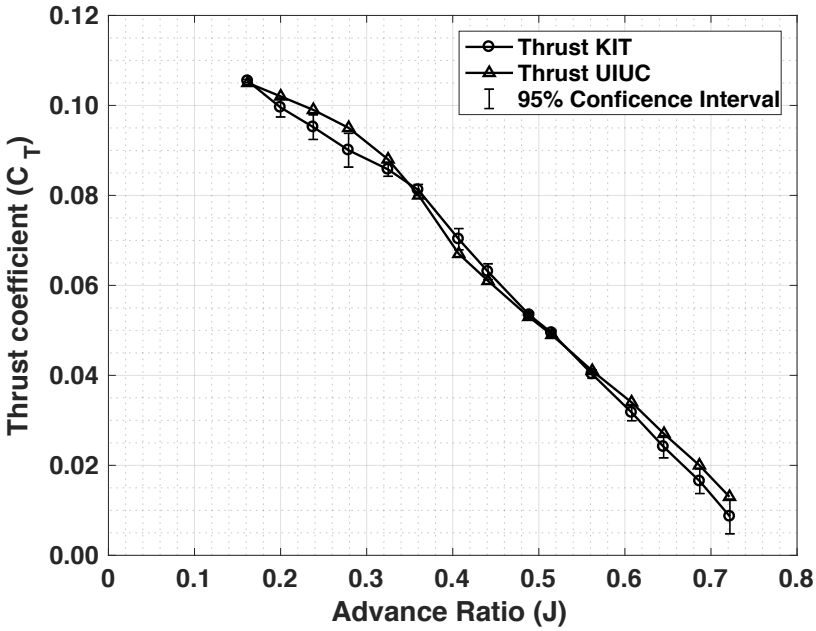

Figure 2-17: Thrust vs advance ratio experiment data from KIT and UIUC including 95% confidence interval

CHAPTER THREE

3 BLADE SHAPE ITERATION (SDL60M)

This chapter describes work undertaken in validating vortex theory in the design of a 2-bladed heavily loaded propeller with a solidity of ≈0.25 and chord based Reynolds number of ≈60k (calculated at 75% radius) at design point. The design was based on minimum induced propeller losses and lifting line theory. 2D-airfoil experiment data of SD7037 collected at Reynolds number of 60k was used for the entire blade design. At design advance ratio, more than 50% of the entire blade radius operated between 40k – 60k Reynolds numbers. A design goal of the propeller was to minimize variation in Reynolds number from hub to tip radius. Amongst other factors, the design of a high-performance propeller requires the accurate knowledge of the 2D airfoil data to be used for the design. Poor or inaccurate 2D airfoil data results in poor propeller performance and discrepancy between vortex theory prediction and experiment data.

Iterating a blade in Xrotor requires 3 steps: provision of atmospheric condition in which the propeller is expected to operate, linearized 2D airfoil force data, and physical propeller parameters such as dimensions.

3.1 Design Atmospheric Data

The design atmospheric data of the propeller is presented in Table 3-1.

Table 3-1 Blade design atmospheric data

Atmospheric Parameter	Value
Density [kg/m^3]	1.21
Speed of Sound [m/s]	339
Dynamic Viscosity [Kg/m-s]	1.78*10^{-05}

3.2 Linearized 2D Airfoil Force Data

Xrotor requires linearized airfoil lift curve slope, $d(C_D)/d(C_L^2)$, and other specific airfoil data from which the linear behavior of the airfoil is fully established. SD7037 was selected for the design of the propeller and its detailed geometric parameters are found in Table 3-2 while its 2D shape is seen in Figure 3-1.

The lift curve slope inputted in to Xrotor for this purpose was derived from H. A Stokely's experiment lift coefficient points shown in Figure 3-2(a). The linearized lift characteristic of SD7037 that is shown in Figure 3-2(a) was modeled using the lift curve slope derived from experiment data. The relationship between drag and square of lift coefficient was derived the between points shown in Figure 3-2(b). Shown in Figure 3-2(a) is the airfoil lift curve slope from UIUC experiment and its linearized form as reconstructed in Xrotor from provided inputs. From this figure, it is clearly observed that at lift coefficient above 0.2, the linearized lift curve slope (Xrotor) slightly departs from experiment values.

Table 3-2: Geometric details of SD7037

Airfoil	Thickness [%]	Max. Thickness Pos. [%]	Max. Camber [%]	Max. Camber Pos. [%]
SD7037	9.20	28.30	3.02	40.42

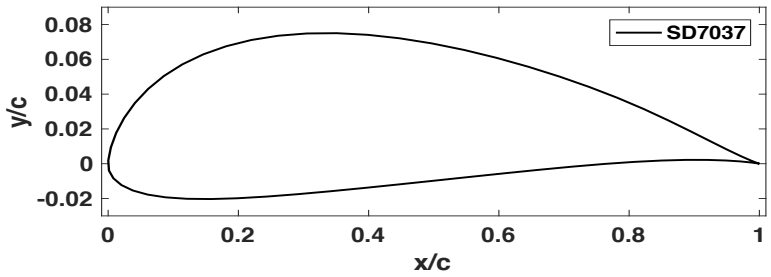

Figure 3-1: SD7037 profile shape

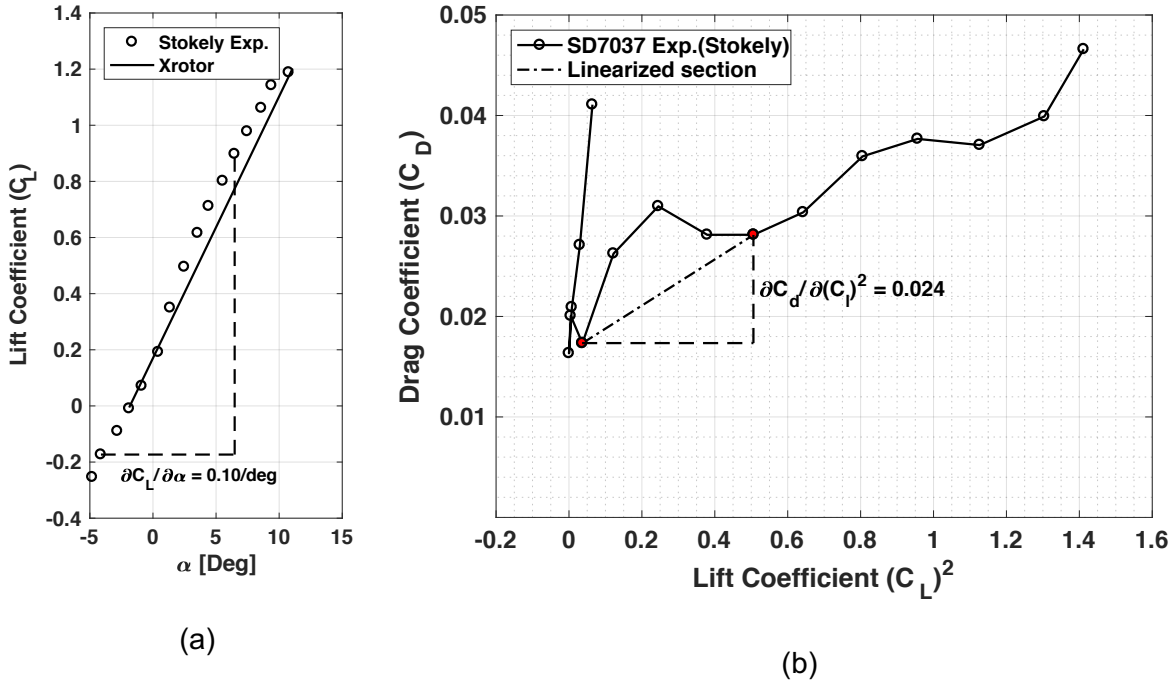

(a) (b)

Figure 3-2: 2D Airfoil aero data (Stokely) showing derivation points. Cl vs AoA (a) and Cd vs C_L^2 (b)

Figure 3-3 shows C_L vs C_D dependence on Reynolds number obtained using equation 3. Xrotor uses equations 39 to relate C_D, C_L and Reynolds number to fit curve the 2D lift and drag force coefficient obtained from experiments that is also shown in Figure 3-3. In design mode, Xrotor accepts design inputs used in the iteration of blade shape and prediction of blade performance. Predicted performance in design mode are always in perfect agreement with corresponding performance from operate mode.

$$C_D = \left| C_{D(0)} + {d(C_D)}/{d(C_L{}^2)} \left(C_{L(0)} - C_L\right)^2 \right| * \left({Re}/{Re_{ref}}\right)^f \quad (39)$$

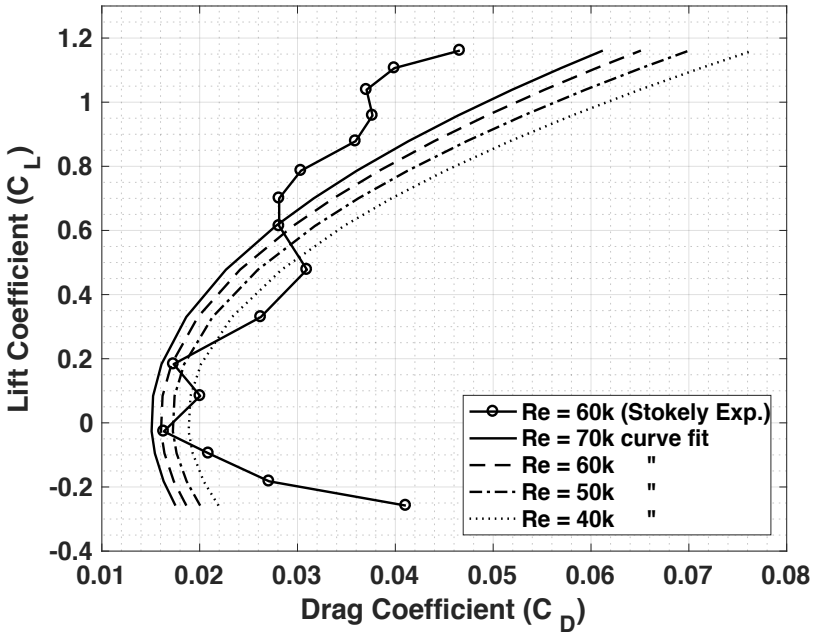

Figure 3-3: C_L vs C_D relationship with changing Reynolds number for SD7037.

3.3 Propeller Design Input Parameters

In design mode, the parameters found in Table 3-3 were used with Blade Element Momentum Theory (BEMT) implementation in Xrotor to iterate the blade pitch and chord.

Table 3-3: Blade design input parameters/requirement

Blade parameters	Value
Number of blades	2
Tip radius [m]	0.0875
Airspeed [m/s]	8.00
Angular speed [RPM]	3300
Constant C_L design	0.3
Lift curve slope [/deg]	0.1
Solidity	0.24
Chord Re @ 75% Radius	60,000

Figure 3-4 shows the blade twist and c/R both as a function of station radius r/R and Figure 3-5 shows the cumulative thrust and Reynolds number as a function of blade station radius. From Figure 3-5, it is seen that the region of the blade radius between 0.32 and 0.88 operates within Reynolds number range of 42k and 58k and produces about 70% of the total propeller thrust. It was desired to have a minimum variation in Reynolds number from the hub to the tip of the propeller. The blade loading of the propeller at design point is 17.43N/m^2.

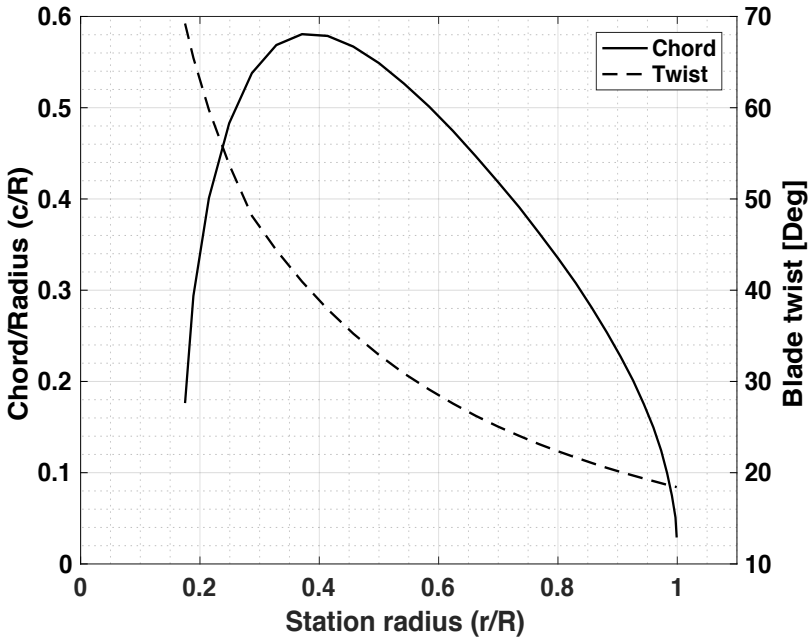

Figure 3-4: Iterated propeller geometry – c/R and twist

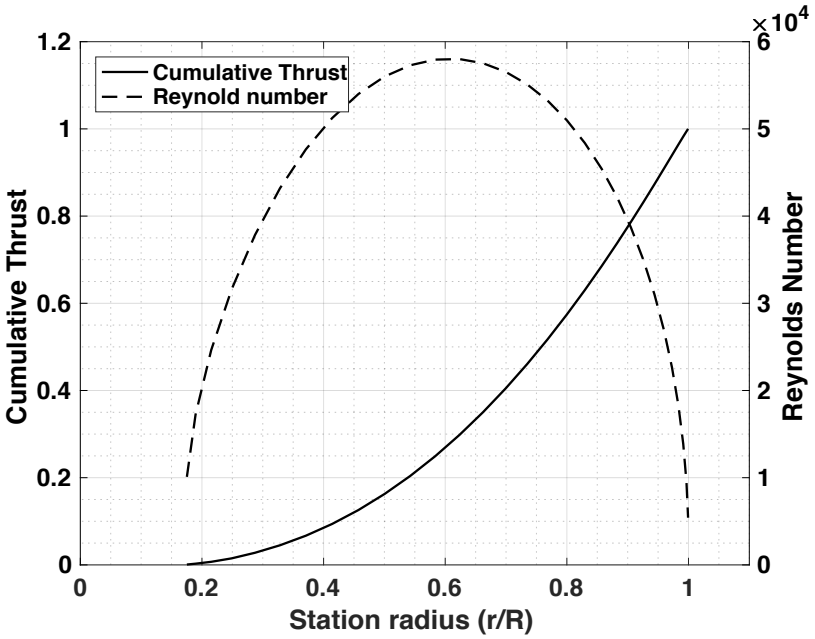

Figure 3-5: Cumulative thrust and Re distribution along blade radius

3.4 Propeller Fabrication

The propeller was 3D printed using formlab stereolithography (SLA) printer. Formlab SLA printer is capable of delivering a resolution between 25 – 100 micron in the Z-axis and 2.8 microns resolution in X-Y axis. The printed propeller was not only smooth and required less effort to finish, but also the printer's resolution allowed for a finite trailing edge thickness of 0.05mm without compromising strength. Figure 3-6 shows the propeller on its printing support structure after it has fully cured and hand finished. The finished propeller was designated SDL60M and it weighed 23g.

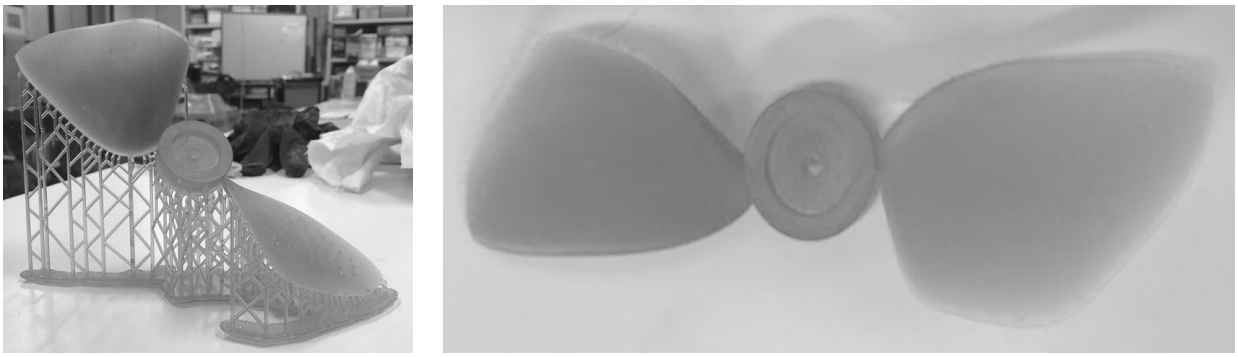

Figure 3-6: 3D printed propeller

3.5 Test Results

3.5.1 Constant Angular Velocity Experiments & Analysis

The wind tunnel experiment was set up as described in the experiment test set up section of this paper. SDL60M was first tested at constant angular velocity of 2300, 3300 and 4300 rpm.

Figure 3-7: Propeller on Wind tunnel test stand (Thrust test configuration)

Figure 3-7 captures the experiment set up in the open test section of the wind tunnel. For each of the RPM tested, 2300, 3300, and 4300, the advance ratio swept range was from 0.3 to 1.3. The constant angular velocity test method allowed a greater range of RPM sweep, thus, the propeller performance was assessed from a lower and much wider advance ratio range.

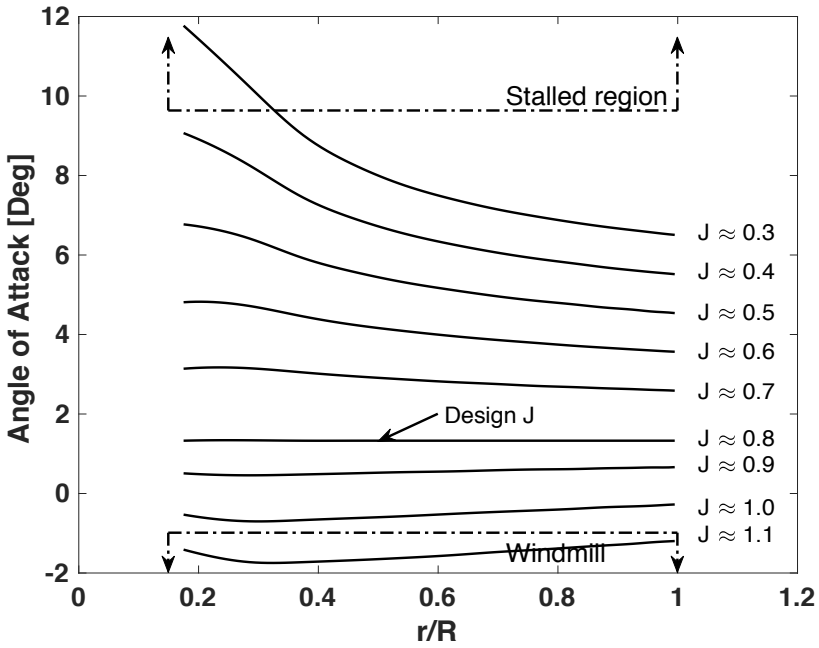

Figure 3-8: AoA vs station radius at constant angular velocity of 3300RPM.

The propeller was tested through the advance ratio range shown in Figure 3-8. At each of the advance ratios, Xrotor was used to estimate the angle of attack distribution along the blade radius. This was performed for the constant 3300RPM test case only. The radial angle of attack distribution at design point is a constant 1.3degrees. However, as advance ratio either increases or decreases, the distribution of angle of attack also increases or decreases.

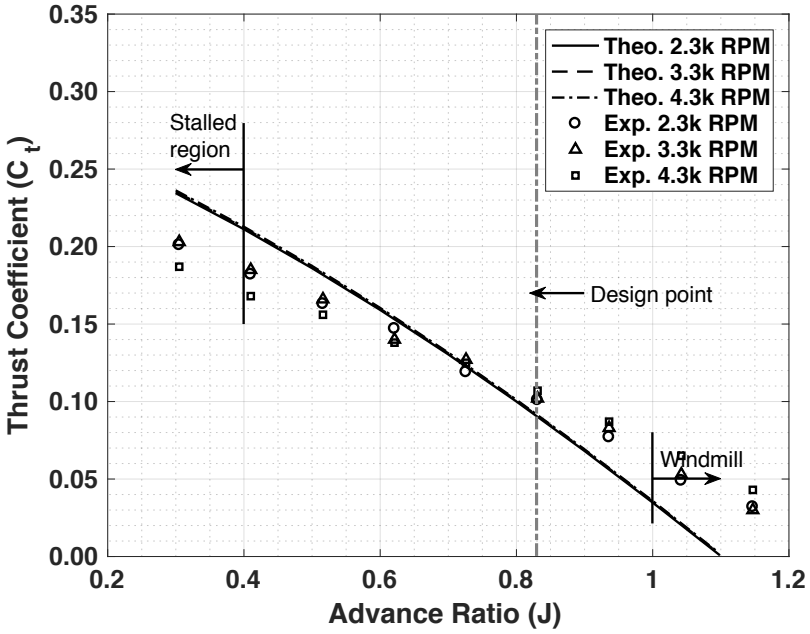

Figure 3-9: Constant angular velocity plots - C_T

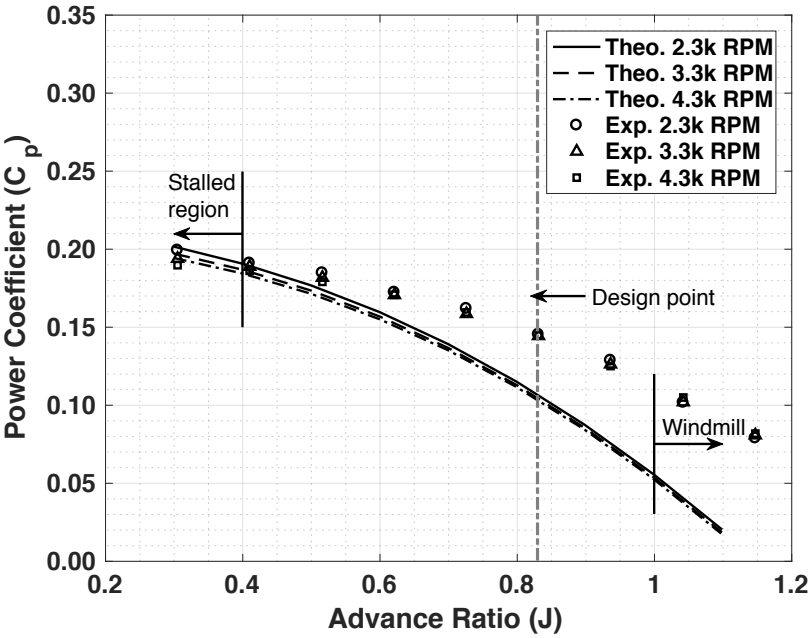

Figure 3-10: Constant angular velocity plots - C_P

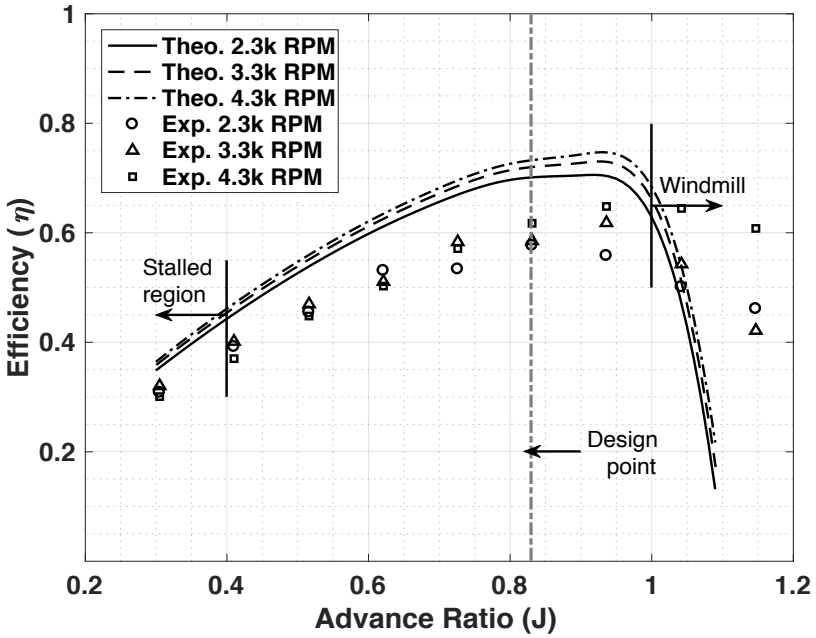

Figure 3-11: Constant angular velocity plots - Efficiency

The thrust coefficient experiment data shown in Figure 3-9 is in good agreement with theory at advance ratios near the design point but begins to depart at lower advance ratio as propeller approaches stall, which occurs around J = 0.45. However, from Figure 3-10 significant power divergence between experiment and theory is observed. As expected, the power divergence resulted in low blade efficiency than designed as seen in Figure 3-11. At design point, BEMT efficiency prediction is 70% while 58% efficiency was obtained from experiment. An overall maximum efficiency of 65% was recorded from SDL60M wind tunnel tests carried out at constant 4300RPM shown in Figure 3-11.

3.5.2 Constant Airflow Velocity Experiment

Constant angular velocity propeller wind tunnel tests were followed by a constant airflow velocity test.

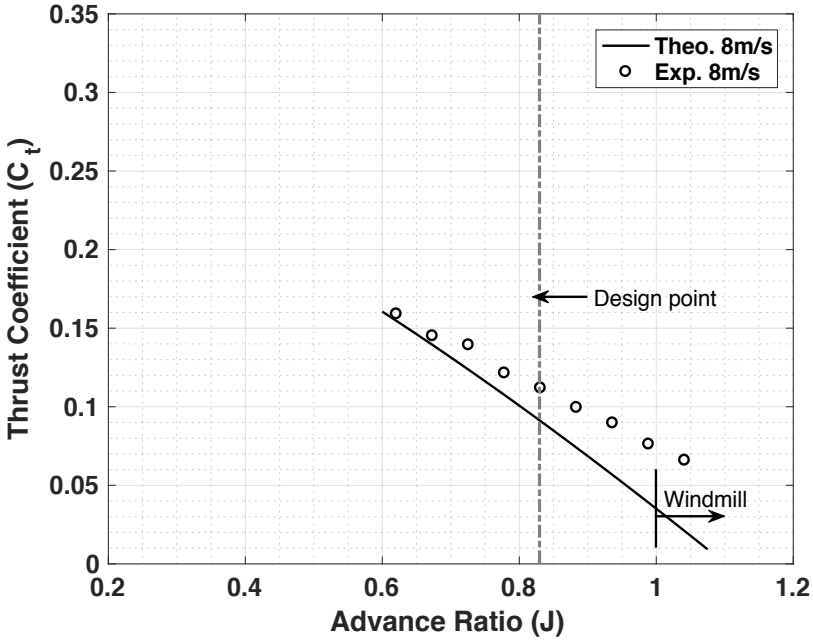

Figure 3-12: Constant 8m/s constant Velocity plots: C_T

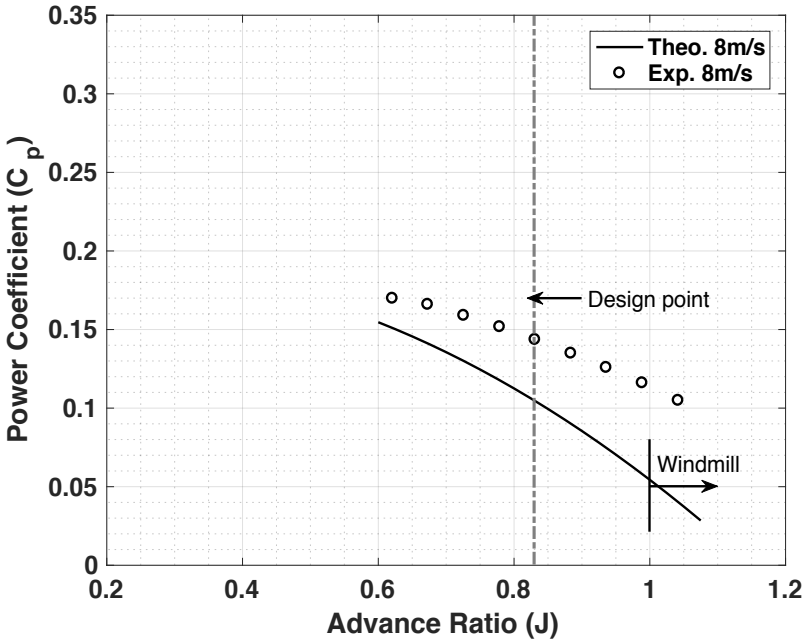

Figure 3-13: Constant 8m/s constant Velocity plots: C_P

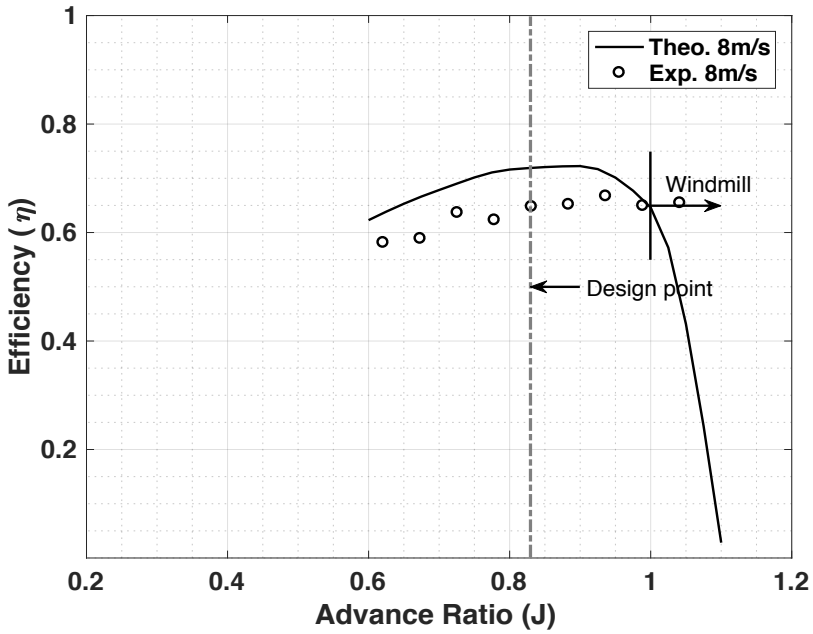

Figure 3-14: Constant 8m/s constant Velocity plots - Efficiency

This additional wind tunnel test was performed by maintaining a constant airflow velocity of 8m/s over the propeller while varying the angular velocity of the propeller to achieve the range of advance ratio sweep shown in Figure 3-12. The experiment value of C_T in Figure 3-12 is about 30% higher than theory prediction of C_T at design point. Further, the power coefficient recorded from experiment shown in Figure 3-13 is 1.4 times higher than corresponding BEMT predictions. Efficiency plot of SDL60M in Figure 3-14 shows that a peak efficiency of 67% was reached from experiment at advance ratio of 0.93, and 65% at design advance ratio of 0.83. BEMT efficiency prediction at design point was 70%.

Although the difference between the maximum efficiency obtained from the BEMT code prediction and experiment is 5% for both test cases, the difference in power is considerable for both cases. The thrust coefficient plot in Figure 3-12 also shows significant difference between BEMT code and experiment at design point. Three (3) potential reasons for design point performance discrepancy were investigated: assumption of perpendicularity of the propeller induced velocity, effect of Reynolds number, and inaccuracy of 2D aerodynamic force coefficient used for the propeller design.

3.5.3 Effect Of Inflow Angle Calculation Assumptions On Performance

The inflow angle (ϕ), defined in equation 40 and 41, is the sum of the advance ratio divided by pi (ϕ_J) plus angle introduced by the induced velocities (ϕ_i). The inflow distribution angle of ϕ_J and ϕ_I for SDL60M at design advance ratio is shown in Figure 3-15. This figure also show the plots of ϕ_J + 10 to ϕ_J – 5 decreased in steps of 5 degrees to investigate the impact of overestimated or underestimated induced velocities on propeller performance. Beside the region below r/R 0.28, having a ϕ_I > 5degrees because of thick airfoil used in this region, other regions of the blade have a ϕ_i < 5degrees. Increasing and decreasing the maximum value of ϕ_i by 200% is equal to ϕ_J + 10 and ϕ_J – 10 respectively. However, from Figure 3-16 (a & b), it is seen that increasing ϕ_i by 10 degrees at all blade section radius results in a thrust coefficient that is below and power coefficient that is above experiment values. Decreasing ϕ_i will have the opposite effect. By using high and unlikely value for ϕ_i, the assumption of perpendicularity of induced velocities is eliminated as a major contributor to the huge discrepancy observed in the measured performance data of SDL60M.

$$cos\phi = \frac{\Omega r - v_t}{\sqrt[2]{(\Omega r - v_t)^2 + (V + v_a)^2}} \tag{40}$$

$$sin\phi = \frac{V + v_a}{\sqrt[2]{(\Omega r - v_t)^2 + (V + v_a)^2}} \tag{41}$$

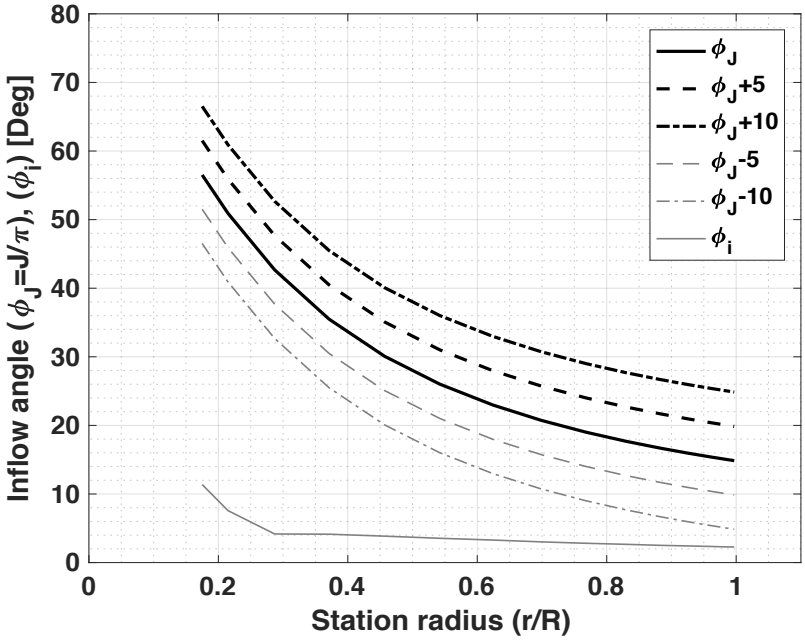

Figure 3-15: Inflow angle (ϕ_J=J/π) Vs blade station radius r/R

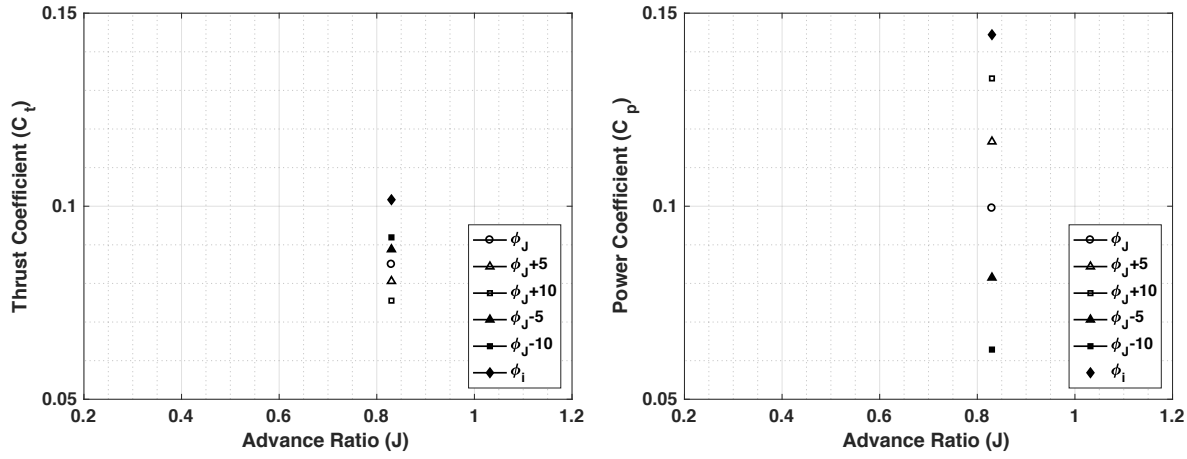

(a) (b)

Figure 3-16: CT Vs J (left) CP Vs J (right)

3.5.4 Effect Of Reynolds Number And Aerodynamic Force Data On Performance

The lift curve slope used in the iteration of SDL60M in the BEMT code was derived from a wide angle of attack range shown in Figure 3-2(a). This range is representative of a wide propeller operation regime, however, it does not accurately represent specific local lift coefficient at corresponding angle of attacks. To investigate the effect of a narrower and more representative local lift curve slope around the design point, a new lift curve slope was derived from the nearest two points around the design lift coefficient. The resulting lift curve was found to be much higher than the lift curve slope used in the iteration of SDL60M. Figure 3-17(a) shows the exact points from which a more representative local lift curve slope was derived. C_L points from which the lift curve slope was derived was also used in deriving $d(C_D)/d(C_L^2)$, which in turn was to establish the linear relationship between C_L and C_D shown in Figure 3-17(b). At C_L = 0.3, good agreement between C_L and C_D is observed in Figure 3-17(a & b).

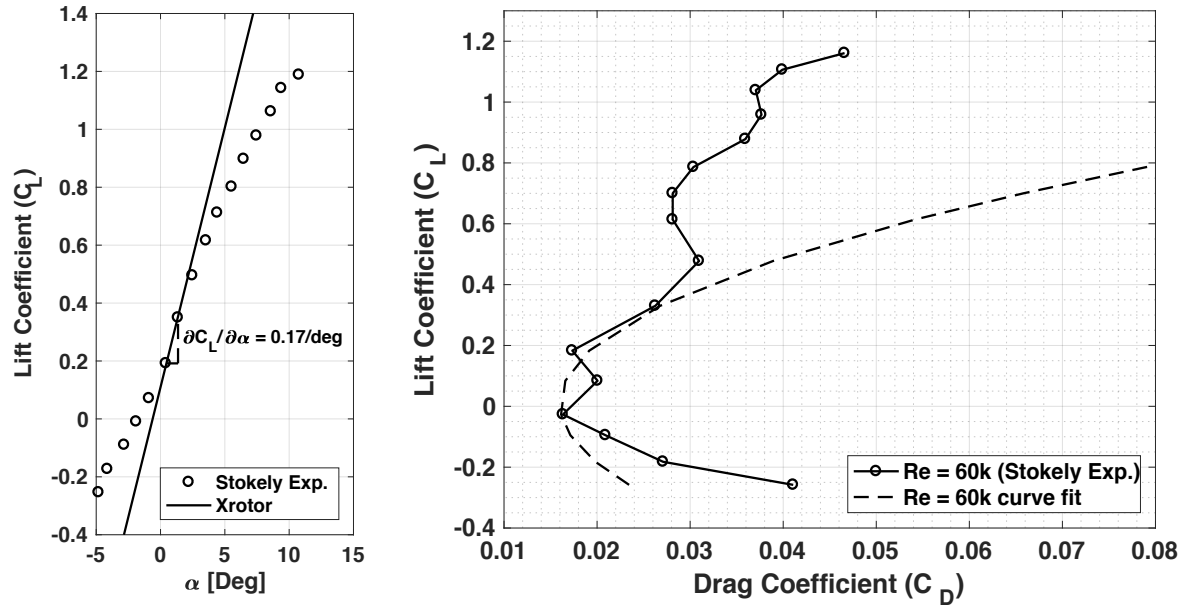

(a) (b)

Figure 3-17: Recomputed lift curve slope (a) and linear relationship between C_L and C_D (b)

The re-computed lift curve slope in Figure 3-17 and $d(C_D)/d(C_L^2)$ were inputted to Xrotor, and used in the performance analysis of the previously iterated blade shape (SDL60M) shown in Figure 3-4. The blade shape performance analysis was performed in operation mode in Xrotor. Re-analysing the shape of the previously printed SDL60M with the new linear airfoil force coefficients was chosen as an alternative to fabricating an entirely new propeller design.

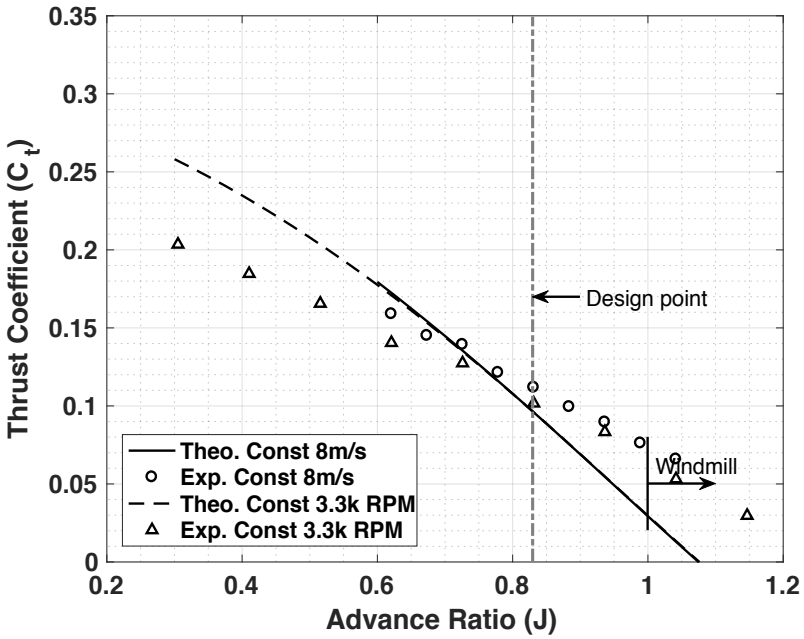

Figure 3-18: C_t vs J for $\delta C_L/\delta\alpha$ = 0.17

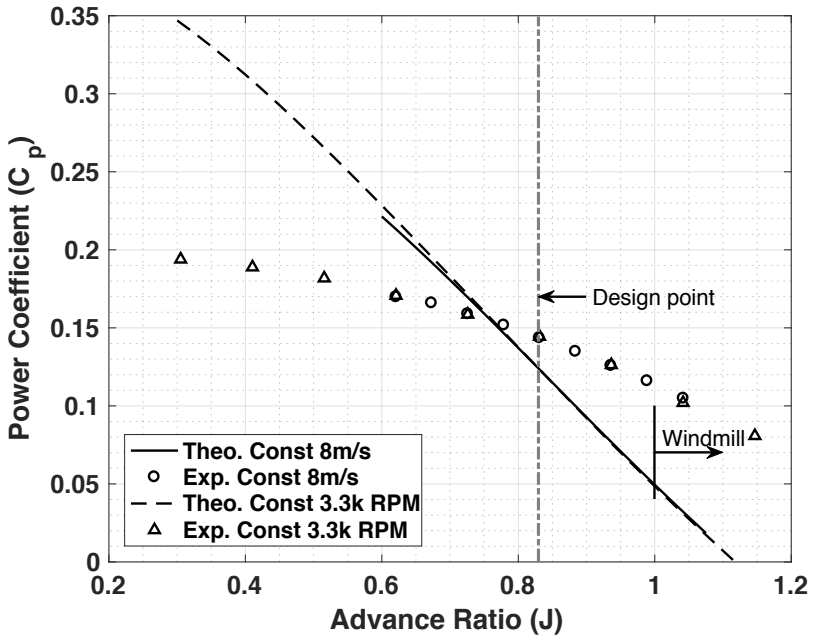

Figure 3-19: C_p vs J for $\delta C_L/\delta\alpha$ = 0.17

Figure 3-18 and Figure 3-19 shows the C_T and C_P plots of the blade analyzed at constant linear velocity and constant angular velocity. For the purpose of comparison, the experiment C_T and C_P shown in Figure 3-18 and Figure 3-19 were re-presented from Figure 3-9 and Figure 3-12. From Figure 3-18 and Figure 3-19, it is observed that BEMT predictions show a significantly improved C_T and C_P agreement at design point. However, at advance ratios other than design, theory C_T and C_P begin to depart from experiment.

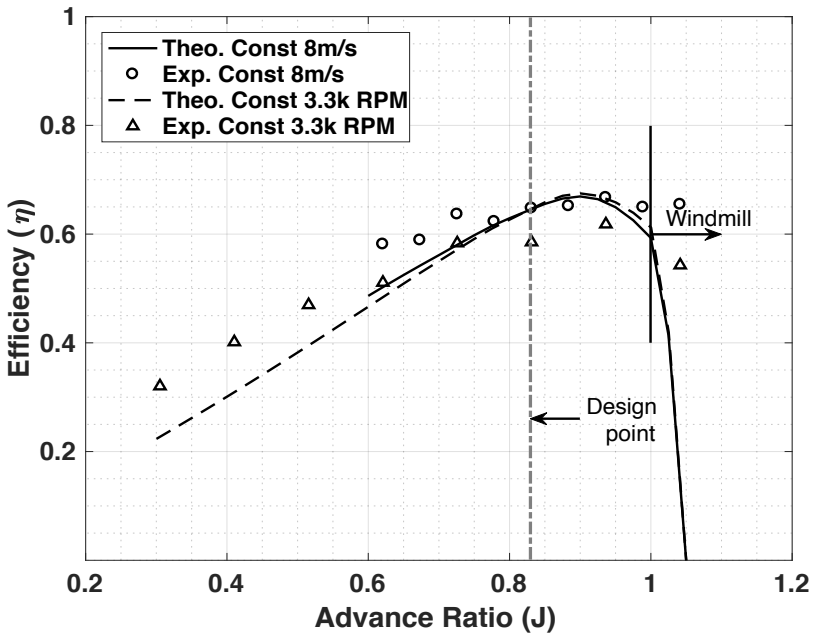

Figure 3-20: η vs J (a) and Reynolds number vs J (b) for $\delta C_L/\delta\alpha = 0.17$

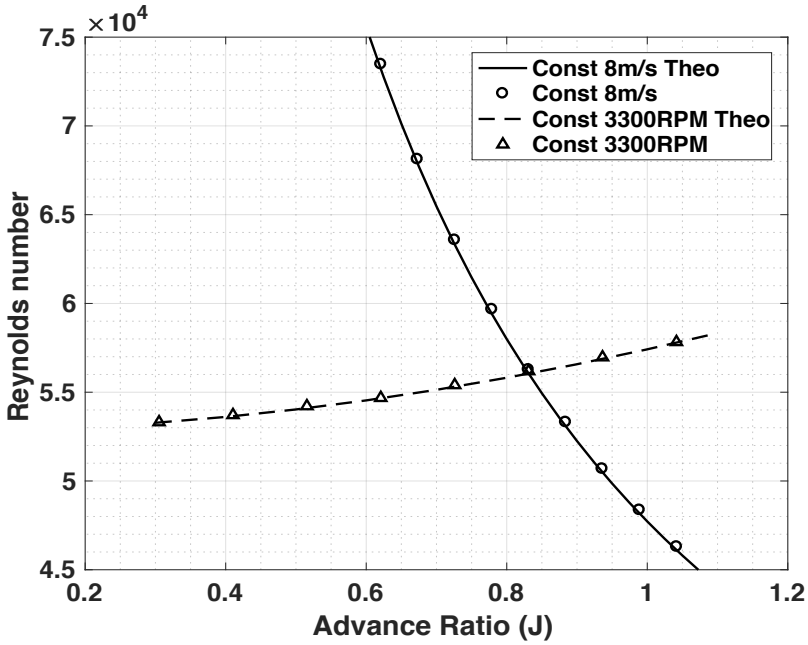

Figure 3-21: Reynolds number vs J for $\delta C_L/\delta\alpha = 0.17$

3.5.5 Reynolds Number Effects

Figure 3-20 shows efficiency as a function of advance ratio and Figure 3-21 shows the Reynolds number profile of the constant airflow velocity and constant angular velocity experiments. Reynolds number analysis is explored in two ways: The effect of variation between the theoretical and experimental values of propeller was extracted from Figure 3-20 and Figure 3-21 by comparing the effect of Reynolds number data obtained from two different experiment methods – blade performance dependence on Reynolds number variation.

As observed in Figure 3-21, there is good agreement between theory and experiment reynolds number values of SDL60M. However, in Figure 3-20, plots of efficiency shows discrepancy between corresponding pairs of theory and experiment data.

The efficiency plots of experiment data obtained from both test methods at same advance ratio shows slight difference due to variation in the respective operation Reynolds numbers, which was minimized from design by ensuring minimum variation from propeller hub to tip radius. The 75% station Reynolds number plots of the propeller as a function of advance ratio shows a range of about 20k between the constant airflow velocity and angular velocity operation cases at advance ratio of 0.61. Hence, it can be inferred that the dependence of propeller performance on Reynolds number is small and not the major contributor to the performance discrepancy between theory and experiment. McCormick (8) asserts that for propellers, dependence of lift curve slope and drag/lift ratio on Reynolds number is small and can be considered negligible.

3.5.6 Aerodynamic Force Data Effects

The region of the blade from 60% station radius outbound to the blade tip generates more than 75% of the total propeller thrust. Moving from inbound of the propeller radius to outbound regions, the local flow angle ϕ of the blade reduces, hence $\cos(\phi)$ in equations 40 dominates $\sin(\phi)$ in equation 42. Since C_L and C_D were the only changed parameters, a theoretical re-analysis and re-evaluation of the performance of SDL60M blade shape carried out under this condition.

In re-analysing the blade shape, the linearized values of C_L and C_D relative to corresponding experiment values applied to equation 23 and 24 could have four effects on the overall predicted thrust delivered and power absorbed by the propeller:

1. If the linearly obtained value of C_L is lower than the experiment values while the linear and experiment values of C_D agree, the estimated propeller thrust and power would be lower than experiment values.
2. If the linearly obtained value of C_L is higher than the experiment values while the linear and experiment values of C_D agree, the estimated thrust and power would be higher than experiment values.
3. If a lower than experiment value of C_D is used in the re-analysis of the blade while the linear and experiment values of C_L agree, the estimated thrust would be higher and power lower than experiment.
4. Lastly, if a higher than experiment value of C_D is used to re-analyze a blade shape while the linear and experiment values of C_L agree, the estimated thrust would be lower and power higher than experiment.

The analysis above assumes that 2D airfoil experiment data are accurate. SDL60M was iterated using a lift curve slope of 0.10/deg and from Figure 3-8, the design C_L of 0.3 corresponds to angle of attack of 1.3deg.

Table 3-4: SD7037 airfoil experiment data & its linearized form (a0 = 0.10/deg) @ Re = 60k

	$C_{L(@a0=0.10)}$	$C_{L(E)}$	$C_{D(@CL=0.3)}$	$C_{D(E)}$
@ AoA = 1.3deg	0.30	0.34	0.020	0.026

Table 3-4 captures the linearized and experiment values of lift and drag coefficient of SD7037 at angle of attack of 1.3deg, taken from Figure 3-2(a) and Figure 3-3(a). From Table 3-4, it is seen that while the linearized lift coefficient, $C_{L(@a0=0.10)}$, used in the iteration of the blade is equal to 0.3, the corresponding experiment value, $C_{L(E)}$, is 11% higher. Consequently, where

the linearized C_L is 0.3, the corresponding linear $C_{D(@CL=0.3)}$ is 0.02, which is 20% less than experiment value of $C_{D(E)}$ compared at same C_L. The combined effect of lower linearized forms of aerodynamic data used for the iteration of SDL60M resulted in lower-than-experiment values of C_T and C_P as seen in Figure 3-9, Figure 3-10, Figure 3-12, and Figure 3-13 at design point.

Table 3-5: SD7037 airfoil experiment data & its linearized form (a0 = 0.17/deg) @ Re = 60k

	$C_{L(@a0=0.17)}$	$C_{L(E)}$	$C_{D(@CL=0.5)}$	$C_{D(E)}$
@ AoA = 1.3deg	0.30	0.30	0.025	0.026

Again, the linearized and experiment aerodynamic data in Table 3-5 were extracted from Figure 3-17 and Figure 3-3. In this case, the experiment and re-computed linear estimates for C_L and C_D are in excellent agreement as shown in Table 3-5. Despite the agreement between experiment and linear estimates of the force coefficients, discrepancies in performance especially in power are observed in Figure 3-18 and Figure 3-19.

Thompson (9), Michaelis (9), and Bregman (10) all performed experiments on SD7037 at Reynolds number of 60k. The results of their experiments are shown in Figure 3-22. From this figure, it is observed that while the lift curve slope of all experiments have similar profiles, the drag profiles show considerable variation between each other. The lift curve slopes of all the experiments at higher angle of attack (>12 deg not shown here) reveal the presence of Aerodynamic hysteresis, indicating the presence of laminar separation bubble. Selig (11) suggests that laminar bubble is responsible for the drastic increase in airfoil drag coefficient mostly occurring about mid lift region. For propellers that operate in low Reynolds flight regime, it is almost certain that within its operational envelope some region of the propeller would contain laminar separation bubble. The presence of laminar separation bubble, which is observed around mid-lift region of Figure 3-22(b), may act to degrade the overall propeller performance.

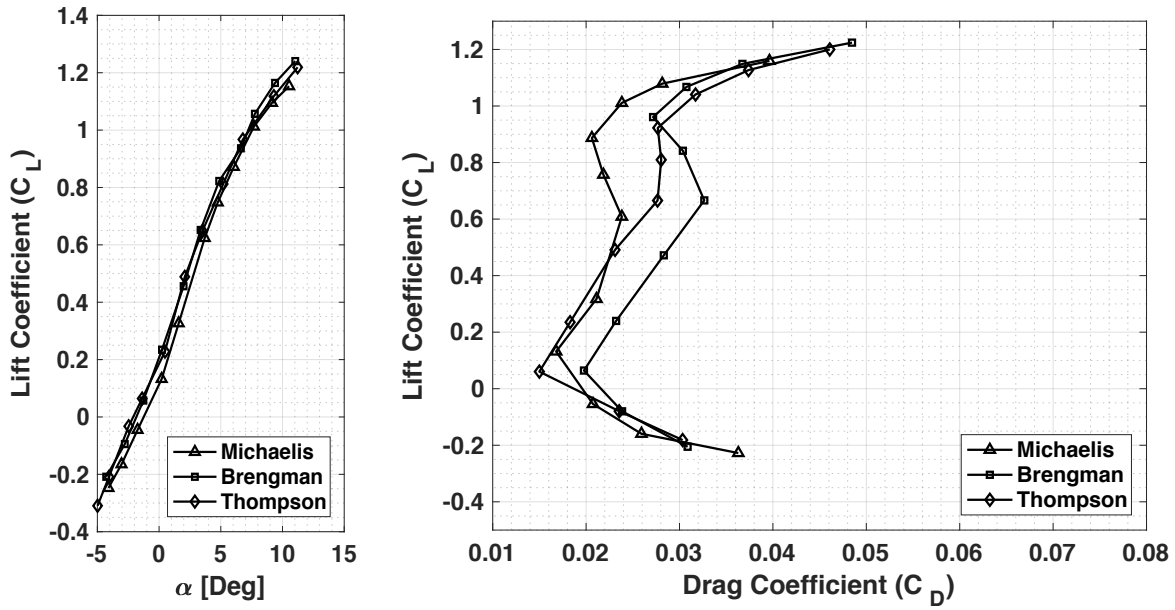

(a) (b)

Figure 3-22: C_L Vs α (a) and C_L Vs C_D (b) for SD7037 at Re=60k

The local C_L and C_D of the blade shown in Table 3-5 at design point are equal to their respective linearized values. Given the sensitivity of overall propeller performance to C_L and C_D, it can be concluded that accurate 2D force coefficients are necessary for accurate prediction of propeller thrust and power. Figure 3-22 (a & b) clearly indicates that inaccuracy in the measured airfoil aerodynamic forces are considerable especially in drag. Taken together, the 2D airfoil aerodynamic measurement inaccuracies, which is due to non-linearity associated with low Reynolds number flows, is a major contributor to the propeller performance discrepancy recorded at these low Reynolds numbers.

CHAPTER FOUR

4 LOW REYNOLDS NUMBER DESIGNS

4.1 Blade Shape Iteration (SDL20M)

SD7037 was selected for the design of the propeller and its detailed geometric parameters are found in Table 3-2 while its 2D shape is seen in Figure 3-1. The lift slope and CL-CD predictions for SD7037 at Reynolds number of 20k was obtained using Xflr-5 and is shown in Figure 4-1.

The blade design used a single airfoil (SD7037) for the entire blade span. For the purpose of this study, the Lift-angle of attack relationship from Xfoil was linearized using equation 42 while the function given in equation 39 was applied to estimate the drag associated to lift.

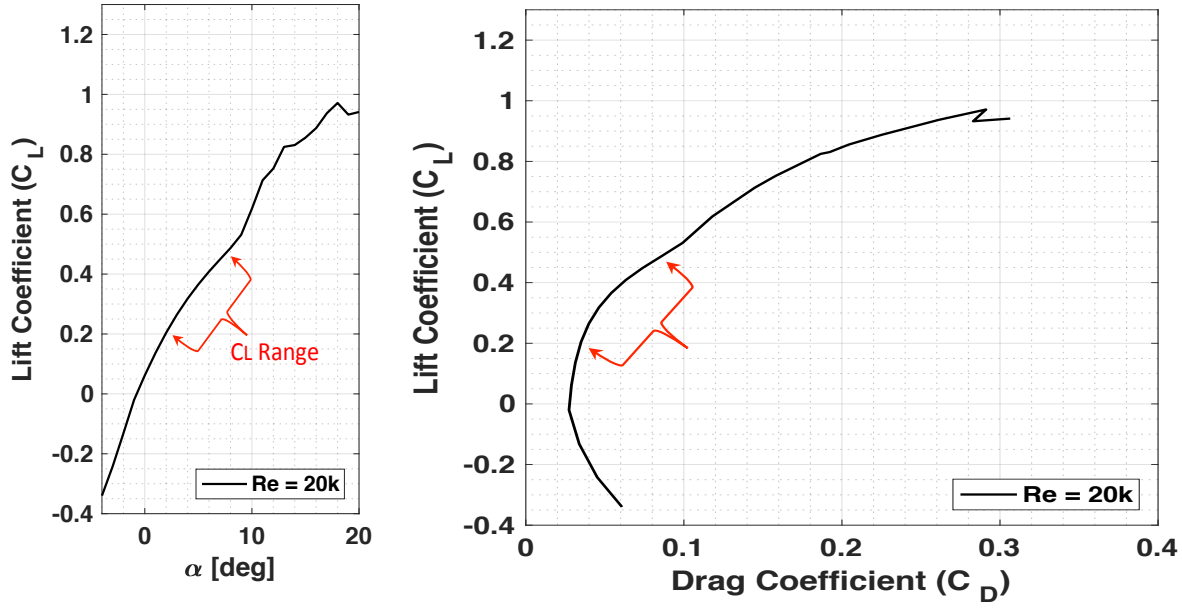

Figure 4-1: SD7037 2D airfoil characteristics data (Mach No=1, Ncrit = 9 and Re = 20k)

The unavailability of 2D force data at these low Reynolds number led to the absolute reliance on predictions from Xflr-5. To ensure that the blade operated within the laminar regime around design point, the choice of design lift coefficient was constrained to operate between 0.2 and 0.5 as shown in Figure 4-1.

Table 4-1: Prepller design atmospheric condition

Atmospheric Parameter	Value
Density [kg/m^3]	1.21
Speed of Sound [m/s]	339
Dynamic Viscosity [Kg/m-s]	1.78*10^{-05}

Table 4-2: Propeller design parameters

Blade parameters	Value
Number of blades	2
Tip radius [m]	0.1
Airspeed [m/s]	8.0
Motor speed [RPM]	3000
Solidity	0.078

Table 4-1 captures the atmospheric condition the blade was design to operate, while Table 4-2 outlines the blade design parameters.

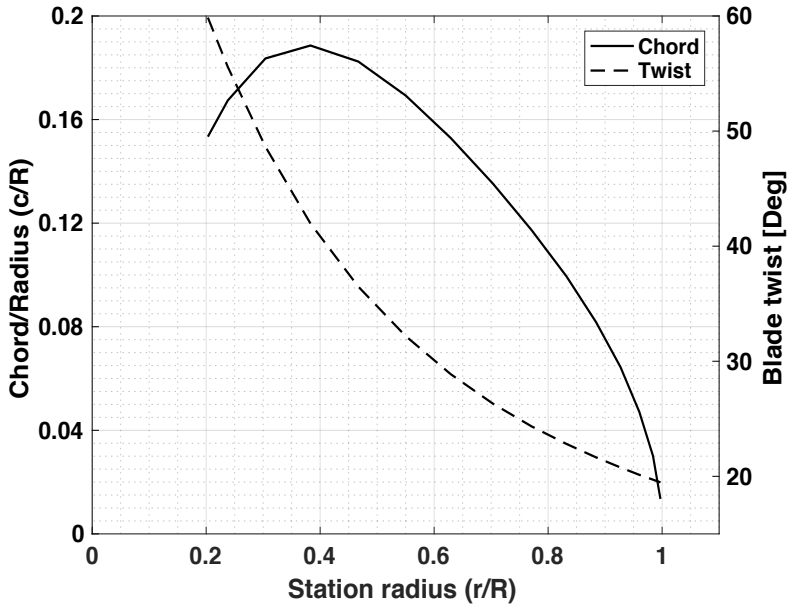

Figure 4-2: c/R, Twist Vs. station radius r/R

An unmodified 2D profile of SD7037 was used in the design of the entire propeller. Figure 4-2 shows the iterated blade shape – twist and chord along the blade radius from root to hub.

4.2 Fabrication And Test Set-Up

The propeller was fabricated using acrylonitrile butadiene styrene material in a Mutoh 2000 3D printer. The printed propeller was hand finished to improve surface smoothness. The post-finished propeller weighed 22g. Figure 4-3(a) and (b) shows the finished propeller while Figure 4-3(c) shows the propeller in wind tunnel test set-up configuration.

(a)

(b)

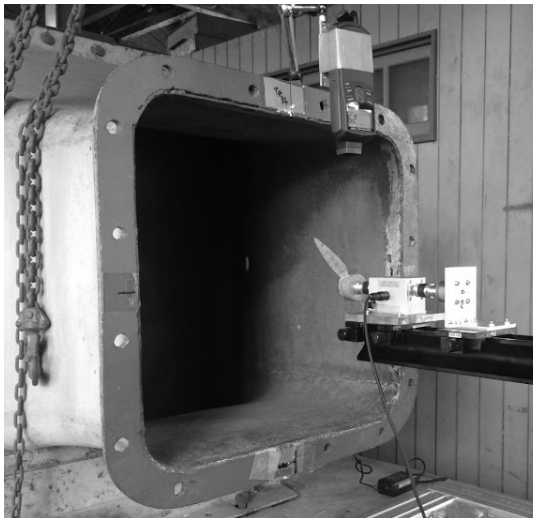

(c)

Figure 4-3: (a) front view of propeller, (b) Side view of propeller and (c) Propeller in test set-up

4.3 Wind Tunnel Test Result

The propeller test was carried out at Kyushu Institute of Technology wind tunnel facility. The propeller was spun at a constant 2000, 3000 and 4000 RPM and at each angular velocity, the wind velocity was adjusted so that the advance ratio ranged from 0.2 and 1.3.

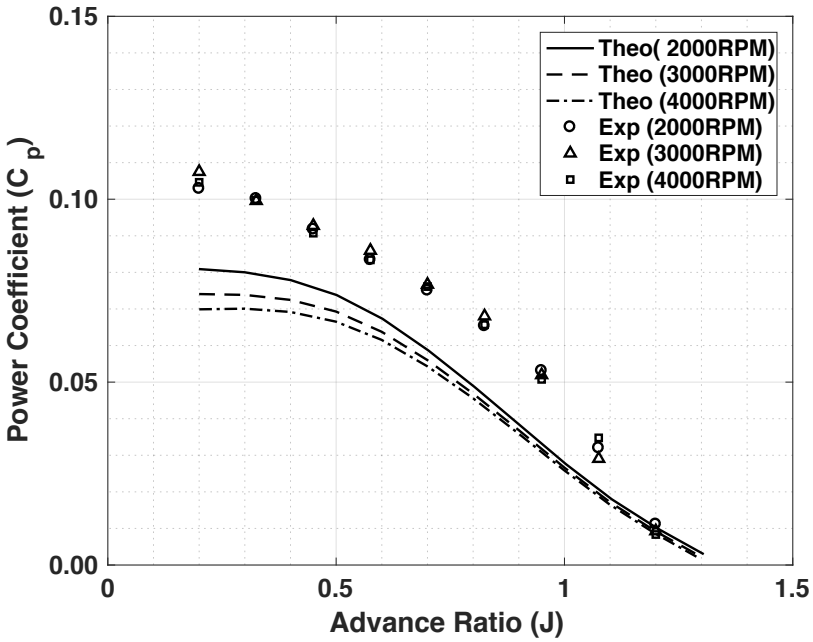

Figure 4-4: C_P Vs. J at constant angular speeds

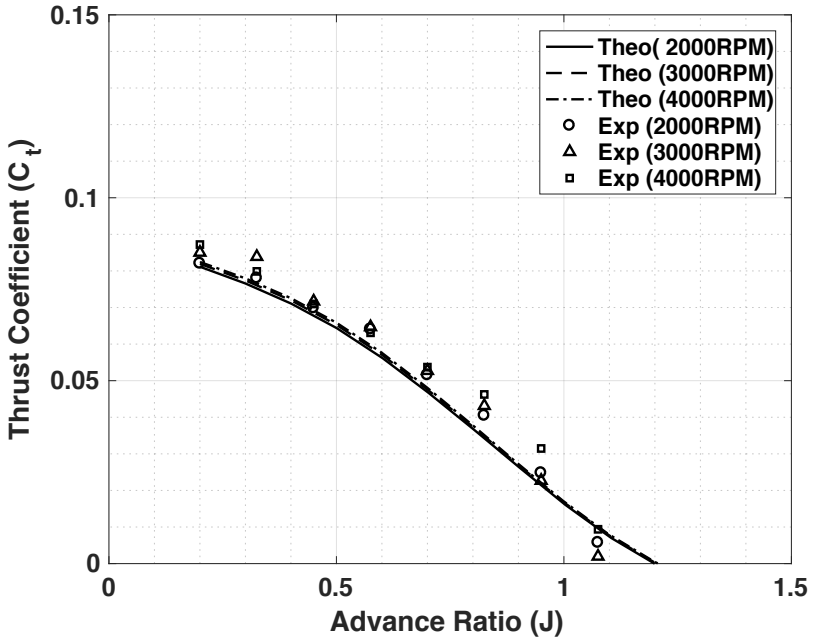

Figure 4-5: C_T Vs. J at constant angular speeds

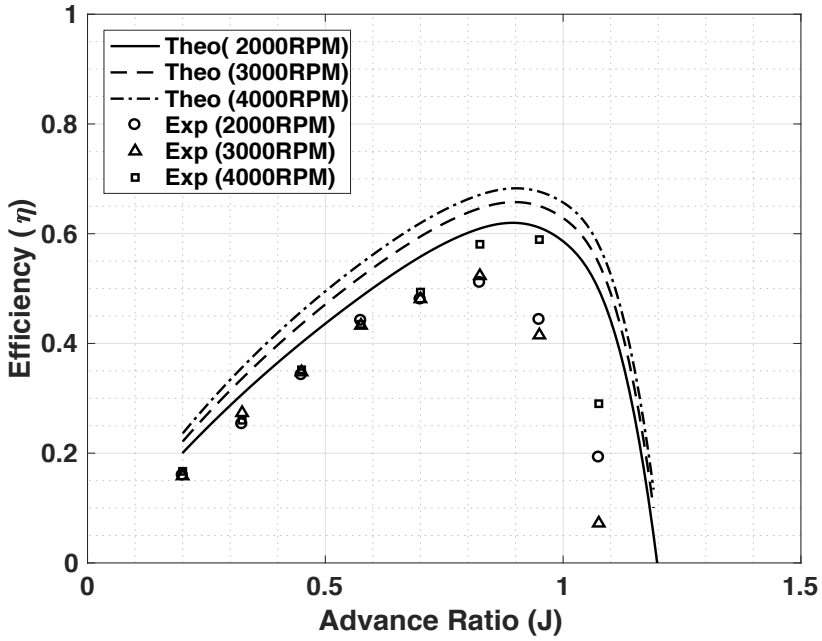

Figure 4-6: Efficiency Vs. J at constant angular speeds

Figure 4-4, Figure 4-5 and Figure 4-6 shows theoretical and experiment power coefficient, thrust coefficient and efficiency plots respectively. Assuming C_P α C_d and C_T α C_L, it can be concluded from Figure 4-4, Figure 4-5 and Figure 4-6 that airfoil drag and lift coefficients were under predicted in Xflr-5 and hence, theoretical C_P and C_T values were correspondingly lower. However, drag coefficient was much more under estimated than was lift coefficient. The experiment peak efficiency for 4000RPM test case is 0.87 of the theoretically predicted value. Beside the observed discrepancy between theoretical performance predictions and experiment in Figure 4-4, the theoretical peak efficiency prediction of 67% was considered low even though the Reynolds number was 30k. A directly driven propeller design for the Black Widow (Grasmeyer & Keennon, Development of the Black Widow Micro Air Vehicle, 2001) achieved efficiency of up to 78%.

CHAPTER FIVE

5 Semi-empirical Correction

METHODOLOGY

Matching wind tunnel experiment with theoretical propeller performance

The use of functions in estimating airfoil lift and drag performance makes Xrotor a good design tool in studying the relationship between airfoil force coefficients and overall propeller performance. Parameters in the lift and drag estimation functions in Xrotor can be individually manipulated and its relationship on the overall propeller performance can be investigated. The wind tunnel performance of of two blade designed designated as SDL60M and SDL20M were matched using Xrotor by manipulating the $C_{L(0)}$ and lift curve slope in equation 42 and the minimum drag and $d(C_D/d(C_L^2)$ in equation 39. Detailed plots of the match are shown in later sections of this work.

Using blade element momentum theory, a blade was designed and fabricated for wind tunnel test. The fabricated blade was designated as SDL20M.

$$C_l = \alpha \, {dC_l}/{d\alpha} + C_{l(0)} \tag{42}$$

Empirical function: Induction factor correction

Once the match between propeller performance test data and theoretical prediction was achieved, a backward iteration to recompute the induced velocities on the propeller plane commences. Firstly, the 2D airfoil data from Xflr-5 would be assumed to be sufficiently representative of 2D airfoil data that would have been accurately obtained from experiment where it possible. The 2D airfoil lift coefficient from xflr-5 is applied to replace parameters from equation 42 and 39 obtained by the manipulation until match is achieved, which was earlier described. Since the design parameters of the blade is expected to be known, including its angle of attack or C_L, blade pitch, airflow velocity, and angular speed, the challenge shifts to recomputing the magnitudes of axial and tangential components of induced velocities.

Empirical relationships between the velocities at propeller wake to velocities acting at the plane of the propeller would be developed by extending the relationship given in Larrabee's work (12).

Wind tunnel tests conducted on SDL60M and SDL20M to measure its performance showed that experiment data differs from theoretical predictions from BEMT. Figure 4-4, Figure 4-5, and Figure 4-6 captures the experiment and theoretical estimates from SDL20M. From these Figures, it is clearly seen that considerable discrepancy exists between experiment and theoretical predictions. The discrepancy may have been recorded for a number of reasons: 2D airfoil force coefficients used for the blade design and off performance analysis were approximated using functions captured in equations 42 and 39; or BEMT code fails to capture the entire flow physics at these low Reynolds number flight regimes. For the purpose of analysis and to investigate the latter reason above, let us assume that the measurements from SDL20M are within acceptable limits and further impose the performance data from experiment on the propeller plane as shown in Figure 5-1(left). Similarly, the velocities in action far aft in the propeller wake as depicted in Figure 5-1 (right) as observed by a stationary observer. it can be shown that axial and tangential components of the induced velocity at the plane and wake of the propeller is related by $w_a = 2v_a$ and $w_t = 2v_t$ as widely assumed in BEMT. Therefore, the problem reduces to quantifying the induced velocity for a propeller with known angle of attack and incident velocity distribution along its span. Using equations 44 and 45, the axial and tangential components of induced velocity at the plane of the propeller can be estimated since $\phi_j + \phi_l$ is equal to the twist of the propeller at station radius r/R.

The following sequence would be applied to match BEMT propeller performance estimate to wind tunnel experiment data:

1. The lift curve slope ($dC_L/d\alpha$), $C_{L(0)}$, $d(C_D)/d(C_L^2)$ and $C_{D(0)}$ in equations 42 and 39, would be manipulated in the BEMT code until a match with experiment data was achieved.
2. Since $\phi_j + \phi_l = \phi$ and ϕ is known, V_R and V_A are known, v_a and v_t would be calculated using the relationship shown in Figure 5-1 and equations 44 and 45.
3. The induced angle of attack ϕ_i is then calculated
4. To proceed, three assumptions are made:
    a. the 2D airfoil force coefficient from Xflr-5 is assumed to be representative of experiment data;

b. the pitch of the propeller is fixed;

c. and the angle of attack remains unchanged.

Following these assumptions, the performance of the airfoil force coefficient in item (1) above is used to obtain a match and then replaced with the performance of SD7037. A new induced angle of attack ϕ_i and thus corresponding, v_a and v_t would be estimated.

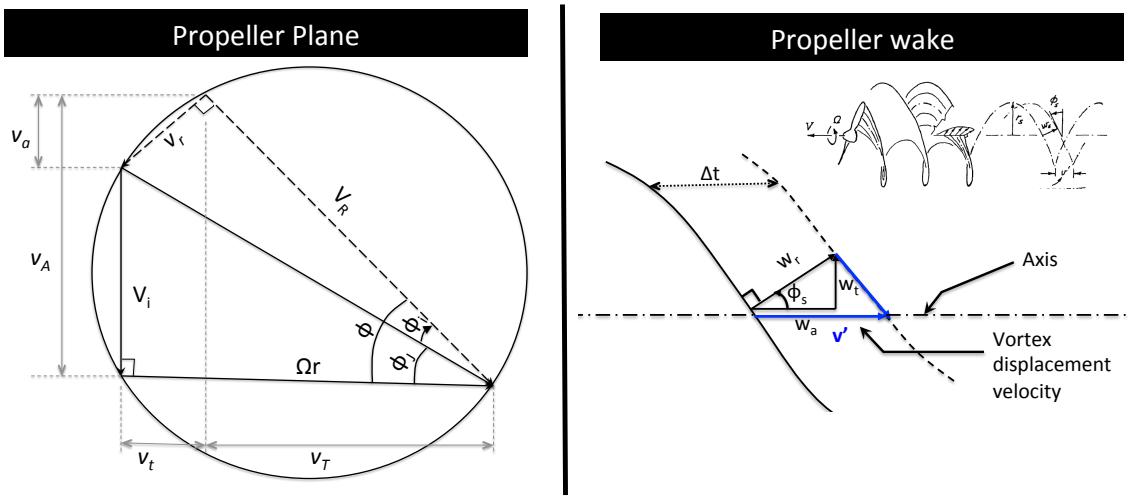

Figure 5-1: Velocities acting at propeller plane (left) and propeller wake (right)

$$v_a = V_R \sin(\phi_j + \phi_i) - V_A \tag{43}$$

$$v_t = \Omega r - V_R \cos(\phi_j + \phi_i) \tag{44}$$

$$V_R = (V_i^2 + \Omega r^2) cos\phi_i \tag{45}$$

5.1 Matching simulation to experiment SDL60M

The propellers tested, SDL60M and SDL20M, both showed discrepancy between experiment and theoretically predicted performance, however, SDL60M showed less discrepancy. (13) and (4)recorded huge discrepancy when the compared performance data from experiment and theory for blades designed to operate at Reynolds number of less than 30,000. In chapter 4, it was shown that the major contributions to the discrepancy observed in SDL60M were as a result of 2D airfoil non-linearity largely from drag data. This uncertainty from 2D airfoil non-linearity result in deviation of the calculated induced velocity along the radius of the blade from the induced velocity in actual blade performance measurements. The effect of 2D airfoil non-linearity on propeller performance was investigated by simulating the propeller wind tunnel test. This was achieved by adjusting lift and drag linearization functions until matching outcomes were obtained. Central to the method is the assumption that the thrust and power coefficient plots are unique solutions from unique 2D airfoil force data.

5.1.1 Effect of lift curve slope

The BEMT code accepts linearized forms of 2D aero data and as earlier mentioned, the lift curve slope. In this section, three different lift curve slope (ao) values were applied and the propeller performance for each was plotted on Figure 5-2, Figure 5-3, and Figure 5-4 along with wind tunnel experiment.

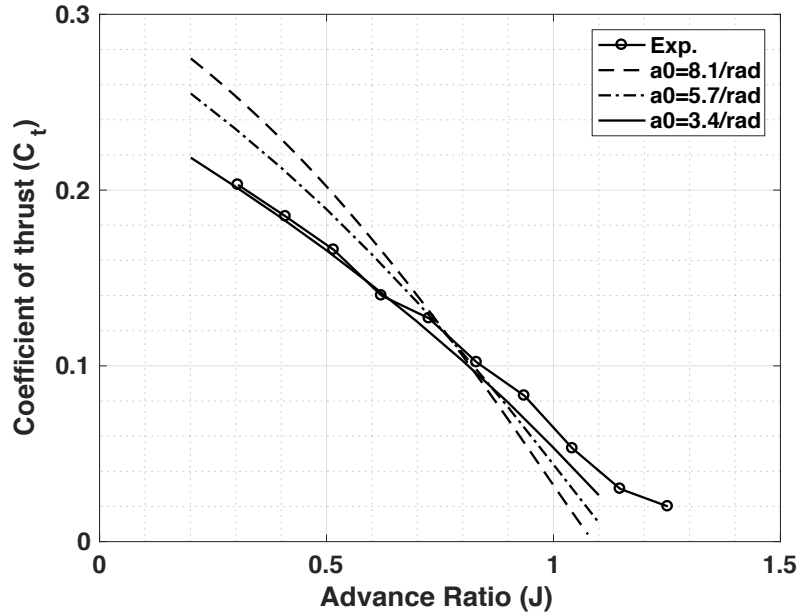

Figure 5-2: Effect of lift curve slope on C_t relative to Experiment data

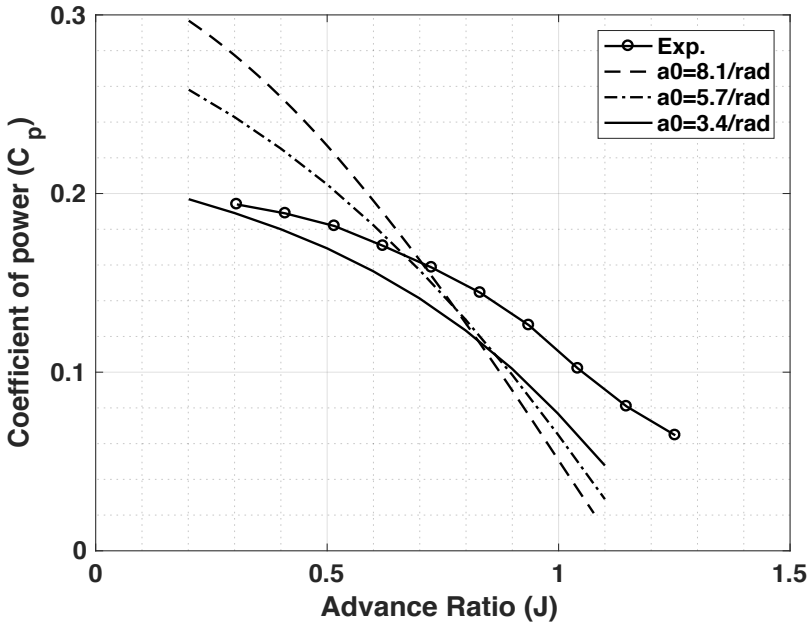

Figure 5-3: Effect of lift curve slope on C_p relative to Experiment data

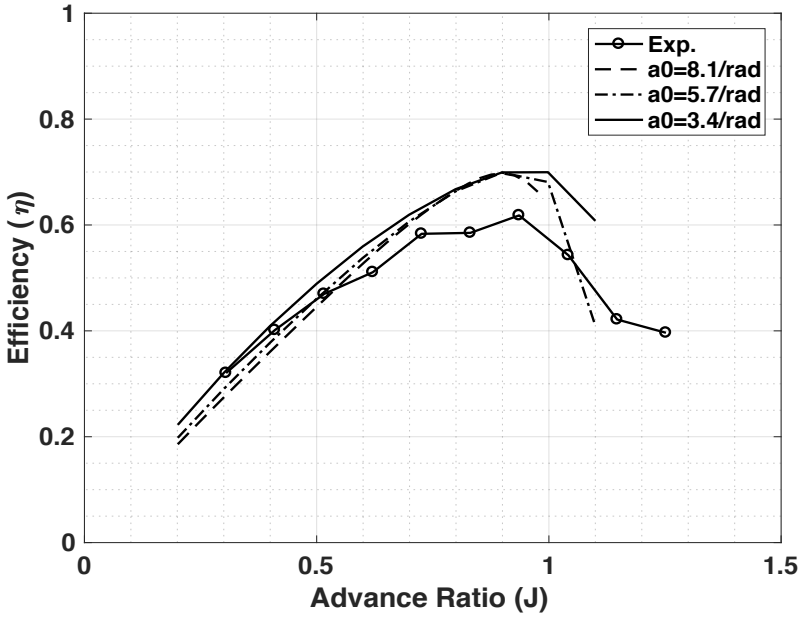

Figure 5-4: Effect of lift curve slope on Efficiency relative to Experiment data

Varying the lift curve slope changed the slopes of both the coefficient of power and thrust as observed in Figure 5-2 and Figure 5-3. However, the overall effect of slope changes on the efficiency of the blade is minimal. In the approach used, matching priority was firstly given to the lift coefficient. Comparing the effect of changing lift curve slope between the thrust and power coefficient from Figure 5-2 and Figure 5-3 respectively, it is seen that the lift curve slope has more impact on the thrust coefficient as expected. A lift curve slope of 3.4/rad matched the plots from experiment as observed in Figure 5-2 and selected for extended matching. Further observed from Figure 5-4 is that at lower advance ratios up to 0.6, good matching was achieved. However, at advance ratios greater than 0.6, sharp increase in thrust coefficient is observed. This increase may have been as a result of minor measurement discrepancies.

5.1.2 Effect of drag to quadratic lift relationship

Following an acceptable match for the thrust coefficient, attention was turned to obtaining acceptable match for coefficient of power. Using the preselected lift curve slope of 3.4/rad, the effect of three values of b on the overall blade performance were analysed and captured in Figure 5-5, Figure 5-6, and Figure 5-7.

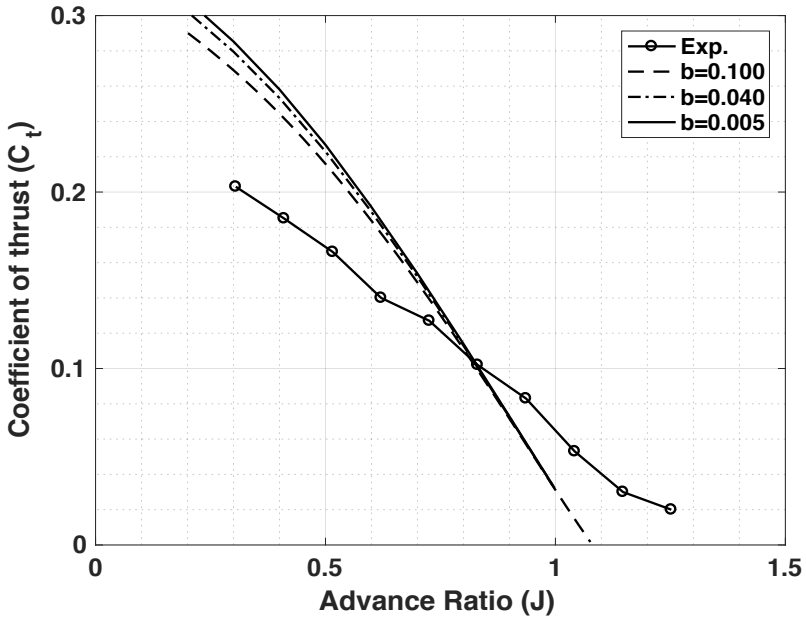

Figure 5-5: Effect of b = dC_D/dC_L^2 on C_t relative to Experiment data

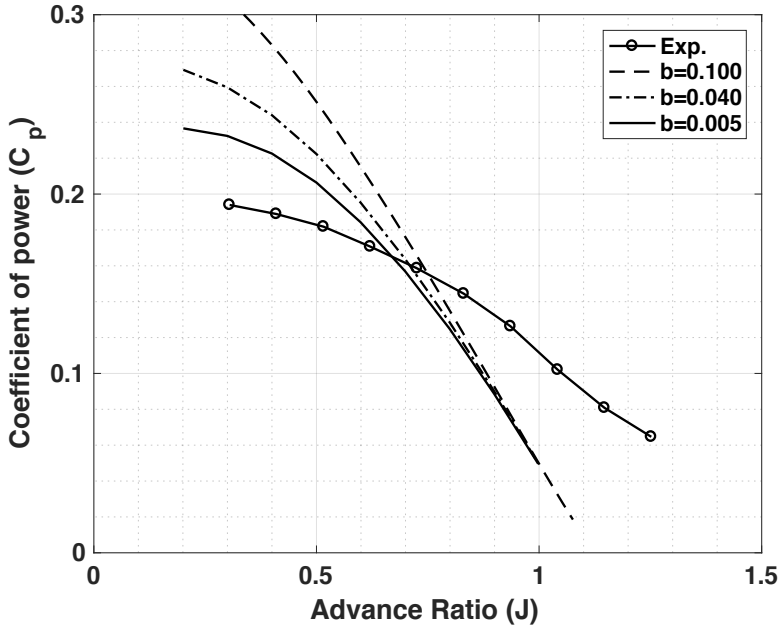

Figure 5-6: Effect of b = dC_D/dC_L^2 on C_p relative to Experiment data

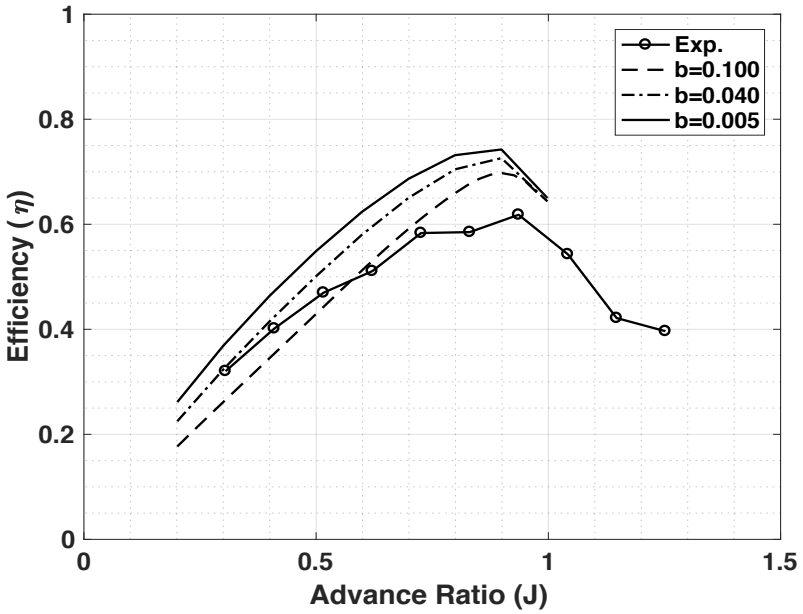

Figure 5-7: Effect of b = dC_D/dC_L^2 on efficiency relative to Experiment data

The effect of b, drag slope parameter that relates drag to quadratic lift changes was observed to have a huge effect on the slope of the coefficient of power. In this case, the slope is modified by lowering C_p at low advance ratio end of the C_p plot as shown in Figure 5-6. While the effect of b is profound on slope of power coefficient, its effect is less so on thrust coefficient plots found on Figure 5-5. As a result, the efficiency curve shows similar trend where the overall effect of b is large in lower advance ratios and tend to converge to a single efficiency value at higher advance ratio.

5.1.3 Effect of minimum airfoil drag

At this point, the combination of lift curve slope of a0 = 3.4/rad and drag slope of b=0.04 resulted to the most acceptable parallel gradient between experiment data and matching with simulation. To study the effect of minimum airfoil drag, a0 and b were fixed to this value, while C_{D0} was varied. Ideally, the C_{D0} value of an airfoil is largely dictated by the thickness and leading-edge radius of the airfoil. A large airfoil thickness and leading-edge radius results in increase of the minimum drag coefficient of the airfoil.

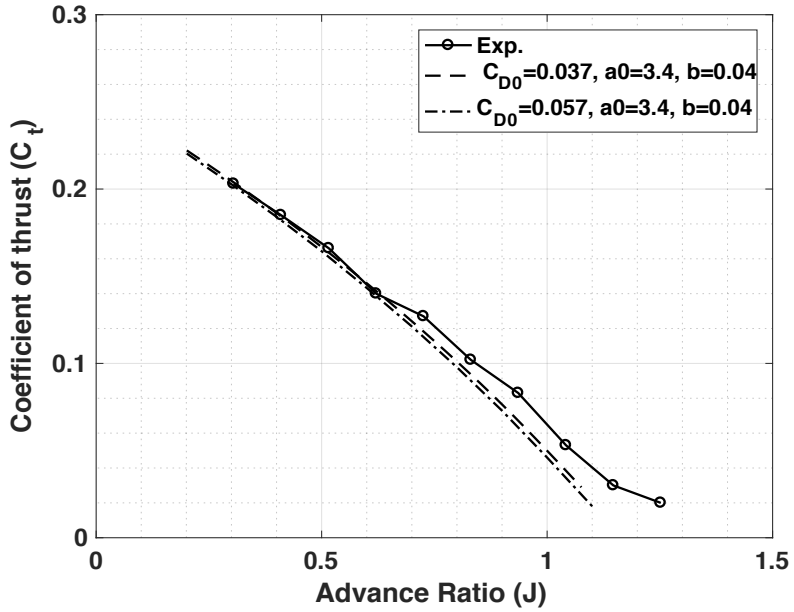

Figure 5-8: Effect of C_{D0} on C_t relative to Experiment data

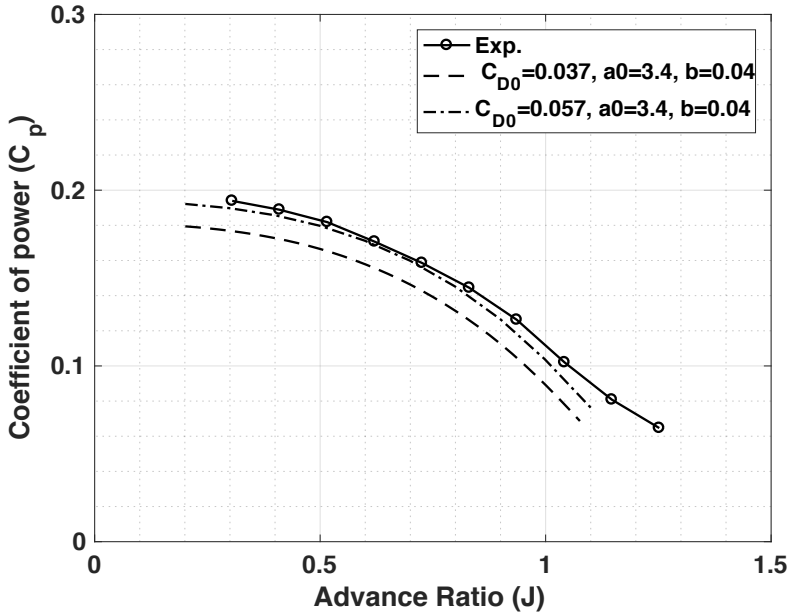

Figure 5-9: Effect of C_{D0} on C_p relative to Experiment data

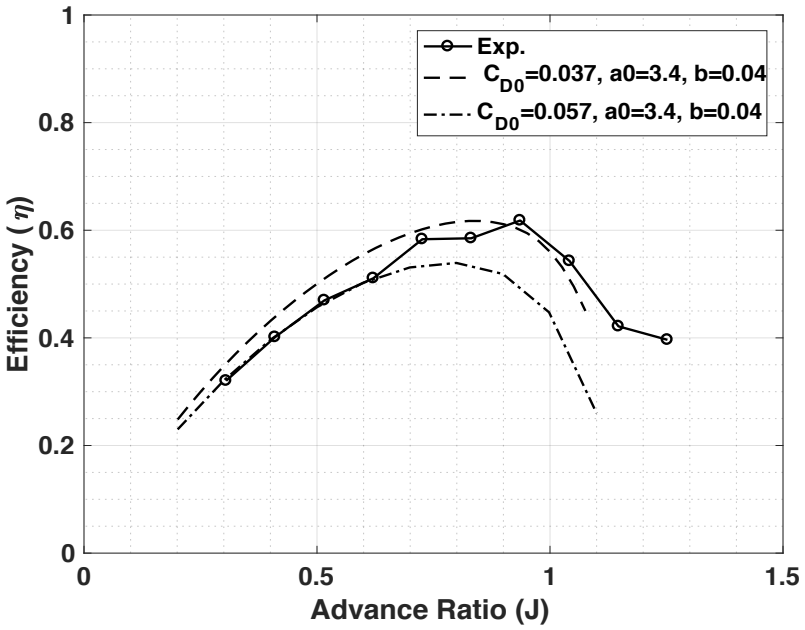

Figure 5-10: Effect of C_{D0} on efficiency relative to Experiment data

The minimal drag (C_{D0}) showed the highest influence on the propeller efficiency by drastically translating the power coefficient curve. Small changes to minimal drag coefficient have significant effect on the propeller performance. Figure 5-9 shows the effect of a 54% increase in C_{D0} from 0.037. While the corresponding increase in thrust coefficient is minimal due to the change, the predicted propeller efficiency is however, decreased from 62% to 46% as seen in Figure 5-10. Finally, by adjusting a0, b and C_{D0} to the values found on Figure 5-10, it was possible to match the performance obtained from wind tunnel tests to simulation for SDL60M.

5.2 Matching simulation to experiment SDL20M

As with SDL60M, a similar approach was employed to simulate the measured propeller performance by manipulating the linearized forms of airfoil force data fed into the blade element momentum software. While the design operation of SDL60M was at 60K Reynolds number, SDL20K was at Reynolds number of 20K.

5.2.1 Effect of lift curve slope

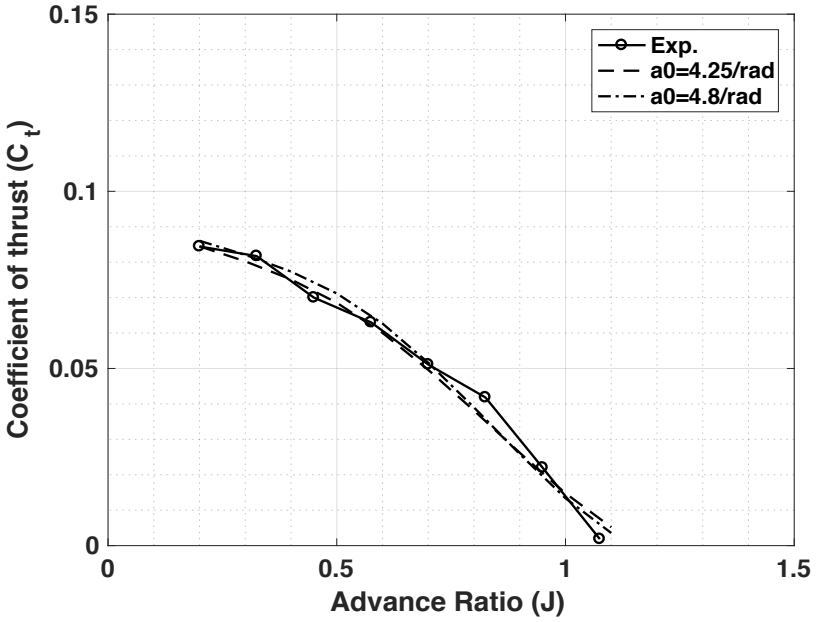

Figure 5-11:Effect of lift curve slope on C_p relative to Experiment data

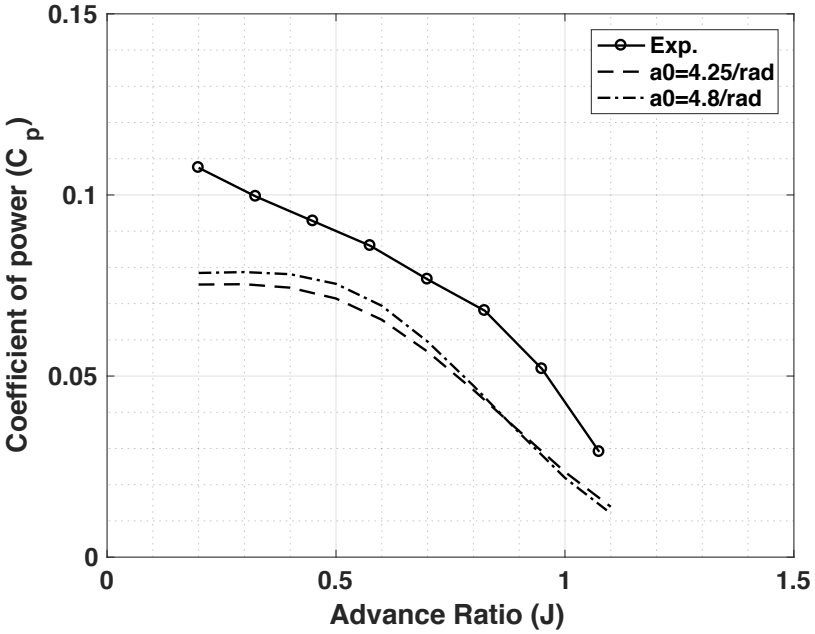

Figure 5-12:Effect of lift curve slope on C_P relative to Experiment data

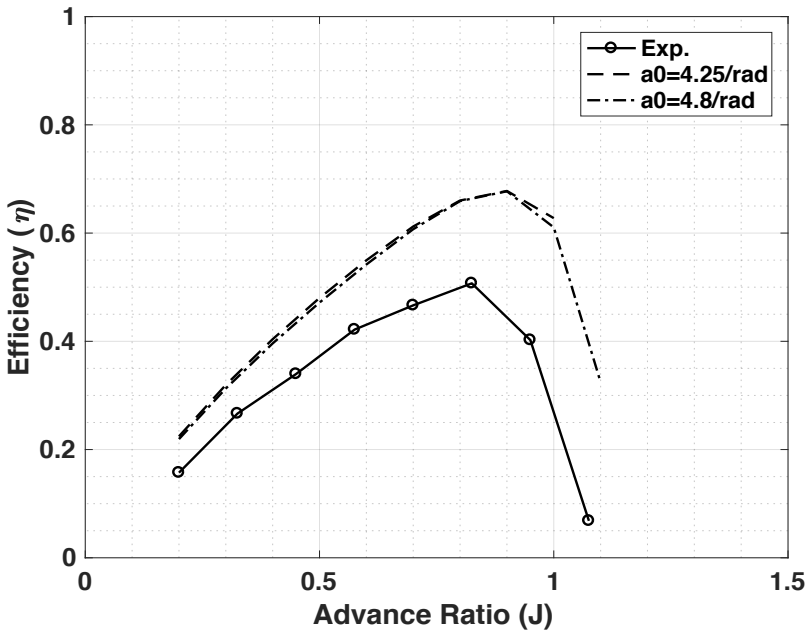

Figure 5-13:Effect of lift curve slope on efficiency relative to Experiment data

From Figure 5-11, a lift curve slope of 4.23/rad clearly shows a better agreement with experiment C_T data and an almost translating relationship with C_P in Figure 5-12. The effect of lift curve slope on efficiency plot is minimal as observed in Figure 5-13.

5.2.2 Effect of drag to quadratic lift relationship

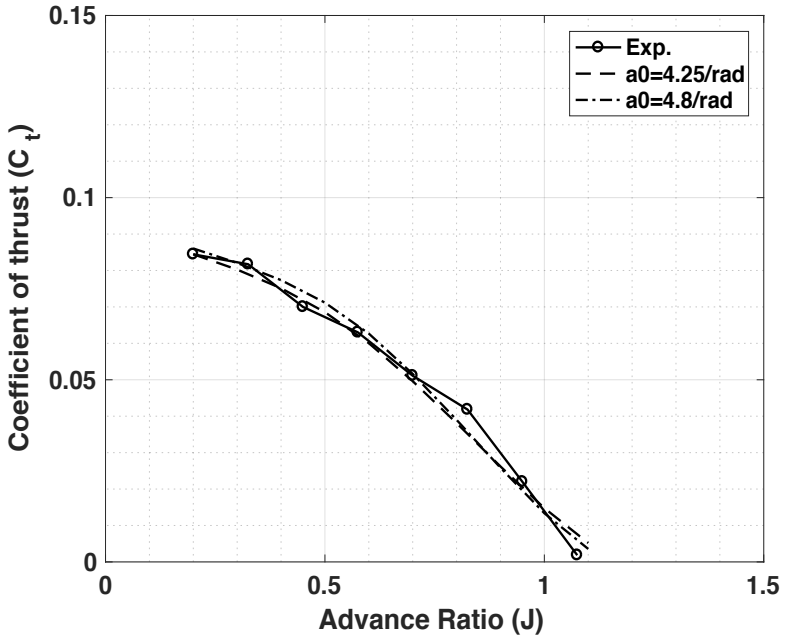

Figure 5-14:Effect of b = dC_D/dC_L^2 on C_p relative to Experiment data

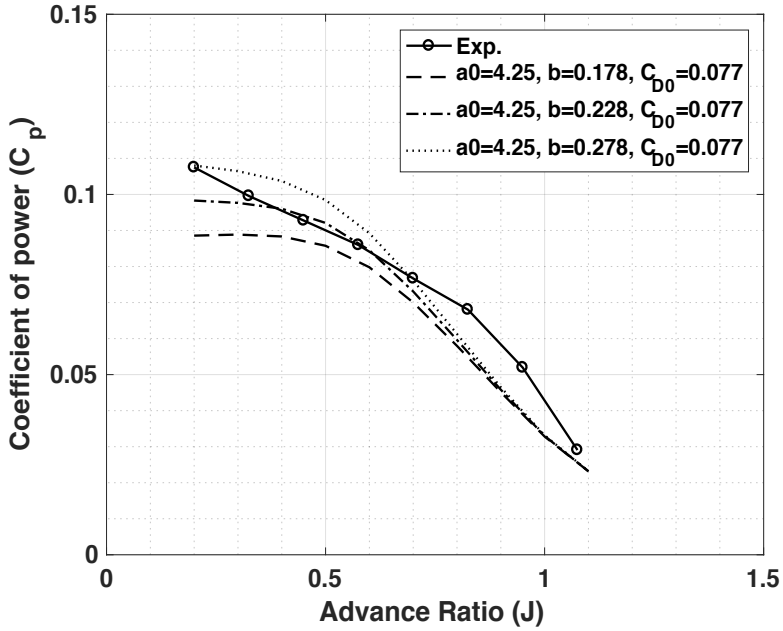

Figure 5-15:Effect of b = dC_D/dC_L^2 on C_t relative to Experiment data

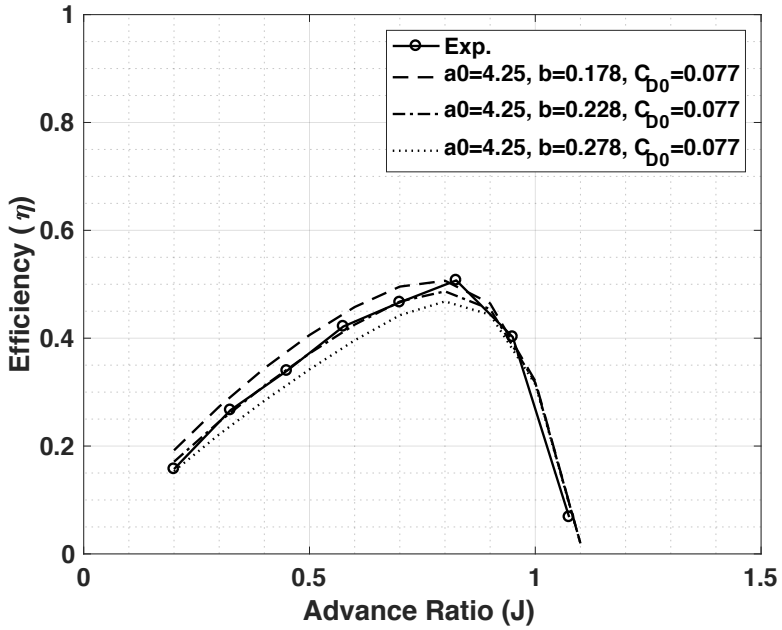

Figure 5-16:Effect of b = dC_D/dC_L^2 on efficiency relative to Experiment data

Figure 5-14 to Figure 5-16 show the plots of three parameter combinations a0, b and C_{D0} to arrive at results that matches wind tunnel results. Again, it is observed from Figure 5-14 that changes in b do no significantly affect the propeller C_T predictions as much as C_P as seen in Figure 5-15. The efficiency plot in Figure 5-16 shows the input parameters to the BEMT code that produces matching results to wind tunnel experiment data: a0 = 4.25/rad; b = 0.278 and C_{D0} = 0.077.

$$\alpha = \beta - \phi \tag{46}$$

5.2.3 Derivation of correction function

To compare the obtained 2D linear force data extracted as a result of matching simulation to experiment results, the 2D airfoil (SD7037) characteristics was predicted in a numeric software Xflr-5. In xflr-5, Ncrit can be set to trigger transition aimed at replicating disturbances in real flows. However, since the propeller experiment data and hence matched data contain these disturbances, the Ncrit was set to 1 to by-pass transitions of linear-instability prediction of the airfoil. The goal is to provide a means to account for the combined non-linear airfoil

characteristics at low Reynolds number and other propeller effects such as 3D effects in the early stage of propeller design during which the airfoil input is linearized. McCrink (14) applied semi-empirical correction developed by Snel (15) and Liu & Janajreh (16) in the BEM modelling of COT propellers.

After matching of simulation to wind tunnel experiment is achieved, as follow up assumption is that the propeller design C_L is unchanged and the backward re-computation process described earlier is carried out. By setting the design angle of attack as the true angle of attack, a new relationship between v_a and v_t is established and applied as a correction function to the analysis of propellers at similar low Reynolds number.

Low Reynolds number propeller designs and analysis have 2 main challenges:

1. How to treat the uncertainties in the 2-D airfoil characteristics
2. The uncertainty in 1 above does not allow for the objective evaluation of lifting line theory as a tool for the design of propellers operating at low and ultra low Reynolds numbers (13).

Although in his work, Kunz (13) was not focus on maximizing the performance of propellers operating in ultra-low Reynold number, results from his propeller show considerable discrepancy in power with increasing advance ratio. test Wind tunnel experiment conducted at university of Osaka to validate the design of a propeller having a diameter of 50cm and design Reynolds number of 10,000 (17), not only showed good agreement at design point, but also reached efficiency of 60% .

From Larrabee's work it can be shown that v_a/w_a and v_t/w_t is averagely taken to be 2. However, Figure 5-17 reveals that the velocity ratios v_a/w_a and v_t/w_t varies along the propeller span. As the advance ratio increases, the velocity ratio and Reynolds number increase. By averaging the velocity ratio at each advance ratio shown in Figure 5-17, the plots in Figure 5-18 was generated.

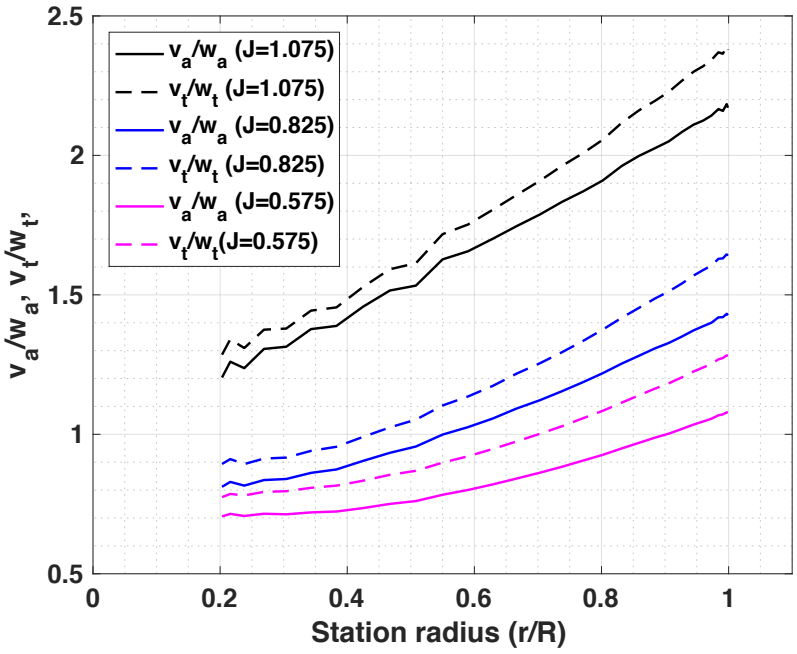

Figure 5-17: v_a/w_a, v_t/w_t as a function of station radius (r/R) at three advance ratios

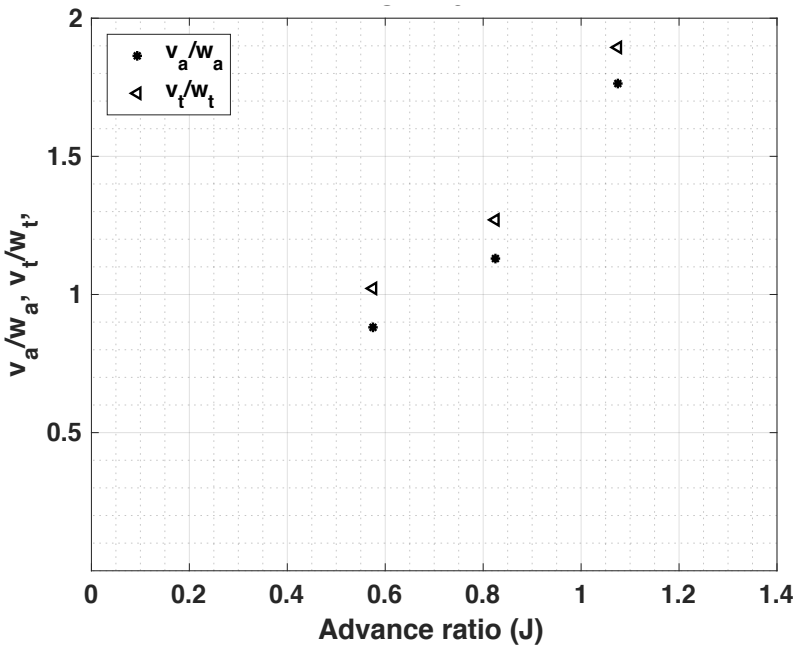

Figure 5-18: v_a/w_a, v_t/w_t as a function of advance ratio

Next, by fitting a curve on the points shown in Figure 5-18, a semi-empiric non-dimensional function that corrects induced velocity estimates at the propeller wake to plane was derived and captured in equations 47 and 48. Where v_a and v_t are re-estimated values derived from experiment matching, while w_a and w_t are BEMT estimate from a location far aft of the propeller

wake as shown in Figure 5-1. Given that v_a = V*a and w_a = 2*v_a, w_a can be replaced in equation 47. along similar lines, v_t = omega*r*a'/60 and w_t = 2*v_t, where w_t can be replaced in equation 48.

$$VA = w_a(3.1\frac{V}{\Omega r}^2 - 3.3\frac{V}{\Omega r} + 1.77) \quad (47)$$

$$VT = w_t(3.0\frac{V}{\Omega r}^2 - 3.2\frac{V}{\Omega r} + 1.88) \quad (48)$$

5.2.3.1 Effect of Induction Factor

In the analysis of arbitrary blades the treatment of axial and tangential induction factors influences the stability of propeller performance prediction. This section explores the effect of clipping maximum axial induction factor (a) and minimum tangential induction factor (a'). However, only results for the axial induction factor is presented here. (18) prescribed clipping a and a' to 0.7 and -0.7 respectively but using these values, which lie between 1 and 0.5 resulted in instabilities at the Reynolds number of interest (Re<25,000).

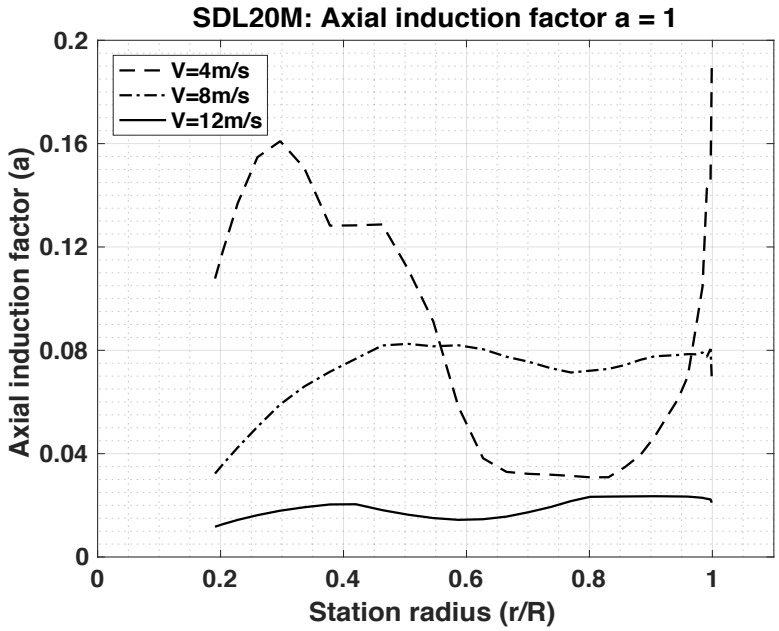

Figure 5-19: Axial Induction factor (a≤1) versus r/R for three airflow velocities(SDL20Y-2)

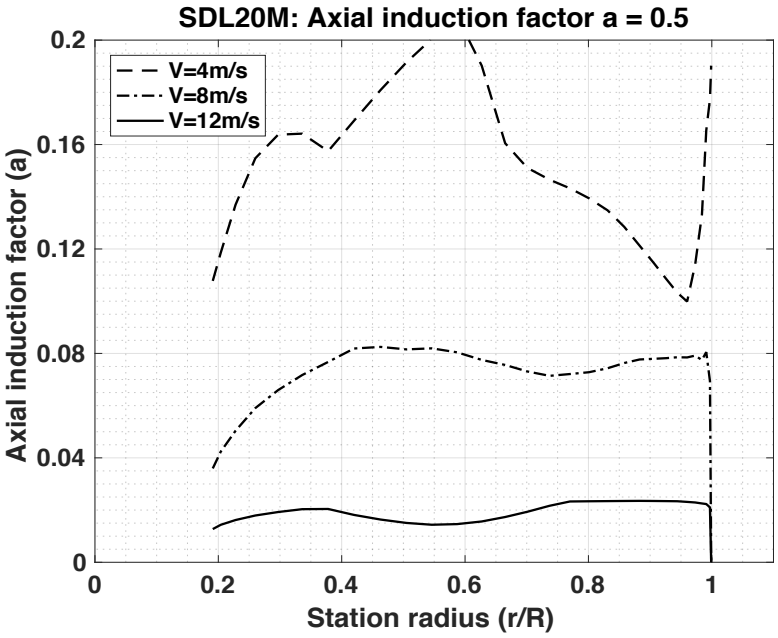

Figure 5-20: Axial Induction factor (a≤ 0.5) versus r/R for three airflow velocities(SDL20Y-2)

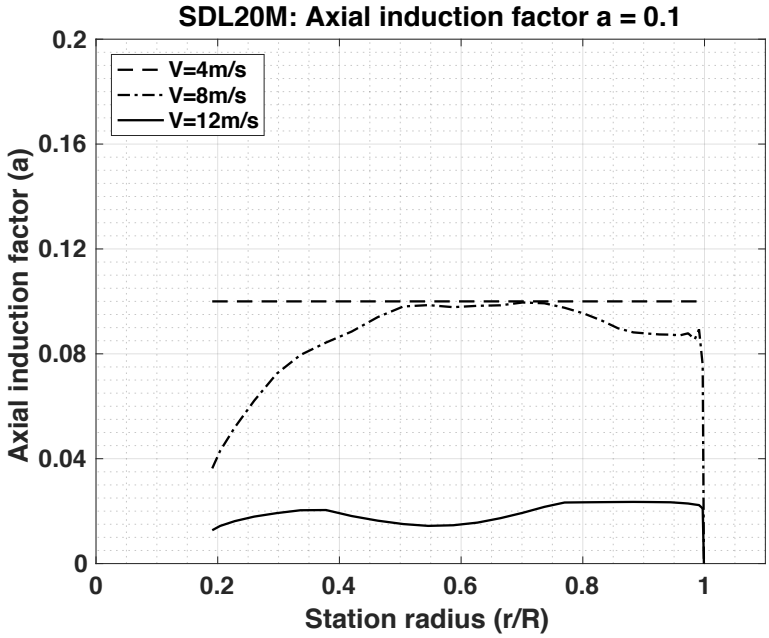

Figure 5-21: Axial Induction factor (a≤ 0.1) versus r/R for three airflow velocities(SDL20Y-2)

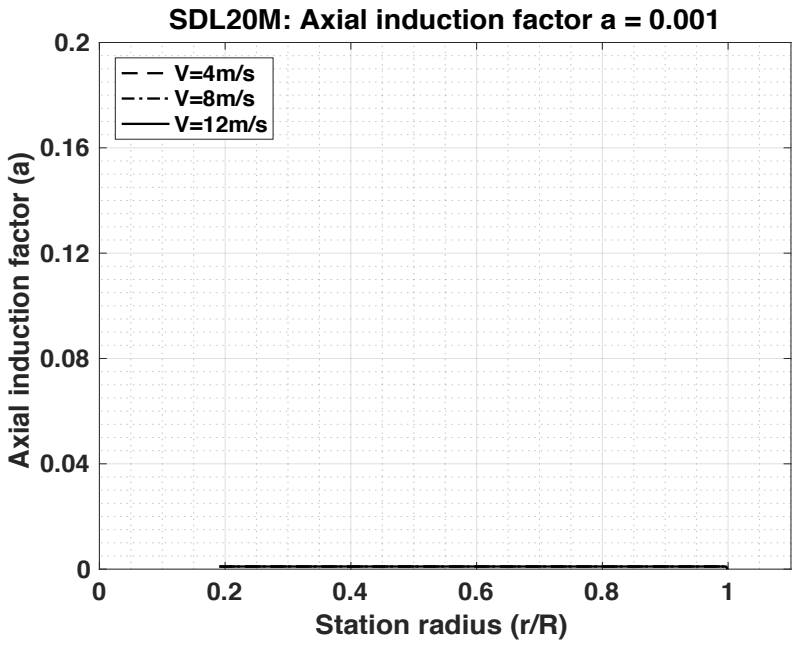

Figure 5-22: Axial Induction factor (a≤ 0.001) versus r/R for three airflow velocities(SDL20Y-2)

Figure 5-19, Figure 5-20, Figure 5-21, and Figure 5-22 captures the effect of 100%, 50%, 10% and 0.1% induction factors respectively. In the BEMT the induction factors are bounded within a range of values. For example, the range for an induction factor of 1 is defines as -1≤a≤1 and -1≤a'≤1. It is necessary to state that the same magnitude of induction factor is implemented on the axial and tangential induction factor (a and a'). For each of the induction factor considered, three (3) velocities 4m/s, 8m/s and 12m/s are presented for study. Figure 5-19 and Figure 5-20 show instability in all three velocities, which are transferred to the non-dimensional thrust and power coefficients. The figures along with Figure 2-7 also confirm, the impossibility of having an induced velocity as much as airflow and tangential velocity of the propeller or even the likelihood of 50%. However as seen in Figure 5-21 where an induction factor of 10% acts to increase magnitude of the airflow and tangential velocities at the plane of the propeller as depicted in Figure 2-7. From Figure 5-21 it is clearly observed that a constant induction is achieved along the propeller span at 4m/s but not at higher velocities shown in this figure. Further decreasing the induction factor to 0.1% or increasing the airflow velocity to by 0.1% results to a stable induced velocity along the entire blade radius span and all velocity considered as shown in Figure 5-22. Additional decrease in induction factor from 0.1% did not bring about any observable change in blade performance. As a result, an induction factor of 0.1% was chosen and implemented in the BEMT code. (19) in their work adopted a 70% induction factor for a propeller Reynolds number design of about 500,000. In

this work, however, the Reynolds number is 20,000, implying a much lower propeller induction at lower Reynolds number and necessitating the need to find an appropriate induction factor boundaries.

5.2.4 Applying correction function to design of a blade

To apply the semi-empirical correction functions developed in this work SDL20Y and SDL20Y-2 were designed. The correction functions in equation 47 and 48 were implemented in the design and analysis of SDL20Y as shown in the flowchart of Figure 5-23. VA and VT replaced induced velocities, v_a and v_t, respectively. However, SDL20Y-2 was designed, fabricated and tested as a control specimen blade and the corrections were not applied in its design.

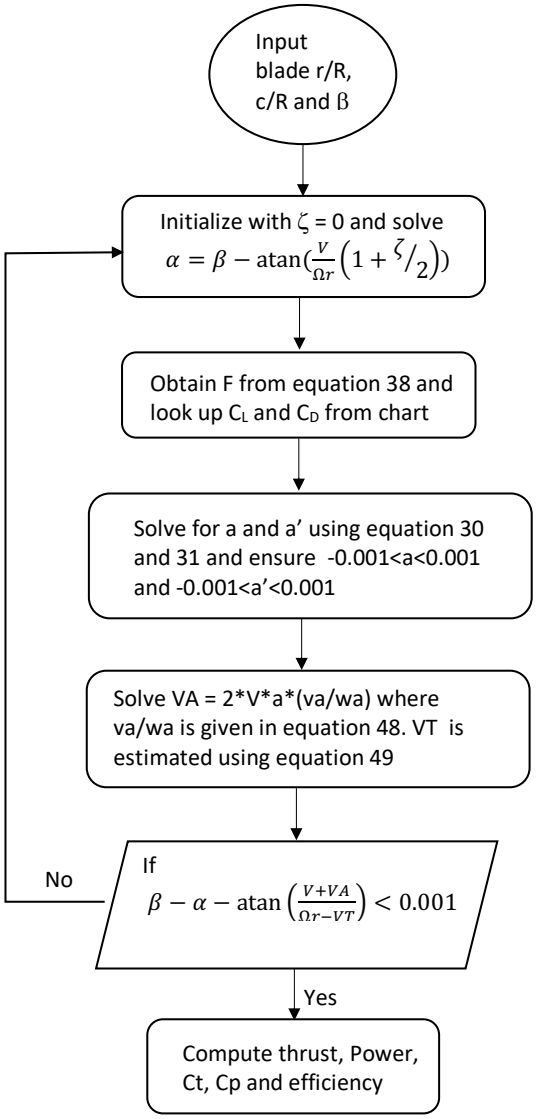

Figure 5-23: Blade analysis BEMT flowchart including the semi-empirical correction functions

The arbitrary blade analysis flowchart shown in Figure 5-23 was implemented in Matlab and can be found in the appendix section of this work. Table 5-1shows the deign blade parameters of SDL20Y-2 and SDL20Y. The table it is clearly seen that the design input for both propellers are same. To re-iterate, the only difference between both blades is the introduction of the semi-empirical correction function captured in equation 47 and 48.

Table 5-1: Blade design parameters. Blade section: SD7037

	SDL20Y-2	SDL20Y
Hub radius [m]	0.013	0.013

Blade tip radius [m]	0.08	0.08
Angular velocity [RPM]	4000	4000
Velocity [m/s]	12	12

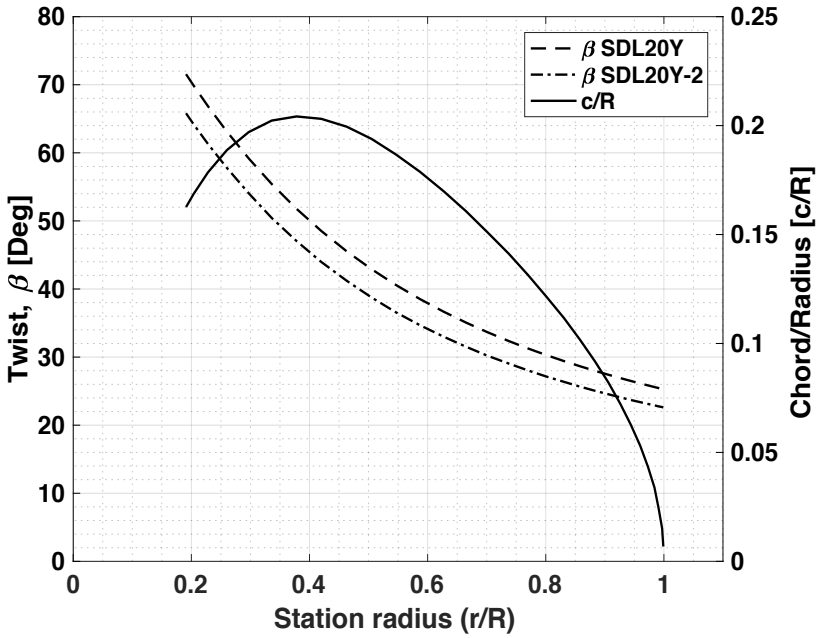

Figure 5-24: Pitch and c/R of SDL20Y-2 and SDL20Y

Figure 5-24 shows the twist for both propellers and the chord to radius distribution across the span of the propeller. From this figure it is clearly observable that the only geometric difference between SDL20Y-2 and SDL20Y is the twist. The c/R and all other physical geometric properties of both propellers are similar as shown in Table 5-1. Both designs, SDL20Y-2 and SDL20Y, were fabricated using formlab's 3D stereolithography (SLA) printer as described in section 4.4 of this work. The printed propeller weighted 8.5g as shown in Figure 5-25. Experiment tests were conducted on SDL20Y-2 and SDL20Y at Kyushu Institute of Technology wind tunnel facility. Figure 5-26 shows SDL20Y-2 in a wind tunnel torque test set-up. The experiment on both propellers were carried out as described in section 2.4 of this work.

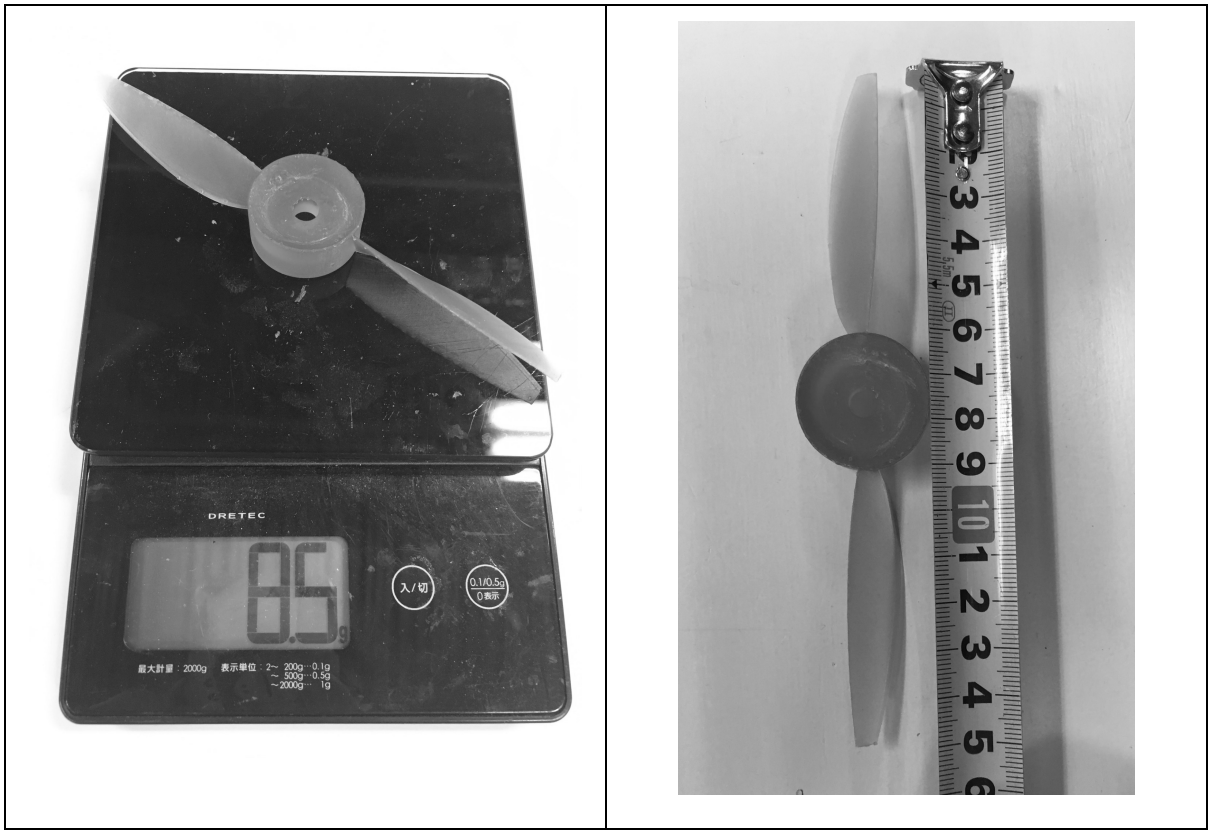

Figure 5-25: SDL20Y-2 on a mass scale (left) and SDL20Y-2 against a meter (right)

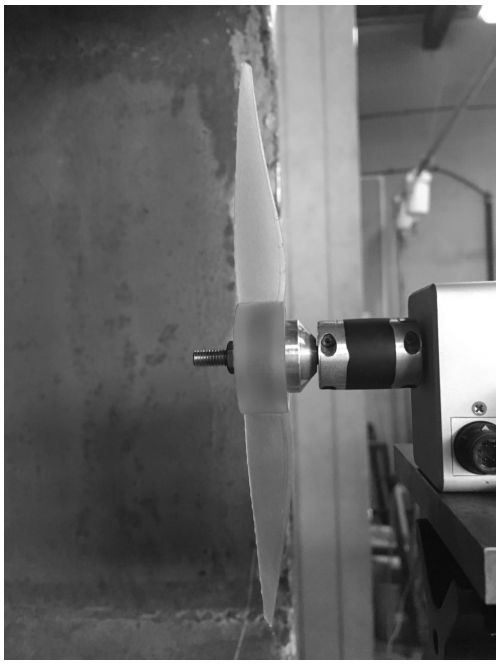

Figure 5-26: SDL20Y-2 in a wind tunnel test set-up

5.3 Test Result and Analysis for SDL20Y-2 and SDL20Y

Parameters of interest in the wind tunnel test of SDL20Y-2 and SDL20Y are thrust and torque. In these experiments, the angular velocity was held at a constant 4000RPM while the airflow velocity is varied to obtain different values for advance ratio. This means that variation in Reynolds number would be less than would have been recorded if advance ratio changes were achieved by varying the angular velocity. The central goal and expectation in the design of SDL20Y-2 and SDL20Y was to use the 2D airfoil force data from xflr-5 in their designs; implement the semi-empirical correction factor derived from SDL20M; and obtain good agreement between theoretical prediction and wind tunnel experiment for SDL20Y and less likely so for SDL20Y-2. While there is plenty of room to improve the overall performance of the blades, this design focussed on improving BEMT performance prediction.

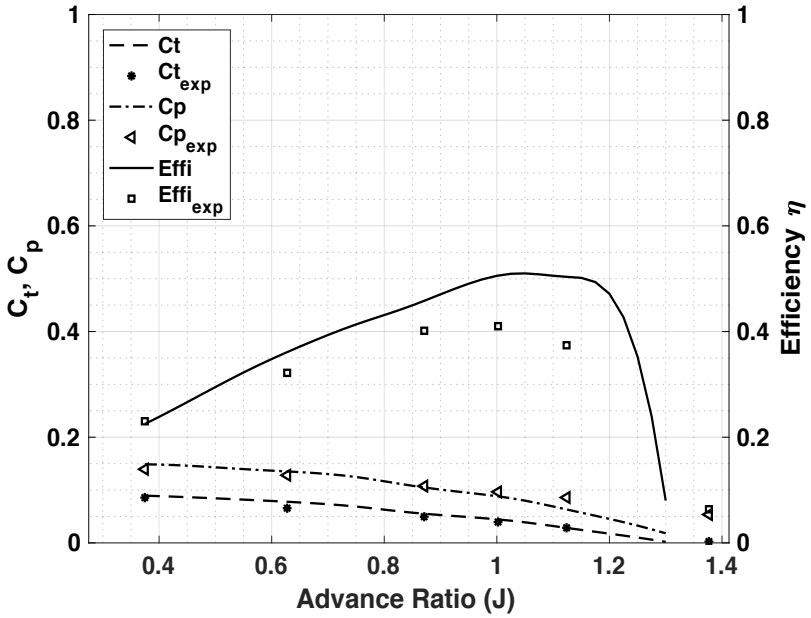

Figure 5-27: SDL20Y-2: C_t, C_p and η versus Advance ratio for wind tunnel test and BEM theory

The coefficient of thrust (Ct), coefficient of power (Cp) and efficiency (η) from theoretical performance prediction and wind tunnel tests for SDL20Y-2 are presented in Figure 5-27. From the figure, it is seen that there is acceptable agreement in the thrust coefficients for theory and wind tunnel tests. However, at advance ratios of 1.15 the experiment value of Cp

is about 33% higher predicted by BEMT code, while there is excellent agreement in CT between theoretical and experiment. The net effect of the discrepancy is observed in the efficiency plot at advance ratio of 1.15, where theoretical efficiency reaches a maximum value of 50% while corresponding experiment values is 38%.

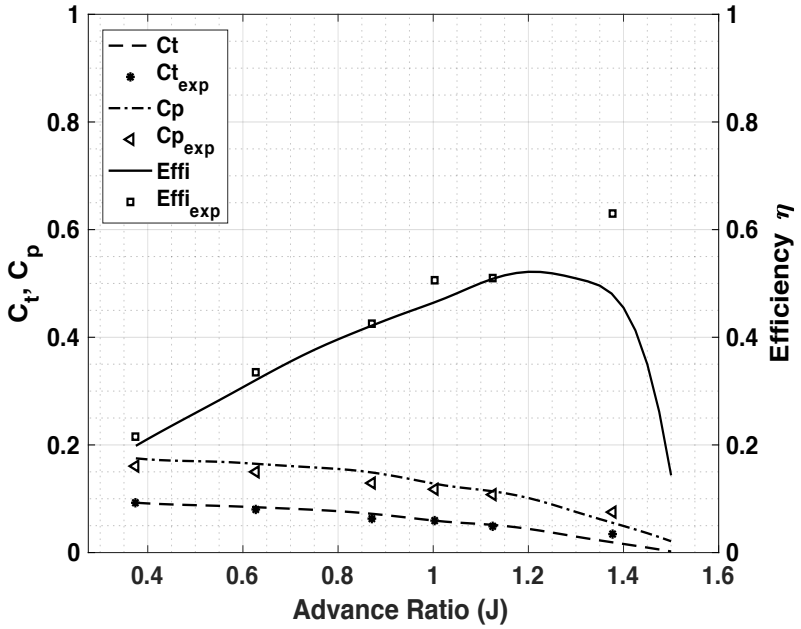

Figure 5-28: SDL20Y: C_t, C_p and η versus Advance ratio for wind tunnel test and BEM theory

The design and off-design performance analysis of SDL20Y incorporated the semi-empirical corrections developed to adjust the relationship between the swirl (w_t) and axial (w_a) velocity of the vortex sheet and the induced component of velocities (v_t and v_a) at the plane of the propeller. Rather than relating the respective pairs, v_a and v_t directly to w_a and w_t, as an average as with conventional BEMT, the semi-empirical correction function introduces advance ratio in the relationship between v_a and w_a. Figure 5-28 presents the theoretical and wind tunnel experiment data for SDL20Y. The figure shows excellent agreement between theoretical performance prediction and wind tunnel experiments. However, some scatter in data points are observed. The only geometric difference between SDL20Y-2 and SDL20Y is the geometric pitch of both propellers, which is as a result of the semi-empirical function incorporated in to the design of SDL20Y. Comparing Figure 5-27 and Figure 5-28 it is seen that the efficiency of both propellers are similar, each reaching a peak efficiency of about 50%

at advance ratio of 1.2. However, while the wind tunnel experiment of SDL20Y-2 in Figure 5-27 is about 33% less than theoretical values from the BEMT code, there is excellent agreement between wind tunnel and theoretical performance prediction as shown in Figure 5-28. This indicates that the semi-empirical function incorporated in the design of SDL20Y largely improved the propeller force coefficient C_t and C_p and ultimately the efficiency.

There are a few corrections the semi-empirical function developed and implemented may serve: (1) the effect of the screwing action of the propeller operating at Reynolds number as low as 20,000 may have been inadequately accounted for (2) the semi-empirical function may have acted to correct flow physics uncaptured in the prediction of the 2D airfoil characteristics (3) In conventional BEMT, the relationship between v_a and w_a is expressed only. However, the semi-empirical function extends the relationship between v_a and w_a to include advance ratio (J). Thus, it may be taken to mean that the relationship between v_a, w_a and J may be no longer negligible as Reynold number falls below 25,000.

6 CONCLUSION

Blade element momentum theory was used in the design of a 2-bladed propeller (designated SDL60M) with solidity of 0.24 and chord based Reynolds number of ≈60k calculated at 75% radius and advance ratio of 0.83. A single 2D experiment data of SD7037 at 60k Reynolds number was employed in the design of more than 75% of the entire blade, which was based on minimum propeller induced losses. From blade design, it was ensured that above 50% of the entire blade radius operated between 40k – 60k Reynolds numbers at design advance ratio. A design goal of the propeller was to minimize variation in Reynolds number from hub to tip radius. Propeller tests were conducted at Kyushu Institute of Technology wind tunnel facility in two ways: A constant angular velocity was maintained while airflow velocities over the propeller was changed at each data point; and a constant airflow over the propeller while changing angular velocity of the propeller at required data points. Performance discrepancy between blade element momentum theory predictions and data from wind tunnel experiment was observed.

The constant angular velocity and air velocity wind tunnel tests both achieved a maximum efficiency of 65%, and respective efficiency of 58% and 65% at design point. However, blade element momentum theory predictions at design point were about 70% efficiency for the both cases. While the maximum efficiencies reached do not significantly differ from theory predictions, thrust and power experiment data show considerable discrepancy with theory at design point.

Because Xrotor accepts airfoil aerodynamic input in linearized forms only, the effect of drag and lift coefficients on propeller performance was investigated in detail by re-computing the lift curve slope from a narrower range that gave a more representative value for the local design angle of attack. Performance of an earlier iterated blade shape, which was fabricated and tested, was re-predicted in operation mode in Xrotor by replacing the lift and drag force coefficients with the re-computed value. The re-computed airfoil force coefficients agreed excellently with experiment data and predicted propeller performance showed better agreement especially in thrust. However, discrepancy in power remained considerable.

For low Reynolds number operating propellers, a major source of performance discrepancy between theory and experiment is inaccurate lift and drag coefficient used in the blade shape iteration. Investigation showed that blade performance is especially sensitive to lift and drag

coefficient, and an unrepresentative value contributes to discrepancies between theory predictions and experiment data. Non-linearity associated with airfoil aerodynamic data that are not captured by linearization result in a less representative modeling of the airfoil force coefficient and consequently, discrepancy in propeller performance between theory and experiment.

The work progressed by investigating validity of using 2D airfoil coefficient for the design of propellers that operate at Reynolds number of 25,000 or less. Typically at these range, it is difficult to obtain 2D airfoil force data from experiment due to low inertia and high sensitivity of the flow to external factors. This section of the work required the design of a propeller to operate at chord-based Reynolds number of 20,000 Reynolds number. The propeller was designated SDL20M. At these low propeller operation Reynolds number, 2D airfoil force data from experiments are not publicly available. Hence, the design of SDL20M was completed using 2D airfoil data obtained from a numeric code that estimates airfoil force coefficient using vortice panel method.

Theoretical efficiency of the fabricated propeller (SDL20M) achieved a maximum of 67%, while experiment data from efficiency was up to 13% less than theoretically predicted value. Inaccurate prediction of 2D airfoil force data was identified as a major contributor to the discrepancy between experiment and theory.

The focus of the work from here turned to investigating why the discrepancies between theoretically predicted propeller performance and wind tunnel test data at Re ≈ 25,000 exist. The challenge of analysing propeller performance designed to operate within this low Re number flight regime is in two folds: (1) Blade Element Momentum Theory (BEMT) code as applied in the design and analysis of propellers operating at Re >5 x 10^5 does not adequately apply to Re <6 x 10^4; (2) at Re < 60,000, obtaining reliable 2D airfoil experiment force data becomes increasingly challenging, largely because of the inherent difficulty in measuring aerodynamic forces acting on an airfoil. To overcome the latter problem, 2D airfoil data at this Reynolds number regime of interest (≈25,000) where experiment data is unavailable, Xflr-5, a numeric code was used to predict the 2D airfoil force data. Then using the airfoil data from numeric source, a propeller was designed to operate at 20k Reynolds number.

The design of SDL20M was carried out using a Minimum Induced Loss BEMT code - Xrotor. In Xrotor, airfoil lift and drag estimates are approximated using a linear function for lift and a

quadratic function for drag coefficient. The use of functions in estimating airfoil lift and drag data makes Xrotor a good design tool to under study relationship between airfoil force coefficients and propeller performance. Parameters in the lift and drag estimation functions in Xrotor can be individually manipulated and the overall effect on propeller performance can be isolated and theoretically studied. Using Xrotor, a propeller designated as SDL20M was designed, fabricated and tested at Kyushu institute of technology wind tunnel facility. The result show discrepancy between predicted propeller performance and wind tunnel test data. Through a careful manipulation of four (4) key parameters in the functions defining lift and drag in Xrotor, it was possible to match predicted propeller performance to wind tunnel test. Following a successful performance matching, a semi-empirical correction function that corrected the flow velocity relationships in the wake and plane of the propeller in classical BEMT formulation was developed.

The final research section of the dissertation deals with the application of the semi-empirical correction function developed in the course of this work. A BEMT code was written in Matlab in which semi-empirical correction function was integrated. 2D airfoil force data is supplied to the BEMT code in a M by N matrix look-up chart which was populated with data from a numerical code. The airfoil force data was obtained from Xflr-5 by setting Ncrit value of 1. Utilizing the developed BEMT code, two (2) propellers designated as SDL20Y and SDL20Y-2 were designed, fabricated and tested in wind tunnel experiments. SDL20Y-2 is a 2-bladed unmodified propeller design output from classical BEMT code written for the purpose of this work, while the design of SDL20Y was modified by applying the semi-empirical correction developed in the course of this research. Beside the semi-empirical correction applied in the design of SDL20Y, all other design parameters were kept exactly the same with SDL20Y-2.

Comparing wind tunnel tests of SDL20Y-2 with SDL20Y, the latter had excellent agreement between predicted performance and wind tunnel test data.

However, while the wind tunnel experiment of SDL20Y-2 was about 33% less than theoretical values from the BEMT code, there is excellent agreement between wind tunnel and theoretical performance prediction for SDL20Y. This indicates that the semi-empirical function incorporated in the design of SDL20Y largely improved the propeller force coefficient C_t and C_p and ultimately the efficiency. The semi-empirical function extends the relationship between v_a and w_a to include advance ratio (J), which is an indication that the relationship between v_a, w_a and J may be no longer negligible as Reynold number falls below 25,000.

The semi-empirical correction functions proposed in this work were shown to be effective in accounting for uncertainties from 2D airfoil data from Xflr-5 by modifying the propeller wake and induced velocities relationship in the BEMT code around Reynolds number of interest, which is 25,000.

6.1 Future work

Is the semi-empirical correction function and design process, which developed using SD7037 applicable to all airfoils? Because the correction function was developed on the assumption that the 2D airfoil force data from the numeric source is accurate, the correction function therefore bears within it all inaccuracies from various sources. The individual contributions from inaccurate 2D airfoil force data and collapse of certain underlying assumptions under low Reynolds number conditions combine to cause performance discrepancy. In future work, it would be necessary to investigate the applicability of semi-empirical function developed in this work on other airfoils.

What is the range of Reynolds number within which the semi-empirical correction function continues to be applicable? The semi-empirical correction function was developed from a propeller operating at Reynolds number of 20,000. Future research would need to be conducted to ascertain the Reynolds number range validity of the semi-empirical function and explore the possibility of a general case.

Lastly, the scope of the current research did not include achieving high propeller efficiency. However, by successfully developing a method that allows for accurate propeller performance prediction at low Reynolds number of interest, it would be necessary to push the envelop and improve the propeller efficiency.

7 REFERENCES

1. **Selig, MichaelS., et al.** *Summary of Low-Speed Airfoil Data.* Virginia : SoarTech , 1995.

2. **Muller, Thomas J.** *Low Reynolds Number Vehicles.* University of Notre Dame. Indiana : Advisory Group For Aerospace Research And Development, 1985.

3. *Effects of Acoustic Disturbances on Low Re Airfoil Flows.* **T.M, Grundy, Keefe G.P and Lowson M.V.** Notre-Dame : AIAA, 2000.

4. *Design, Fabrication, Analysis and Testing of a Micro Vehicle Propeller.* **Smedresman, Adam, Yeo, Derrick and Shyy, Wei.** Hawaii : AIAA, 2011. AIAA 2011-3817.

5. **Christopher, Lyon A, et al.** *Summary of Low-Speed Airfoil Data.* Virginia : SoarTech Publication, 1997.

6. **Joseph, Herrig, Emery James and Erwin John.** *Effct of Section Thickness and Trailing-edge Radius on the Performance of NACA 65-series Compressor Blades in Cascade at Low Speeds.* Washington : National Advisory Committee for Aeronautics, 1951.

7. **Drela, Mark.** XFOIL: An Analysis and Design System for Low Reynolds Number Airfoils. [ed.] T.J Muller. 1989, Vol. 54.

8. **McCormick, Barnes.** *Aerodynamics of V/STOL Flight.* London : Academic Press INC., 1967.

9. **Michael, Selig, et al.** *Summary of Low-Speed Airfoil Data.* Virginia : SoarTech, 1995. Vol. 1.

10. **Michael, Selig, et al.** *Summary of Low-Speed Airfoil Data.* Virginia : SoarTech Publications, 1996. Vol. 2.

11. **Michael, Selig, Donovan and Fraser.** *Airfoils at Low Speeds.* Virginia : H A Stokely, 1989.

12. *Design of Propeller for Motor Soarers.* **Larrabee, Eugene.** 1980, pp. 285 - 303.

13. **J, Kunz P.** *Aerodynamics and Design for Ultra-Low Reynolds Number Flight.* Stanford University. 2003. Dissertation.

14. *Blade Element Momentum Modeling of Low-Re Small UAS Electric Propulsion Systems.* **Mccrink, Mathew and Gregory, James W. .** Texas : AIAA, 2015. 33rd AIAA Applied Aerodynamics Conference.

15. **Snel, H, Bosschers, J and Houwink , R .** *Sectional prediction of lift coefficients on rotating wind turbine blades in stall.* Nederland : Petten Netherlands Energy Research Foundation ECN, 1993.

16. *Development and application of an improved blade element momentum method model on horizontal axis wind turbines.* **Su Liu and Janajreh, Isam.** Berlin : Springer Berlin Heidelberg, 2012, International Journal of Energy and Environmental Engineering. 2251-6832.

17. *Experimental and Numerical Investigations of Three-Dimensional Flows around Propellers in Low-Reynolds Number Flows.* **Yonezawa, Koichi, et al.** 2014, JSASS Aerospace Tech., pp. 65 - 70.

18. *Theoretical and Experimental Power from Large Horizontal Axis Wind Turbines.* **Viterna, A and Janetzke, D.** s.l. : DOE/NASA-LeRC, 1980.

19. *Design of Optimum Propellers.* **Charles, Adkin and Liebeck, Robert.** 1994, Journal of Populsion and Power.

20. **Betz, Albert.** *The Theory of the Screw propeller.* s.l. : National Advisory Committee for Aeronautics, 1921.

21. *On the Vortex Theory of Screw Propellers.* **Goldstein, Sydney.** s.l. : Royal Society Publishind, 1929.

22. **Drela, Mark.** qprop_theory.pdf. [Online] 06 2006. [Cited: 10 03 2016.] http://web.mit.edu/drela/Public/web/qprop/qprop_theory.pdf.

23. **Drela, Mark and Youngren, Harold.** Xrotor_doc.txt. [Online] 13 11 3003. [Cited: 28 02 2016.] web.mit.edu/drela/Public/web/xrotor/xrotor_doc.txt.

24. *Test, Analysis and Design of Propeller propulsion Systems for MAVs.* **Youngren, Harold.** Florida : AIAA, 2011. AIAA 2011-876.

25. *Reynolds Number Effects on the performance of Small-scale Propellers.* **Deters, Robert, Ananda, Gavin and Selig, Michael.** Georgia : AIAA, 2014. 2014-2151.

26. *Development of the Black Widow Micro Air vehicle.* **Grasmeyer, Joel and Keennon, Mathew.** Nevada : AIAA, 2001. 2001-0127.

27. *The Design of Airfoils at Low Reynolds Numbers.* **Michael, Selig.** Nevada : AiAA, 1985. 85-0074.

28. **Michael, Selig and Ananda, Gavin.** UIUC Propeller Database - Volume 1. *University of Illinois Urbana Champaign.* [Online] 11 01 2015. [Cited: 22 06 2017.] http://m-selig.ae.illinois.edu/props/volume-1/propDB-volume-1.html.

29. **Christopher, Lyon A, et al.** *Summary of Low-Speed Airfoil Data.* Virginia : SoarTech Publication, 1997. Vol. 3.

8 Appendices

8.1 Appendix 1

```
%%%%%%%%%%%%%%%%%%%%%%%%%%%%%%%%%%%%%%%%%%%%%%%%%%%%%%%%%%%%%%%%%%%%%%%%%%
%%%%%%%%%%%%%%%%%%%%%%%%
% ======== Arbitrary Propeller geometry Performance Analysis
=====================                    %
%      Reuben Umunna Jikeme 2019
%
% This file determines the performance of an arbitrary geometry of a
propeller.It outputs
% the lateral 2D propeller geometry.
%
%
% References:
%  [1] Chales Adkins and Robert Liebeck "Design of Optimum Propellers"
1994
%
%  [2] E E Larrabee "DESIGN OF PROPELLERS FOR MOTORSOARERS"
%
%%%%%%%%%%%%%%%%%%%%%%%%%%%%%%%%%%%%%%%%%%%%%%%%%%%%%%%%%%%%%%%%%%%%%%%%%%
%%%%%%%%%%%%%%%%%%

global SD7037


clc
clear all
Arb_Blade   =   input ('Input arbitrary blade shape file in single
quotes:  ');  %
Arb_Blade = strcat(Arb_Blade,csv);
Bshape = csvread(Arb_Blade);
Nelements =  length(Bshape);
r2R = Bshape(1:Nelements,1);
c2R = Bshape(1:Nelements,2);
pitch = (pi/180)*Bshape(1:Nelements,3);
PitchD = Bshape(1:Nelements,3);
Bshape = [r2R c2R pitch];


Rt   =   input ('Input Propeller tip radius. (m):  ');
Nb   =   input ('Input the number of blades.:  ');

zeta = 0;
stop = 0;
count = 0;
i = 0;

%%%%%%%%%%%%%%%%%%%%%%%%%%%%%%%
```

```
%  2D airfoil charateristics    %
%%%%%%%%%%%%%%%%%%%%%%%%%%%%%%%%

a0 = 0.0907*180/pi ;       % Lift curve slope /deg
Cl0 = 0.2143;        % Cl when angle of attack = 0
Clmax = 1.15;        % Maximum Cl
Clmin = 0.12;        % Minimum Cl

Cdmin0 = 0.022 ;     % Minimum Cd
b = 0.0318;          % d(Cd)/d(Cl^2)
Clmin0 = 0.103;      % Cl at minimum cdmin
f_Re = -0.4;
Re_ref = 20000;      % Reference reynolds number 2D airfoil data was
collected

%%%%%%% Beginning of Calculations %%%%%%%%%%%%%%%%%%%%%%%%%%%%%%%%%%%
atmaltitude =   100; % input ('Altitude (meters): ');

[atmtemperature, atmpressure, atmdensity,atmVsound, atmviscosity] =
AtmosProp(atmaltitude);

y_location = r2R.*Rt;

dy_location = [y_location;Rt];

for m = 1:30
    dy(m,:) = dy_location(m+1) - dy_location(m);
end


Off_perf   =   input ( ['Choose between Velocity sequence or angular
velocity sequence', ...
    '\n 1 = Velocity sequence,   2 = angular velocity sequence:    ']);

if Off_perf == 1

    V_Ini   =   input ('Input initial Vel. (m/s):  ');
    V_Fin   =   input ('Input final Vel. (m/s):  ')  ;
    V_inc   =   input ('Input increment Vel. (m/s):  ');
    blade_omega = input('Rotational Rate (RPM): '); %4000;
    blade_omega_Ini = blade_omega;
    blade_omega_Fin = blade_omega;
    blade_omega_Inc = blade_omega/blade_omega;

elseif Off_perf == 2
    blade_omega_Ini   =   input ('Input initial angular Vel. (RPM):  ');
    blade_omega_Fin   =   input ('Input final angular Vel. (RPM):  ');
    blade_omega_Inc   =   input ('Input increment angular Vel. (RPM):
');
    V   =   input ('Input initial Vel. (m/s):  ');

    V_Ini = V;
```

```
    V_Fin = V;
    V_inc = V/V;
end

Ask2Save = input('Do you want to save propeller performance data? Y = 1 N
= 0:     ');
Yes = 1;
No  = 0;
if Ask2Save == 1

    savefolder_name     = 'Type the folder name:     ';
    savefolder_name_str = input(savefolder_name,'s');
    savefolder          = strcat(savefolder_name_str,'/');
    mkdir(savefolder);
    Propname = savefolder_name_str;
    csv = '.csv';

elseif Ask2Save == 0
    disp('Propeller data would not saved')

end

    for V = V_Ini:V_inc:V_Fin
        for blade_omega = blade_omega_Ini:blade_omega_Inc:blade_omega_Fin

     i = i + 1;
     Vel(i,:) = V;
     blade_RPM(i,:)   = blade_omega;

    bladeomega = (2*pi*blade_omega/60);
    lambda = (V/(bladeomega*Rt)).*r2R;
    x = (bladeomega.*y_location)./V;
    V_R = sqrt(V.^2 + ((bladeomega.*y_location).^2));


   Phi_tip = atan(lambda(Nelements,1)*(1+zeta/2));

phi = atan([tan(Phi_tip)./r2R]);

Phi_rad = phi;


while stop == 0


for N = 1:Nelements


AoA(N,:) = pitch(N,1)- Phi_rad(N,1);
AoA_deg = AoA*180/pi;
```

```
f(N,:) = (Nb/2).*(1-r2R(N))./tan(Phi_tip);    % this uses Glaucert
sin(phi_tip)
F(N,:) = (2./pi).*acos(exp(-1.*(f(N))));




%%%%%%% 2D Airfoil characteristics calculation
%%%%%%%%%%%%%%%%%%%%%%%%%%%%

% [C_L, C_D] = AerodynamicCoefficientx()

c(N,:) = c2R(N).*Rt;
Re(N,:) = atmdensity.*V_R(N,1).*c(N)/atmviscosity;

AeroCoeff = AeroCoefficientx( AoA(N), Re(N));

Cl(N,:) = AeroCoeff(1);
Cd(N,:) = AeroCoeff(2);
e(N,:) = Cd(N)./Cl(N);


Cy(N,:) = Cl(N).*(cos(Phi_rad(N,1)) - e(N).*sin(Phi_rad(N,1)));
Cx(N,:) = Cl(N).*(sin(Phi_rad(N,1)) + e(N).*cos(Phi_rad(N,1)));
K(N,:) = Cy(N)./(4.*sin(Phi_rad(N,1)).^2);
Kprime(N,:) = Cx(N)./(4.*sin(Phi_rad(N,1)).*cos(Phi_rad(N,1)));
sigma(N,:) = (Nb.*c(N))./(2.*pi.*r2R(N).*Rt);

% Uprime = 1;

a(N,:) = (sigma(N).*K(N))./(F(N) - sigma(N).*K(N));

alim = 0.001;
if a(N) > alim
    a(N,:) = alim;
    if a(N) < -1*alim
      a(N,:) = -1*alim;
    end
end

aprime(N,:) = (sigma(N).*Kprime(N))./(F(N) + sigma(N).*Kprime(N));
if aprime(N) > alim
    aprime(N,:) = alim;
    if aprime(N) < -1*alim
      aprime(N,:) = -1*alim;
    end
end

%%%%% Proposed correction of induced velocities %%%%%
va = V.*a;
```

```
wa = 2.*va;
vt = (blade_omega./60).*r2R(N).*Rt.*aprime;
wt = 2.*vt;

adv_R = V/((blade_omega./60)*Rt*2);

VA = wa.*(3.1*adv_R^2 - 3.3*adv_R + 1.77);
VT = wt.*(3.0*adv_R^2 - 3.2*adv_R + 1.88);




%%%% Correction included of induced velocities in iteration %%%%
W(N,:) = (V + VA(N))./sin(Phi_rad(N,1));
PhiNew(N,1) = atan((V + VA(N))./(bladeomega.*r2R(N).*Rt - VT(N)));

if abs(Phi_rad(N,1) - PhiNew(N,1))<0.001
    stop = 1;

 end;
 count = count + 1;
 if (count>1000)
    stop = 1;
    disp(' Maximum number of iterations exceeded')
    end;
     Phi_rad(N,:) = PhiNew(N,1);
end;
end



%%%%%% Classical
dL1 = 0.5.*atmdensity.*(V_R).^2.*c.*Cl.*dy;
        dD1 = 0.5.*atmdensity.*(V_R).^2.*c.*Cd.*dy;

        dT = Nb.*(dL1.*cos(Phi_rad)-(dD1.*sin(Phi_rad)));
        T(i,:) = sum(dT)

        dQ = 1.4.*Nb.*r2R.*Rt.*(dD1.*cos(Phi_rad) + (dL1.*sin(Phi_rad)));
%          Q(i,:) = sum(dQ)
         P(i,:) = (sum(dQ).*bladeomega)
Ct(i,:) = sum(dT./(atmdensity.*(blade_omega./60).^2.*(2.*Rt).^4))
Cp(i,:) = P(i)./(atmdensity.*(blade_omega./60).^3.*(2.*Rt).^5)
J(i,:) =V*60/(blade_omega*2*Rt)
Effi(i,:) = (T(i).*V)./(P(i))



if Off_perf == 1  && Ask2Save == 1
```

```
    filename =
strcat(Propname,'_','Vel',int2str(V),'_','RPM',int2str(blade_omega),csv);




elseif Off_perf == 2 && Ask2Save == 1
    filename =
strcat(Propname,'_','RPM',int2str(blade_omega),'_','Vel',int2str(V),csv);

end

filename_Data = strcat(filename,'_Data.txt');
     outfile   = strcat(savefolder,filename_Data);
    fid = fopen(outfile,'wt');

    fprintf(fid,'\t\t %s \n\n',filename_Data);
    fprintf(fid,'\t\t Propeller off performance data \n\n');

    fprintf(fid,'Propeller tip radius \t = %.4f m\n',    Rt);
    fprintf(fid,'Number of Blades     \t = %.0f\n',       Nb);
    fprintf(fid,'Propeller Speed      \t = %.0f RPM\n',    blade_omega);
    fprintf(fid,'Airspeed Speed       \t = %.4f m/s\n',    V);
    fprintf(fid,'Advance ratio        \t = %.4f \n',    J(i));
    fprintf(fid,'Power                \t = %.4f W\n',    P(i));
    fprintf(fid,'Thrust               \t = %.4f N\n',    T(i));

     fprintf(fid,' \n');
    fprintf(fid,' \n');

    %%% ==========================Atmospheric
data=============================================================%%
    fprintf(fid,'\t\t Propeller atmospheric data \n\n');

    fprintf(fid,'Altitude        \t = %.4f m\n',    atmaltitude);
    fprintf(fid,'Density         \t = %.4f kg/m^3\n',    atmdensity);
    fprintf(fid,'Speed of Sound  \t = %.4f m/s\n',    atmVsound);
    fprintf(fid,'Viscosity       \t = %.9f m/s^2\n',    atmviscosity);



 fprintf(fid,' \n');
    fprintf(fid,' \n');



    fprintf(fid,'No    r/R    c/R      Beta     Cl     Cd/Cl     Re\t
a\t  aprime\t\n');
    fprintf(fid,'\t   \t     \t      \t       \t    \t  \n');
```

```
    for k = 1:Nelements

        fprintf(fid, '%2.0f   %5.4f  %5.4f  %5.4f  %5.4f  %5.4f  %5.2f
%1.5f  %1.5f\n',...
                k,
r2R(k),c2R(k),PitchD(k),Cl(k),e(k),Re(k),a(k),aprime(k));

    end

    fprintf(fid,' \n\n');
    fprintf(fid,'Coefficient of thrust (Ct)  \t  = %.4f \n',    Ct(i));
    fprintf(fid,'Coefficient of power (Cp)   \t  = %.4f \n',    Cp(i));
    fprintf(fid,'Efficiency                  \t  = %.4f \n',    Effi(i));
    fclose(fid);


zeta = 0;
stop = 0;
count = 0;
clear AoA  Re e Cy Cx K Kprime a aprime W Phi_rad PhiNew %Ct CtPrime Cp
Effi T P
    end
    end

    SaveOrNot = input('Do you want to save off-performance data? Y = 1 N
= 0:    ');
Yes = 1;
No  = 0;

if SaveOrNot == 1
    filename = strcat(Propname,csv);

    filename_Data = strcat(filename,'_Data.txt');
     outfile   = strcat(savefolder,filename_Data);
    fid = fopen(outfile,'wt');

    fprintf(fid,'\t\t %s \n\n',filename_Data);
    fprintf(fid,'\t\t Propeller off performance data \n\n');


    fprintf(fid,'Propeller tip radius \t = %.4f m\n',    Rt);
    fprintf(fid,'Number of Blades     \t = %.0f\n',        Nb);


     fprintf(fid,' \n');
     fprintf(fid,' \n');

    %%% Atmospheric data%%
    fprintf(fid,'\t\t Propeller atmospheric data \n\n');
```

```
    fprintf(fid,'Altitude          \t = %.4f m\n',    atmaltitude);
    fprintf(fid,'Density           \t = %.4f kg/m^3\n',    atmdensity);
    fprintf(fid,'Speed of Sound    \t = %.4f m/s\n',    atmVsound);
    fprintf(fid,'Viscosity         \t = %.9f m/s^2\n',    atmviscosity);



    fprintf(fid,' \n');
    fprintf(fid,' \n');



    fprintf(fid,'No    V     RPM       J      Ct      Cp       Eff
Thr    Pow\t\n'); %
    fprintf(fid,'     \t     \t     \t      \t       \t    \t  \n');

     if Off_perf ==1;
      Nos =  ((V_Fin - V_Ini)/V_inc)+1;

     elseif Off_perf ==2;
      Nos = ((blade_omega_Fin - blade_omega_Ini)/ blade_omega_Inc )  +1;
     end


    for k = 1:Nos

        fprintf(fid, '%2.0f  %5.2f  %5.2f  %5.4f  %5.4f  %5.4f  %5.4f
%5.4f  %5.2f\n',...

k,Vel(k),blade_RPM(k),J(k),Ct(k),Cp(k),Effi(k),T(k),P(k));

    end

    fclose(fid);

elseif SaveOrNot == 0
    disp('Propeller data would not saved')
end




%%% Blade performance plot
PlotOrNot = input('Do you want to plot experiment data data? Y = 1 N = 0:
');
Yes = 1;
No  = 0;

[Jplot, Num] = PerfPlot(J, Ct, Cp, Effi, Nos, Off_perf, Propname,
PlotOrNot);
outfile2   = strcat(savefolder,Propname);
saveas(Num,outfile2,'pdf')
```

```
%%% Blade geometry Plot
[LE, TE ] = BladeGeometry(r2R, c2R, Nb);
```

8.2 Appendix 2

```
%%%%%%%%%%%%%%%%%%%%%%%%%%%%%%%%%%%%%%%%%%%%%%%%%%%%%%%%%%%%%%%%%%%%%%%%%%%%%%%%
%%%%%%%%%%%%%%%%%%%%%%%%
% ======== Atmospheric model  ======================             %
%                            Reuben Umunna Jikeme 2019
%
% This function is used to estimate the atmospheric condition where
% propeller is to operate
%

%%%%%%%%%%%%%%%%%%%%%%%%%%%%%%%%%%%%%%%%%%%%%%%%%%%%%%%%%%%%%%%%%%%%%%%%%%%%%%%%
%%%%%%%%%%%%%%%%%%

function [atmtemperature, atmpressure, atmdensity,atmVsound,
atmviscosity] = AtmosProp(atmaltitude);


%%%%%%%%%%%%%%%%%%%%%%%%%%%%%%
%Constants
%%%%%%%%%%%%%%%%%%%%%%%%%%%%%%
gamm = 1.4;                         %Air Constant
R = 286;                            %
atmviscosity = 1.7332*10^-5;        %Standard Viscosity of Air
%%%%%%%%%%%%%%%%%%%%%%%%%%%%%%%%%%%%%%%%%%%%%%%%%%%%%%%%%%%%%%%%%%%%%%%%%%%%%%%%


if atmaltitude >= 25000
    atmtemperature = (-131.21 + 0.00299*atmaltitude)
%Temperature [deg C]
    atmpressure = 2.488*(atmtemperature + 273.1/216.6)^-11.388;
%Pressure [Kpa]
    atmdensity = atmpressure/(0.2869*atmtemperature) ;
%Density [kg/m^3]
    atmVsound = sqrt(gamm*(atmtemperature+ 273.1)*R);
%Speed of Sound [m/s]
end


if atmaltitude <= 11000
    atmtemperature = (15.04-0.00649.*atmaltitude);
%Temperature [deg C]
    atmpressure = 101.29.*((atmtemperature +273.1)./288.8).^5.256;
%Pressure [Kpa]
    atmdensity = atmpressure./(0.2869.*(atmtemperature+273.1)) ;
%Density [kg/m^3]
    atmVsound = sqrt(gamm*(atmtemperature +273.1)*R);
%Speed of Sound [m/s]

end

if atmaltitude >= 11000
```

```
    if atmaltitude <= 25000
        atmtemperature = -56.46
%Temperature [deg C]
        atmpressure = 22.65*exp(1.73 - (0.000157*atmaltitude));
%Pressure [Kpa]
        atmdensity = atmpressure/(0.2869*(atmtemperature+273.1)) ;
%Density [kg/m^3]
        atmVsound = sqrt(gamm*(atmtemperature +273.1)*R);
%Speed of Sound [m/s]
    end
end
```

8.3 Appendix 3

```
function AeroCoeff = AeroCoefficientx( AoA, Re)
%#codegen

global SD7037

    C_L          = csvread('SD7037_Aero_CL.csv');
    C_D    = csvread('SD7037_Aero_CD.csv');


    alpha_deg    = 180/pi*AoA;
    Rey_No       = Re;

    cl           = interpter2(      C_L, Rey_No, alpha_deg);
    cd           = interpter2(      C_D, Rey_No, alpha_deg);



AeroCoeff = [cl;  cd;];
end
```

8.4 Appendix 4

```
function [C_L, C_D] = AerodynamicCoefficientx()

    C_L          = csvread('SD7037_Aero_CL.csv');
    C_D    = csvread('SD7037_Aero_CD.csv');


    AoA_min    = min(CL(2:end,1));
    AoA_max    = max(CL(2:end,1));
    Re_min     = min(CL(1,2:end));
    Re_max     = max(CL(1,2:end));

end
```

8.5 Appendix 5

```
function idx = BinarySearch(x,xi)

n = numel(x);
maxLength = n + 1;
ax = 2;

if xi < x(1)
    dx = 1;
elseif x(n) <= xi
    dx = n-1;
else
    dx = floor(maxLength / 2);

    while xi < x(dx) || x(dx + 1) <= xi
        ax = ax * 2;
        step = floor(maxLength / ax);
        if step < 1
        step = 1;
          if xi < x(dx)
              dx = dx - step;
          else
              dx = dx + step;
          end
        end
    end
end

idx = dx;
```

8.6 Appendix 6

```
%%%%%%%%%%%%%%%%%%%%%%%%%%%%%%%%%%%%%%%%%%%%%%%%%%%%%%%%%%%%%%%%%%%%%%%%%%%%%%%%
%%%%%%%%%%%%%%%%%%%%%%%%
% ======== Propeller geometry Plot  ====================              %
%               Reuben Umunna Jikeme 2019
%
% This function plots the 2D geometry of a propeller
%%%%%%%%%%%%%%%%%%%%%%%%%%%%%%%%%%%%%%%%%%%%%%%%%%%%%%%%%%%%%%%%%%%%%%%%%%%%%%%%

function [ LE, TE ] = BladeGeometry(r2R, c2R, Nb )

Rx=0;
Ry=0;
Rh = r2R(1);
th = 0:pi/50:2*pi;
xunit = Rh * cos(th) + Rx;
yunit = Rh * sin(th) + Ry;

LE = c2R.*0.25;
TE = c2R.*-0.75;

figure(2)
plot(xunit,yunit,'-k',r2R,LE,'-k',r2R,TE,'-k','LineWidth',2)
hold on

if Nb >= 2
    for i = 2:Nb
New_XLE(i,:) = r2R.*cos((i-1).*2.*pi./Nb) - LE.*sin((i-1).*2.*pi./Nb);
New_YLE(i,:) = r2R.*sin((i-1).*2.*pi./Nb) + LE.*cos((i-1).*2.*pi./Nb) ;

New_XLE_2(i,:) = r2R.*cos((i-1).*2.*pi./Nb) - TE.*sin((i-1).*2.*pi./Nb);
New_YLE_2(i,:) = r2R.*sin((i-1).*2.*pi./Nb) + TE.*cos((i-1).*2.*pi./Nb);

plot(New_XLE(i,:),New_YLE(i,:),'-k',New_XLE_2(i,:),New_YLE_2(i,:),'-
k','LineWidth',2)
if Nb <= 2
    pbaspect([5 1 1])
else
axis square
end
    end
end
end
```

8.7 Appendix 7

```
function [] = CreateFile(Yes, No);

if Yes == Ask2Save

    savefolder_name     = 'Type the propeller name : ';
    savefolder_name_str = input(savefolder_name,'s');
    savefolder          = strcat(savefolder_name_str,'/');
    mkdir(savefolder);
    Propname = savefolder_name_str;

    csv = '.csv';
    filename = strcat(Propname,csv);
    data_str  = {'r2R','c2R','Pitch','f_tip','F', 'phi'};
    Bshape = [r2R c2R Bpitch f F phi];
    Value_c   =  num2cell(Bshape);
    Simu_data   = cell2table(Value_c,'VariableNames',data_str);
    outfile   = strcat(savefolder,filename);
    writetable(Simu_data, outfile);

    file = strcat(savefolder,'/',Propname,csv);
    Array = readtable(file,'ReadRowNames',false);
    pitch = Array(1:30, 3);
    csvwrite(filename,Bshape)

else
    if No == Ask2Save
        disp('Propeller data not saved')
    end

end
```

8.8 Appendix 8

```
%%%%%%%%%%%%%%%%%%%%%%%%%%%%%%%%%%%%%%%%%%%%%%%%%%%%%%%%%%%%%%%%%%%%%%%%%%%%%%%%%%%%%%%%%%%%%%%%%%%%%%%
% ======== Propeller Performance Plots  =====================
%
%              Reuben Umunna Jikeme 2019
%
% This function plots the performance parameter Ct, Cp and Efficiency Vs
Advance ratio of the propeller
%
%

%%%%%%%%%%%%%%%%%%%%%%%%%%%%%%%%%%%%%%%%%%%%%%%%%%%%%%%%%%%%%%%%%%%%%%%%%%%%%%%%%%%%%%%%%%%%%%%%%

function [Jplot, Num ] = PerfPlot(J, Ct, Cp, Effi, Nos, Off_perf,
Propname, PlotOrNot)

Num = 1;
if Off_perf == 1
    incre = 0.025;
    JMax = J(Nos) + 0.1;
    JMin = J(1) -  0.1;

elseif Off_perf == 2
    incre = -0.025;
    JMax = J(1) +  0.1;
    JMin = J(Nos) - 0.1;
end

Jplot = J(1):incre:J(Nos);
Ct_plot = spline(J,Ct,Jplot);
Cp_plot = spline(J,Cp,Jplot);
Effi_plot = spline(J,Effi,Jplot);


if PlotOrNot == 0

plot (Jplot, Ct_plot,'--',Jplot, Cp_plot,'-.','LineWidth',1.5);
xlabel('Advance Ratio (J)')
ylabel('C_t, C_p')
set(gca,'FontName','Arial','Fontsize',16,'FontWeight','bold');
set(gca,'XLim',[JMin JMax],'YLim',[0 1]);
yticks([0:0.2:1]);
%xtickformat('%.2f')
hold on

yyaxis right
plot(Jplot,Effi_plot,'-m','LineWidth',1.5)

ylim([0 1])
```

```
yticks([0:0.2:1]);

ylabel('Efficiency \eta')
set(gca,'FontName','Arial','Fontsize',16,'FontWeight','bold');
set(gca,'ycolor','k');

grid on
grid minor
legend('Ct','Cp','Effi','location', 'NorthWest')
hold on

end



if PlotOrNot == 1
ExpData = input('For SDL20Y = 1, SDL20Y-2 = 2, SDL18Y = 3,  Read new file
= 4:      ');

if ExpData == 1
ExpData = 'SDL20Y_Exp';  % Experiment CSV data order: J Thrust Ct Power
Cp Efficiency

elseif ExpData == 2
ExpData = 'SDL20Y_2_Exp'; % Experiment CSV data order: J Thrust Ct Power
Cp Efficiency

elseif ExpData == 3
ExpData = 'SDL18Y_Exp'; % Experiment CSV data order: J Thrust Ct Power Cp
Efficiency

elseif ExpData == 4
ExpData    =    input ('Input arbitrary blade shape file in single quotes:
');
end

csv = '.csv';

file = strcat(ExpData,csv);
Array = dlmread(file);
J_exp = Array(1:end,1);
T_exp = Array(1:end,2);
Ct_exp = Array(1:end,3);
P_exp = Array(1:end,4);
Cp_exp = Array(1:end,5);
Effi_exp = Array(1:end,6);



figure(Num)
plot (Jplot, Ct_plot,'--k', J_exp, Ct_exp,'*k',Jplot, Cp_plot,'-
.k',J_exp, Cp_exp,'<k','LineWidth',1.5);
```

```
xlabel('Advance Ratio (J)')
ylabel('C_t, C_p')
set(gca,'FontName','Arial','Fontsize',16,'FontWeight','bold');

set(gca,'XLim',[JMin JMax],'YLim',[0 1]);
yticks([0:0.2:1]);
%xtickformat('%.2f')
hold on

yyaxis right
plot(Jplot,Effi_plot,'-k',J_exp,Effi_exp,'sk','LineWidth',1.5)

ylim([0 1])
yticks([0:0.2:1]);

ylabel('Efficiency \eta')
set(gca,'FontName','Arial','Fontsize',16,'FontWeight','bold');
set(gca,'ycolor','k');

grid on
grid minor
legend('Ct','Ct_e_x_p','Cp','Cp_e_x_p','Effi','Effi_e_x_p','location',
'NorthWest')
hold on


end
end
```

8.9 Appendix 9

```
%%%%%%%%%%%%%%%%%%%%%%%%%%%%%%%%%%%%%%%%%%%%%%%%%%%%%%%%%%%%%%%%%%%%%%%%%
%%%%%%%%%%%%%%%%%%%%%%%%
% ======== Arbitrary Propeller geometry Performance Analysis
=====================             %
%     Reuben Umunna Jikeme 2019
%
% This file determines the performance of an arbitrary geometry of a
propeller.It outputs
% the lateral 2D propeller geometry.
%
%
% References:
%  [1] Chales Adkins and Robert Liebeck "Design of Optimum Propellers"
1994
%
%  [2] E E Larrabee "DESIGN OF PROPELLERS FOR MOTORSOARERS"
%
%%%%%%%%%%%%%%%%%%%%%%%%%%%%%%%%%%%%%%%%%%%%%%%%%%%%%%%%%%%%%%%%%%%%%%%%%
%%%%%%%%%%%%%%%%%%

clear all;
clc;

%%%%%%%%%%%%%%%%%%%%%%%%%%%%%%%
%  2D airfoil charateristics    %
%%%%%%%%%%%%%%%%%%%%%%%%%%%%%%%

a0 = 0.0907 ;       % Lift curve slope /deg
Cl0 = 0.2143;       % Cl when angle of attack = 0
Clmax = 1.15;       % Maximum Cl
Clmin = 0.12;       % Minimum Cl

Cdmin0 = 0.022 ;    % Minimum Cd
b = 0.0318;         % d(Cd)/d(Cl^2)
Clmin0 = 0.103;     % Cl at minimum cdmin
f_Re = -0.4;
Re_ref = 20000;     % Reference reynolds number 2D airfoil data was
collected

%%%%%%%%%%%%%%%%%%%%%%%%%%%%%%%
%  Variable Initialization    %
%%%%%%%%%%%%%%%%%%%%%%%%%%%%%%%
stop = 0;
count = 1;

zeta = 0.5;
atmaltitude = 100;

%%%%%%%%%%%%%%%%%%%%%%%%%%%%%%%
%Beginning of the Main Program%
```

```
%%%%%%%%%%%%%%%%%%%%%%%%%%%%%%%%
[atmtemperature, atmpressure, atmdensity,atmVsound, atmviscosity] =
AtmosProp(atmaltitude);

%%%%%%% Determine the Blade Parameters %%%%%%%%%%%%%%%%%%%%%%%%%%%%%%%%

Nelements       = input ('Number of Elements: ');
Nb         = input ('Number of Blades: ');
Rt     = input ('Blade Radius (meters): ');
Rh =input ('Blade Hub Radius (meters): ');

blade_omega = input('Rotational Rate (RPM): ');
V = input('flight velocity (m/s): ');
Cl = input('input a constant lift coefficient: ');
P = 0;
T = 0;

PorT    =    input ('Include Power or Thrust:    (1 = Power,     2 = Thrust)
');

if PorT == 1
    P    =    input ('Power (Watts):   ');
    Pc = 2*P/(atmdensity*V^3*pi*Rt^2);

elseif  PorT == 2
    T    =    input ('Thrust (N):   ');
    Tc = 2*T/(atmdensity*V^2*pi*Rt^2);

end

bladeomega = (2*pi*blade_omega/60);                          %RPM -> RPS
Vtip = Rt*bladeomega;  %Rotor Tip Speed

Cl = Cl.*ones([Nelements,1]);

%%%%%%% Calculation of Element Properties %%%%%%%%%%%%%%%%%%%%%%%%%%%%%%%
dy = (Rt-Rh)/Nelements;
dr = (1/Nelements);

for i = 1:Nelements
    y_location(i,:)   = Rh+dy.*(i-1);
    r2R(i,:)             = y_location(i)./Rt;
end

x = (bladeomega.*y_location)./V;
V_R = sqrt(V^2 + (bladeomega.*y_location).^2);

r2R_tip = r2R(Nelements,1);
lambda = (V/(bladeomega*Rt)).*r2R;

while stop == 0
```

```
    Phi_tip = atan(lambda(Nelements,1)*(1+zeta/2));  % think more about
what exactly should be phi tip

    phi = atan([tan(Phi_tip)./r2R]);

    f = (Nb/2).*(1-r2R)./sin(Phi_tip);
    F = (2./pi).*acos(exp(-1.*(f)));
    G  = F.*cos(phi).*sin(phi);

    Wc = 70.*4.*pi.*V.*Rt.*zeta.*lambda.*G./(Cl*Nb);
    c2Rt = 4.*pi.*zeta.*lambda.*G./(sqrt(x.^2 + 1).*Cl*Nb);
    Vc = Wc;   % m^2/s
    KinVsou = atmviscosity/atmdensity;  % m^2/s
    Re = atmdensity.*Wc./atmviscosity

    %%%%%%% 2D Airfoil characteristics calculation
%%%%%%%%%%%%%%%%%%%%%%%%%%%%%

    AoA = (Cl - Cl0)./a0;  % AoA in deg
    Cd = abs(Cdmin0 + (b.*(Clmin0-Cl).^2)).*(Re./Re_ref).^f_Re;
    e = Cd./Cl;

    %%%%%%% impact factor calculation %%%%%%%%%%%%%%%%%%%%%%%%%%%%
    Vavg = 2;
    a = (zeta/Vavg).*cos(phi).^2    %.*(1-e.*tan(phi));
    aPrime = (zeta./(Vavg.*x)).*cos(phi).*sin(phi)    %.*(1+e./tan(phi));

    %%%%%%% Blade parameters calculation %%%%%%%%%%%%%%%%%%%%%%%%%%%%
    W = (V.*(1+a))./sin(phi);
    V1 = V.*(1+a);
    c = 1000.*Wc./W;
    Re2 = atmdensity.*V_R.*c./(1000.*atmviscosity)
    c2R = c./(Rt.*1000);
    Bpitch = AoA+(phi.*180./pi);

    [I11, I22, J11, J22] = Derivatives(r2R, G, e, phi, lambda);

    %%%%%%% Blade parameters calculation %%%%%%%%%%%%%%%%%%%%%%%%%%%%

    if PorT == 2
        zetaNew = (I11/(2*I22)) - sqrt((I11/(2*I22))^2 - (Tc/I22))
        Pc = J11*zetaNew + J22*(zetaNew^2);
    end

    if PorT == 1
        zetaNew = (-J11/(2*J22) + sqrt((J11/(2*J22))^2 + (Pc/J22)));
        Tc = I11*zetaNew - I22*(zetaNew^2);
    end

    if abs(zetaNew-zeta)<0.1
        stop = 1;
    end;
```

```
    zeta = zetaNew;
    count = count + 1;
    if (count>100)
        stop = 1;
        disp('count exceeded')
    end;
end;
J =V*60/(blade_omega*2*Rt)
P = Pc*atmdensity*V^3*pi*Rt^2/2
Pc
Tc
Ct = T/(atmdensity*(blade_omega/60)^2*(2*Rt)^4);
Cp = P/(atmdensity*(blade_omega/60)^3*(2*Rt)^5);
Effi = Tc/Pc


Ask2Save = input('Do you want to save propeller name? Y = 1 N = 0:     ');
Yes = 1;
No  = 0;
if Ask2Save == 1

    savefolder_name     = 'Type the propeller name:    ';
    savefolder_name_str = input(savefolder_name,'s');
    savefolder          = strcat(savefolder_name_str,'/');
    mkdir(savefolder);
    Propname = savefolder_name_str;

    csv = '.csv';
    filename = strcat(Propname,csv);

    filename_Data = strcat(filename,'_Data.txt');
     outfile   = strcat(savefolder,filename_Data);
    fid = fopen(outfile,'wt');

    fprintf(fid,'\t\t %s \n\n',filename_Data);
    fprintf(fid,'\t\t Propeller off performance data \n\n');

    fprintf(fid,'Propeller tip radius \t = %.4f m\n',    Rt);
    fprintf(fid,'Number of Blades     \t = %.0f\n',       Nb);
    fprintf(fid,'Propeller Speed      \t = %.0f RPM\n',    blade_omega);
    fprintf(fid,'Airspeed Speed       \t = %.4f m/s\n',    V);
    fprintf(fid,'Advance ratio        \t = %.4f \n',     J);
    fprintf(fid,'Power                \t = %.4f W\n',     P);
    fprintf(fid,'Thrust               \t = %.4f N\n',     T);
    fprintf(fid,'Cp                   \t = %.4f N\n',     Cp);
    fprintf(fid,'Ct                   \t = %.4f N\n',     Ct);
    fprintf(fid,'Efficiency           \t = %.4f N\n',     Effi);


     fprintf(fid,' \n');
    fprintf(fid,' \n');
```

```
    %%% ==========================Atmospheric
data=============================================================%%
    fprintf(fid,'\t\t Propeller atmospheric data \n\n');

    fprintf(fid,'Altitude        \t = %.4f m\n',    atmaltitude);
    fprintf(fid,'Density         \t = %.4f kg/m^3\n',    atmdensity);
    fprintf(fid,'Speed of Sound  \t = %.4f m/s\n',    atmVsound);
    fprintf(fid,'Viscosity       \t = %.9f m/s^2\n',    atmviscosity);



 fprintf(fid,' \n');
    fprintf(fid,' \n');

    %%% ====================================Airfoil data
    %%% data%%==================================

    fprintf(fid,'\t\t 2D airfoil data \n\n');
    fprintf(fid,'a0 (Lift curve slope)             \t = %.4f per deg\n',
a0);
    fprintf(fid,'Cl (when angle of attack is zero) \t = %.4f \n',
Cl0);
    fprintf(fid,'Maximum Cl                        \t = %.4f \n',
Clmax);
    fprintf(fid,'Minimum Cl                        \t = %.4f \n',
Clmin);

    fprintf(fid,'Cdmin0  (Minimum Cd)              \t = %.4f \n',
Cdmin0 );
    fprintf(fid,'b (d(Cd)/d(Cl^2))                 \t = %.4f \n',    b);
    fprintf(fid,'Clmin0 (Cl at minimum cdmin)      \t = %.4f \n',
Clmin0);
    fprintf(fid,'Re_ref (Reference reynolds no)    \t = %.2f \n',
Re_ref );


    fprintf(fid,' \n');
    fprintf(fid,' \n');


    fprintf(fid,'No    r/R    c/R      Beta     Cl     Cd/Cl
Re\t\n'); % add mach no
    fprintf(fid,'\t   \t     \t      \t       \t    \t  \n');



    for k = 1:Nelements

        fprintf(fid, '%2.0f   %5.4f  %5.4f  %5.4f  %5.4f  %5.4f
%5.2f\n',...
                k, r2R(k),c2R(k),Bpitch(k),Cl(k),e(k),Re(k));
```

```
    end

    fclose(fid);



elseif Ask2Save == 0
    disp('Propeller data not saved')
end


%%% Plots of blade shape
[LE, TE ] = BladeGeometry(r2R, c2R, Nb);
```

8.10 Appendix 10

```
function [I11, I22, J11, J22] = Derivatives(r2R, G, e, phi, lambda);

I1 = 4.*r2R.*G.*(1 - e.*tan(phi));
I2 = lambda.*(I1./2.*r2R).*(1 + e./tan(phi).*sin(phi).*cos(phi));
J1 = 4.*r2R.*G.*(1 + e./tan(phi));
J2 = (J1./2).*(1 - e.*tan(phi).*cos(phi)).^2;

I11 = sum(I1);
I22 = sum(I2);
J11 = sum(J1);
J22 = sum(J2);
```

8.11 Appendix 11

	5000	10000	15000	20000	25000	30000	35000	40000	45000	50000	55000	60000
0												
-4	0.06074	0.07125	0.06581	0.06087	0.05476	0.05206	0.03043	0.02867	0.02717	0.02587	0.02475	0.02376
-3	0.05422	0.05948	0.04999	0.04519	0.04162	0.03867	0.02645	0.02506	0.02386	0.0227	0.0217	0.02083
-2	0.05093	0.03676	0.03874	0.0338	0.03176	0.03044	0.02284	0.02157	0.02046	0.01951	0.01887	
-1	0.05071	0.03682	0.03083	0.02733	0.02499	0.0233	0.02109	0.01992	0.01894	0.01813	0.01745	0.01687
0	0.05157	0.03801	0.03222	0.02888	0.02667	0.02508	0.02026	0.01905	0.01808	0.01731	0.01666	0.01612
1	0.0533	0.04008	0.03453	0.03137	0.02931	0.02787	0.02087	0.01951	0.01841	0.01752	0.01677	0.01612
2	0.05593	0.04313	0.03788	0.03496	0.03311	0.03182	0.02178	0.02042	0.01933	0.01843	0.01768	0.01704
3	0.05958	0.04733	0.04247	0.03987	0.03826	0.03775	0.02302	0.02166	0.02054	0.01963	0.01889	0.01823
4	0.06439	0.05285	0.04847	0.04624	0.04544	0.04674	0.02463	0.02319	0.02207	0.02116	0.02034	0.01964
5	0.07049	0.05981	0.05593	0.05403	0.05705	0.05399	0.02665	0.02521	0.02401	0.023	0.02215	0.02142
6	0.07794	0.06823	0.06485	0.06321	0.06723	0.06122	0.02928	0.02768	0.02638	0.02531	0.02434	0.02349
7	0.08672	0.07802	0.07517	0.07383	0.07813	0.07002	0.03249	0.03075	0.02936	0.02805	0.02695	0.02603
8	0.09668	0.08904	0.08673	0.08574	0.09104	0.08309	0.03666	0.03478	0.03305	0.03159	0.03041	0.02936
9	0.10758	0.10097	0.09919	0.09921	0.10845	0.09781	0.04202	0.03973	0.03773	0.03606	0.03466	0.03339
10	0.11923	0.11348	0.11217	0.11802	0.1224	0.1153	0.04931	0.0465	0.04413	0.0421	0.04023	0.03864
11	0.13158	0.12651	0.12561	0.14483	0.13766	0.14256	0.05978	0.05631	0.05329	0.05098	0.0486	0.04649
12	0.1447	0.14015	0.14801	0.15817	0.1533	0.15237	0.07451	0.07096	0.06728	0.06421	0.06221	0.06067
13	0.15869	0.15428	0.16382	0.18654	0.18059	0.16762	0.09544	0.09032	0.08699	0.08453	0.08366	0.08228
14	0.17347	0.1695	0.18225	0.19232	0.19075	0.21002	0.12297	0.11588	0.11184		0.10904	0.10805
15	0.18955	0.18618	0.20452	0.20434	0.20176	0.2043	0.15274	0.14552	0.14038		0.13506	0.1342
16	0.20732	0.21781	0.23736	0.22499	0.22103	0.24002	0.17893	0.17582	0.16831		0.1619	0.16026
17	0.22625	0.24428	0.25325	0.26137	0.24026	0.2449	0.20294	0.20141	0.19881		0.1907	0.18818
18	0.24641	0.26365	0.26993	0.29117	0.26154	0.28209	0.22882	0.22663	0.2241	0.22128	0.21947	0.21837
19	0.26766	0.28376	0.28532	0.28303	0.28629	0.27895	0.25282	0.25098	0.24863	0.24748	0.24709	0.24661
20	0.28981	0.31056	0.31429	0.30648	0.32441	0.32826	0.27603	0.27427	0.27285	0.27268	0.27251	0.27234

Figure 8-1: 2D airfoil Lift data (C_L) for SD7037. Angle of Attack vs Reynolds predicted using Xflr-5 at Ncrit = 1

8.12 Appendix 12

	5000	10000	15000	20000	25000	30000	35000	40000	45000	50000	55000	60000
0												
-4	-0.0815	-0.3351	-0.3461	-0.3398	-0.3086	-0.3151	-0.158	-0.152	-0.1448	-0.1373	-0.1302	-0.1235
-3	-0.1239	-0.329	-0.2671	-0.2421	-0.2268	-0.2097	-0.0519	-0.0434	-0.0351	-0.0271	-0.0197	-0.0127
-2	-0.1011	-0.11	-0.1991	-0.1322	-0.1129	-0.1095	0.0563	0.0672	0.0773	0.0864	0.0944	
-1	-0.0248	-0.023	-0.0213	-0.0201	-0.0194	-0.0189	0.1607	0.1758	0.1881	0.1975	0.2043	0.2098
0	0.0515	0.0569	0.06	0.0618	0.0626	0.0631	0.2795	0.2858	0.2904	0.2963	0.3027	0.3085
1	0.1252	0.1319	0.1352	0.1367	0.1371	0.1373	0.3894	0.4001	0.408	0.414	0.4185	0.4223
2	0.1949	0.2014	0.2038	0.2045	0.2045	0.204	0.4937	0.5032	0.5101	0.5156	0.5201	0.5247
3	0.259	0.2639	0.2649	0.2647	0.264	0.2831	0.5936	0.6022	0.6091	0.615	0.6203	0.6253
4	0.3171	0.3196	0.3191	0.3181	0.3316	0.4655	0.6889	0.6979	0.7054	0.7119	0.7184	0.7241
5	0.3689	0.3691	0.3674	0.3656	0.5026	0.6061	0.7795	0.7892	0.7981	0.8061	0.8132	0.8194
6	0.415	0.4132	0.4108	0.4085	0.6158	0.7039	0.8643	0.8763	0.8865	0.8954	0.9042	0.9123
7	0.4559	0.4526	0.4502	0.4482	0.6941	0.7845	0.9431	0.9564	0.9677	0.9798	0.9904	0.9995
8	0.493	0.4896	0.4879	0.4868	0.781	0.8089	1.0108	1.0249	1.0405	1.0544	1.0661	1.0766
9	0.5278	0.5248	0.524	0.5312	0.7196	0.8292	1.0604	1.0782	1.0961	1.1124	1.1274	1.1413
10	0.5613	0.5594	0.5597	0.6183	0.6845	0.8294	1.0926	1.1129	1.1317	1.1492	1.1672	1.1831
11	0.5943	0.5938	0.5953	0.7132	0.73	0.7763	1.1026	1.1247	1.1459	1.1622	1.1814	1.1996
12	0.627	0.6284	0.6726	0.7524	0.7692	0.7911	1.0933	1.1119	1.1342	1.1532	1.1651	1.174
13	0.6595	0.663	0.7313	0.8247	0.8347	0.8213	1.0592	1.0848	1.1017	1.1147	1.1186	1.1252
14	0.6916	0.6973	0.781	0.8308	0.8474	0.9158	1.0111	1.0401	1.0577		1.0717	1.0768
15	0.7232	0.7309	0.8268	0.8555	0.8638	0.8887	0.9681	0.9918	1.0109		1.0319	1.0362
16	0.754	0.8106	0.8853	0.8874	0.888	0.9405	0.9535	0.9634	0.9834		1.004	1.0094
17	0.7832	0.8575	0.904	0.9371	0.9126	0.9365	0.9546	0.9593	0.9663		0.9865	0.9933
18	0.8109	0.8848	0.9185	0.9712	0.9268	0.9798	0.9553	0.9614	0.9678	0.9744	0.9793	0.983
19	0.8364	0.9032	0.9237	0.9324	0.9467	0.9406	0.9597	0.9656	0.9715	0.9755	0.9782	0.9809
20	0.8593	0.9291	0.9478	0.9412	0.9906	1.0071	0.9591	0.9658	0.9712	0.9744	0.9773	0.9798

Figure 8-2: Figure 8-3: 2D airfoil Drag data (C_D) for SD7037. Angle of Attack vs Reynolds predicted using Xflr-5 at Ncrit = 1